Spectroscopic studies of supergiant elliptical galaxies

Inglis, Iain

Spectroscopic Studies of Supergiant Elliptical Galaxies

PhD Thesis
University of Durham

Iain Inglis BSc

No part of this thesis has previously been submitted for a degree in this or any other university. Except where otherwise indicated, this work is entirely my own.

Iain Inglis

WK1AAW

Spectroscopic Studies of Supergiant Elliptical Galaxies

Iain Inglis BSc

ABSTRACT

This investigation reports on detailed spectroscopic observations of four southern supergiant elliptical galaxies. A Fourier Difference method is derived to analyse absorption-line data to obtain velocities, velocity dispersions and line-strengths. The method is then applied to the galaxy sample to provide rotation curves and velocity dispersion profiles. A dynamical model is used to assist interpretation, in which a normal elliptical galaxy is placed in a massive background of dark material.

The observations indicate that supergiant elliptical galaxies do not rotate; are over-luminous for their central velocity dispersions and have velocity dispersion profiles which depend on the location of the galaxy within the cluster. Modelling of the profiles suggests that any dark background has a density scale length less than or equal to the cluster galaxies themselves. Two dumb-bell galaxies included in the sample are probably merging.

The conclusion of this work is that the formation of supergiant elliptical galaxies is primarily an evolutionary process [eg galactic cannibalism], but does depend on certain initial conditions which affect the way in which that evolution proceeds [eg tidal stripping].

CONTENTS LIST

CONTENTS contd

CONTENTS contd

1 CHAPTER ONE : INTRODUCTION & REVIEW

1.1 INTRODUCTION

The first-ranked galaxy in a cluster of galaxies is simply the brightest galaxy in the cluster. The aim of this thesis is to examine some of the dynamical properties of these galaxies, in order to help understand the properties of galaxy clusters as a whole. There are two main areas of astronomical interest which require a detailed knowledge of the properties of first-ranked cluster galaxies.

Firstly, since these galaxies and their clusters are in some ways quite remarkable, there are many investigators simply interested in defining the properties of these objects in order to discover the mechanisms which account for their formation and general characteristics. Clearly, a study of the properties of first-ranked cluster ellipticals will increase our knowledge of galaxy clusters as a whole, and might possibly provide some insights into the more normal types of elliptical galaxy. This thesis is part of such a programme.

Secondly, a considerable effort has been made to understand first-ranked cluster ellipticals with a view to their use as "standard candles" in the Hubble diagram [apparent magnitude - redshift]. Since nearby first-ranked galaxies are remarkably similar in luminosity, it is essential to know how that luminosity might change with time, which requires knowledge of both the first-ranked galaxies themselves and their cluster environment.

Comprehensive reviews of galaxy clusters and their evolution have been given by Bahcall (1977) and Dressler (1984b). The kinematics and dynamics of normal elliptical galaxies have been reviewed by Binney (1982). It is not the intention of this introduction to provide an exhaustive review of galaxy cluster astronomy, but rather to illustrate the general characteristics of first-ranked cluster galaxies and to discuss the main topics relevant to the work presented here. Section 1.2 provides a review of first-ranked galaxies, cD galaxies and their cluster environment. The morphology of first-ranked cluster ellipticals and their clusters is described first and then some more specific work is reviewed. A discussion of the theories of the formation of supergiant galaxies is given, followed by a brief description of some of the results which suggest that kinematical studies might provide some particularly useful techniques for examining the properties of first-ranked galaxies.

Section 1.3 describes the arrangement of the material presented in this thesis, and section 1.4 lists the adopted values of the astronomical and physical quantities which are used in the various calculations performed throughout the text.

1.2 REVIEW

1.2.1 Morphology

In their discussion of the identification of extragalactic objects with radio sources Matthews, Morgan & Schmidt (1964) identified a class of strong sources associated with D galaxies [Morgan (1958)]. These D galaxies have a characteristic optical morphology consisting of an elliptical-like nucleus and central region, embedded in an extensive low surface-brightness envelope [possibly reaching to several hundred kpc]. They also noted the frequent occurence of double or multiple nuclei in the supergiant D galaxies, or "cD" galaxies. The name "dumb-bell" galaxy and the abbreviation "db" was given to those systems having double nuclei of roughly comparable brightnesses. A characteristic cluster morphology is found to be typical of clusters containing cD galaxies: the cD galaxy is large, dominant and centrally located in the cluster; the cluster itself is usually centrally concentrated and contains predominantly elliptical galaxies [Oemler (1974)]. The D galaxies have a very wide range in radio luminosity and subsequent searches turned up numerous candidates, many of which had no detectable radio emission. Morgan & Lesh (1965) conducted such an optical search and found cD galaxies in 22 of the 85 Abell clusters with richness class R>2 [Abell (1958)].

A classification of galaxy clusters specifically designed to identify cD galaxies was defined by Bautz & Morgan (1970) and has been used extensively ever since. The form type is based upon the degree by which the first-ranked galaxy stands out relative to the rest of the cluster: cD galaxies are to be found in type I clusters [BMI, Al413], and clusters with progressively less dominant first-ranked galaxies are classed type II or type III [BMII or BMIII]. Some very bright D galaxies and cluster ellipticals are found in BMII clusters [A754, Coma] and dumb-bell galaxies may sometimes be found in clusters of all BM types. A particularly important feature of the BM typing system is the lack of correlation between BM types and richness [variously defined, but always finding a similar lack of correlation].

An example of the application of the BM typing system to a large sample of galaxy clusters is the work of Leir & van den Bergh (1977), who surveyed 1889 Abell clusters and were therefore able to examine correlations between cluster properties and BM type with some hope of success. For the 104 clusters with Abell distance class between 1 and 4 they found the following distribution of BM types: BMI,11%; BMI-II,9%; BMII,21%; BMII-III,19% and BMIII,40%. One problem with the BM typing scheme is that a foreground elliptical galaxy can change the form class from BMIII to BMI, though typing on plates taken in two wavebands could help eliminate discrepant cases.

Leir & van den Bergh also found that, on average, the first-ranked galaxy in BMI clusters was closer to the cluster centre than in types BMII or BMIII. A similar kinematical result was found by Sandage (1972c), who argued that the rms velocity deviation of first-ranked galaxies from the mean redshift velocity of their clusters [ie the mean Hubble line] must be less than 100 kms^{-1}. Quintana & Lawrie (1982) analysed the distribution of velocity differences between first-ranked galaxies in BMI clusters and their mean cluster velocities - and found similar results [cf Beers et al (1984)]. This association of first-ranked galaxies with the spatial and kinematical cluster centre might be due to some form of dynamical evolution which tended to bring bright galaxies to the cluster centre, or because supergiant galaxies are preferentially formed at the centres of clusters. An alternative view is that supergiant galaxies formed early in the cluster history and preferentially survive at the cluster centre [Merritt (1984a)]. The central location of first-ranked cluster ellipticals also has important implications for the understanding of the radio and X-ray properties [Bahcall (1977)].

Another very interesting property found by Leir & van den Bergh was that first-ranked cluster galaxies in BMI clusters appeared to be significantly flattened as compared with all BM types. The average axial ratio for BMII-III and BMIII agreed well with that found for normal field ellipticals, $\langle b/a \rangle = 0.79 \pm 0.04$, whereas BMI and BMI-II first-ranked galaxies had $\langle b/a \rangle = 0.64 \pm 0.04$.

Another classification of clusters relevant to the properties of cD galaxies is that of Rood & Sastry (1971), updated in Struble & Rood (1982). The method used here is to define a set of transitional types between irregular [I] clusters and regular [cD] clusters. Struble & Rood suggested that the sequence might be one of increasing dynamical evolution [see, for example, the N body experiment in White (1976)]. The six major classes [called RS types] of the scheme are cD [dominant, supergiant galaxy], B [supergiant binary: Coma, for example], C [core-halo], L [line], F [flat] and I [irregular]. Struble & Rood classed 18.5% of the 276 Abell clusters in their catalogue as cD, where the revised RS class "cD" generally corresponds to BMI, BMI-II or BMII. The RS classification scheme is based upon the relative spatial distribution of the ten brightest galaxies and might, therefore, be prone to foreground contamination in the same way as the BM system.

One further classification scheme is particularly relevant to rich clusters with D or cD galaxies - that of Oemler (1974). He classed the 15 clusters in his sample in terms of the morphological type of the cluster galaxies. As with other form types, this scheme is important because it is found to correlate with many cluster properties, including the appearance of the cluster on the sky. The three cluster categories defined by Oemler are "cD", "spiral-poor" and "spiral-rich". A cD cluster is characterised by a central dominant cD galaxy, surrounded by a smooth, approximately spherical, distribution of mostly elliptical galaxies. Indeed, there is a pronounced deficiency of spirals in the

cores of rich cD clusters and perhaps some evidence for segregation by mass as well [Dressler (1980a) gives a detailed discussion of the distribution of morphological types in clusters]. The spiral-poor clusters tend to be dominated by S0 galaxies but are not as smooth, populous or as concentrated as the cD clusters. The spiral-rich clusters are typified by a field distribution of galaxy types with an irregular and unsegregated appearance. Oemler made the suggestion that the sequence spiral-rich, spiral-poor, cD is one of increasing dynamical evolution.

The problem of dynamical evolution in clusters is a difficult one, because so many of the necessary parameters of any realistic model are unknown. The masses of galaxies must be known, their likely velocities, the distribution of material within galaxies and within clusters: all require more observations. It is not even agreed whether much evolution is expected after virialisation [Roos & Norman (1979)].

Lynden-Bell (1967) derived the form of "violent relaxation" which is thought to account for the observed approximately Maxwellian distribution of cluster galaxy velocities. Violent relaxation tends to equalise energy per unit mass [ie velocities], whereas classical two-body relaxation tends to equalise energies between particles of differing mass [Chandrasekhar (1960)]. Massive galaxies will therefore sink towards the centre of the cluster and less massive galaxies will be flung out to the edges. Such mass segregation is the subject of a certain amount of observational controversy. In cD

clusters the situation as regards mass segregation is even more confused. If a "cannibal" cD galaxy grows by accretion of other "victim" galaxies, it will tend to disrupt exactly those massive galaxies which are being investigated. Without a much more complete knowledge of cluster properties it is difficult to say whether an excess or deficiency of bright galaxies is expected at the centre of a cD cluster. Oemler (1974) claims support for mass segregation in his 15 clusters, whereas others [Green (1977), Dressler (1978b)] find a deficiency of bright galaxies in cluster cores.

A new element entered the discussion of the morphological nature of first-ranked galaxies with the discovery by Morgan, Kayser & White (1975) [MKW] of galaxies with D or cD appearance in compact clusters too poor to be in the Abell catalogue. They stressed the similarity in the types of galaxies found in rich and poor cD clusters but, in the poor clusters, the supergiant galaxy was not always found at the centre of the group. They also remarked that when D galaxies are not bright enough to dominate their cluster they often have a surrounding group of fainter galaxies. However, Thuan & Romanishin (1981) found that the "cD" galaxies in poor clusters did not have the extensive envelopes typical of cD galaxies in rich clusters.

The search for cD galaxies in poor clusters was continued in Albert, White & Morgan (1977) [AWM] and summarised by White (1978). White found, as Oemler had done, that compact clusters tend to be dominated by galaxies having the most evolved stellar populations [ie elliptical galaxies], while in more

open clusters the galaxies tend to have less evolved stellar populations [ie spirals]. White also found that D and cD galaxies are always associated with local density concentrations of galaxies within possibly quite open clusters [judged by their global appearance]. He was therefore able to identify some D galaxies in all Bautz-Morgan types, but with the larger, more obvious, D galaxies occuring in BMI clusters. Beers & Geller (1983) have further specified this tendency by calculating the distances of luminous halo galaxies from the nearest density maximum in the clusters listed in the Dressler (1980b) catalogue. They found that the mean distance of bright D and cD galaxies from a local density maximum in the cluster was only of the order of the size of the galaxies themselves. Also, those density maxima associated with D galaxies were typically 2-3 times denser than those maxima which had no associated D or cD galaxy.

So far as cluster morphology is concerned, the definition of a D galaxy has a surprisingly wide applicability - from the enormous cD galaxy in Abell 1413 down to the MKW D galaxies. However, there is a continuity of properties between the D galaxies in poor groups and the cD galaxies in rich clusters, which provides a great deal of evidence to confront theories of supergiant galaxy formation; these properties are dealt with in the rest of this introduction.

1.2.2 First-Ranked Galaxies and their Clusters

1.2.2.1 Photometric Observations

If there is a class of astronomical objects the members of which have fixed intrinsic luminosities, then a correlation of the apparent magnitude of these objects with their redshifts [the Hubble diagram] will provide information about the luminosity-distance relation [for some assumed cosmology]. First-ranked cluster galaxies might constitute such a class and have therefore been the subject of a great deal of observational attention. Though this study is not directly concerned with the cosmological implications of these observations, some discussion is given here because many of the better established results concerning first-ranked cluster galaxies come from such cosmologically motivated studies.

In a Euclidean space the luminosity-distance relation would be the familiar inverse-square law. However, Friedmann-Robertson-Walker [FRW] solutions of the Einstein equations of general relativity [for an isotropic, zero-pressure and homogeneous universe] result in a redshift-distance relation which is linear only at small redshifts: Hubble's Law [$v = H.r$, where v is the redshift velocity, H is Hubble's constant and r is the distance]. At higher redshifts, departures from linearity might be observable, and would provide a means of testing cosmological theories. The second order term in the Taylor expansion of the FRW redshift-distance relation is parameterised as "q_0", the "nought"

signifying that the present-day value is to be used [Weinberg (1972)]. The astronomical significance of q_0 is that its value determines whether there is enough matter in the universe to halt the observed expansion [assuming FRW solutions] - the critical value being one half, below which the universe will continue expanding indefinitely. No cosmological discussion is appropriate here, save to say that present estimates of q_0 are consistent with FRW universes, which justifies the choice of $q_0 = +1$ for this study.

The classic treatment of first-ranked cluster galaxies and groups of galaxies in the Hubble diagram is that of Humason, Mayall & Sandage (1956). They found a surprisingly small scatter of $0^m.32$ in the magnitudes of their first-ranked cluster galaxies. Twenty-seven years later, Schneider, Gunn & Hoessel (1983a) have only managed to reduce this scatter to $0^m.29$. Part of the importance of the work done by investigators interested in q_0 is the provision of extensive photometry, with which the properties of D and cD galaxies can be compared. It is this aspect of their work which is of particular relevance here.

Sandage & Hardy (1973) performed a detailed analysis of the work begun in Sandage (1973b) and came to several very important conclusions which bear on the problem of first-ranked galaxy formation. Firstly, a correlation of residuals from the Hubble diagram with BM type revealed that first-ranked galaxies in BMI clusters were, on average, $0^m.6$ brighter than first-ranked galaxies in BMIII clusters. This confirmed the findings of Bautz & Abell (1973), who

came to similar conclusions based on the differences between the magnitudes of first-ranked galaxies [M(1)] and an assumed universal Abell M* for the cluster luminosity function [Abell (1973)]. Moreover, Sandage & Hardy found that the second- and third-ranked galaxies were, on average, $0^m.5$ fainter in BMI than in BMIII clusters. This gives us our first important clue to the nature of cD galaxies: first-ranked galaxies in BMI clusters are bright "at the expense of the fainter members". A new result has recently been found by Struble & Rood (1982). They analysed the separation distances of first- and second-ranked cluster galaxies in their catalogue of clusters and found the average separation between first- and second-ranked galaxies in cD clusters to be 0.5 Mpc larger [ie a typical cluster core radius] than in core-halo clusters. This is consistent with Sandage & Hardy's result, but Struble & Rood go on to say that at lower redshifts the 0.5 Mpc "gap" has been somewhat filled in. If borne out by future observations, this suggests that cD galaxies actually consume other galaxies [also see Hickson, Richstone & Turner (1977)].

Sandage & Hardy found no significant correlation of the first-ranked galaxy magnitude with richness, but found that second- and third-ranked galaxies are $0^m.5$ brighter in richer clusters [Abell richness class 4] than in poorer clusters [richness 0]. It therefore appears that the first-ranked galaxy magnitude [M(1)] is not determined by statistical sampling of a luminosity function, whereas the magnitudes of the second- and third-ranked galaxies [M(2) and M(3)] might be. This is because, in the statistical view, a correlation of M(N) with

richness would be expected if the chance of getting a brighter M(N) increases with the number of samples of the luminosity function [ie as the number of galaxies in the cluster increases]. The lack of correlation of M(1) with richness is taken to indicate a very steep luminosity function at the bright end. Summing up this extensive programme of observations, Sandage (1976) concluded that there was no currently known luminosity function steep enough at the bright end to ensure the small correlation of M(1) with richness, over such a wide range in richness - the first-ranked galaxy must therefore have a special formation mechanism, different from that which creates the other cluster galaxies.

The values that Sandage (1976) found for the average galaxy magnitudes are of general interest here: he found the difference between M(1) in BMI and BMIII clusters to be $-0^m.59$ [ie BMI brighter] and $+0^m.5$ for M(2); the difference between M(1) and M(2) in BMI clusters was $-1^m.46$ and $0^m.37$ in BMIII; the mean V magnitude for first-ranked galaxies in BMI clusters was $-23^m.68$. Kristian, Sandage & Westphal (1978) found $\langle M(1)_V \rangle = -23^m.28$ and $\langle M(1)_R \rangle = -24^m.09$ [averaged over all BM types].

The complicated problem of sampling a universal luminosity function with various forms of fitted luminosity function [and selection effects] has been tackled by Geller & Peebles (1976) and Schechter & Peebles (1976). They concluded, in contrast to Sandage (1976), that it is indeed possible to reproduce the observations of the magnitudes of the first few ranked galaxies without recourse to an

artificially steep luminosity function. However, doubt has been cast on the universality of cluster luminosity functions by evidence for real [ie non-random] variations of the Schechter (1976) absolute M^*, calculated from luminosity functions of a sample of twelve very rich clusters [Dressler (1978a)]. Using a technique which does not assume a universal cluster luminosity function [but does make other assumptions] Tremaine & Richstone (1977) developed a series of statistical tests to examine the truth of statistical sampling as compared with special formation. Analysing the Sandage & Hardy data they concluded [provisionally] that special formation is required. Using the same technique applied to photometry of first- and second-ranked galaxies in the MKW and AWM groups, Schild & Davis (1979) concluded that <u>all</u> first-ranked galaxies need "special formation". Clearly, the discussion of the special formation of first-ranked galaxies, as compared with the statistical hypothesis, is not yet concluded [Godwin & Peach (1979)].

A source of error in the formal estimate of q_0 is the accuracy with which the mean [or mean corrected] absolute magnitude of first-ranked cluster ellipticals is known. In an effort to improve the estimate of $\langle M(1) \rangle$, Hoessel, Gunn & Thuan (1980) [HGT] observed the first-ranked galaxy in 116 Abell clusters. Using a metric aperture magnitude system of monochromatic magnitudes the scatter in their observations was initially $0^m.35$, reduced to $0^m.30$ with BM and richness corrections. Unlike Sandage they did find a significant correlation of M(1) with richness, at a level of $0^m.1$ per Abell richness class and a difference between M(1) in BMI and BMIII

clusters of $0^m.41$ [the metric radius of the aperture used by Sandage was 43 kpc, for H_0 = 50 $kms^{-1}Mpc^{-1}$ and q_0=+1, whereas HGT used a smaller aperture: 16 kpc, for H_0 = 60 $kms^{-1}Mpc^{-1}$ and q_0=+½].

Hoessel (1980) replaced the magnitude corrections for BM type and richness made in HGT by a single correction, in terms of the luminosity growth curve slope parameter, α [Gunn & Oke (1975) - the growth curve is parameterised $L(\gamma) = L_S.(\gamma/\gamma_S)^{\alpha}$, where γ is the aperture size and L_S and γ_S are constants]. Hoessel found that first-ranked galaxies in BMI clusters had larger values of α [ie were more distended] than those in BMIII clusters, and a similar but weaker correlation with richness. The work has been continued in Schneider, Gunn & Hoessel (1983a,b).

1.2.2.2 Individual Objects

Only the properties of the class of first-ranked galaxies have been discussed so far. A considerable amount of work has been done on individual objects, particularly the more spectacular cD galaxies and clusters of galaxies.

Oemler (1973) studied the cD galaxy in A2670 and found that the luminosity profile is similar to that of an elliptical galaxy out to a distance of 30 kpc, when the extensive envelope becomes apparent. The envelope can be followed to a distance of 1 Mpc, giving an integrated visual magnitude of $-25^m.2$. The photometric study of elliptical and cD galaxies is continued in Oemler (1976). A1413 is included in

Oemler's sample, for which a magnitude brighter than -26^m is given, and the envelope is traced out to more than 2 Mpc. First-ranked cluster ellipticals show a wide variety of luminosity profiles, with the larger galaxies having surface-brightness profiles flatter than r^{-2}. Bahcall (1977) comments that $r^{-1.6}$ fits cD profiles quite well. An unusual feature found in some cD galaxies is a very low surface-brightness core [Kron & Albert (1982)] - an example of this phenomenon is the multiple nucleus cD in A2199 [NGC6166]. Oemler found a correlation between the first-ranked galaxy luminosity and the total luminosity of the cluster, in the sense of increasing first-ranked luminosity with increasing cluster luminosity [cf Thuan & Romanishin (1981)].

Dressler (1978a,b) investigated the luminosity functions and cluster dynamics of 12 very rich clusters. He found it difficult to correlate the properties of the central cD galaxy with the appearance of its cluster luminosity function - of the BMI clusters in his sample the ones with the fewest bright galaxies did indeed have the brightest cD galaxies, but he found examples of non-cD clusters with unusually steep bright-end slopes as well. He also found that BMI clusters, though not necessarily the richest clusters, did always have average or higher than average central galaxy densities [cf White (1978), Beers & Geller (1983)]. The density profiles of his sample clusters were adequately represented by King models [King (1966)] with an average core radius of 0.47 ± 0.11 Mpc. This is rather at odds with the Bahcall (1975) estimate of 0.25 ± 0.04 Mpc, but disagreement should not be taken too seriously as the data used in the

studies are significantly different - later in this work a representative value of cluster core radius is determined. The sizes of galaxy clusters may be appreciated by considering the estimates of de Vaucouleurs effective radii included in Dressler (1978a), who found $\langle r_e \rangle = 3.8 \pm 1.3$ Mpc.

1.2.3 cD Galaxy Formation

There is mounting evidence that first-ranked cluster galaxies, and cD galaxies in particular, grow by the accretion of material originally attached to other cluster galaxies. There are three principal mechanisms currently proposed which may be able to account for the accretion by a galaxy at the dynamical centre of its cluster of large amounts of stellar [or non-stellar] material: tidal stripping, galactic cannibalism and gas accretion.

1.2.3.1 Tidal Stripping

Gallagher & Ostriker (1972) investigated the possibility that tidal encounters between cluster galaxies might strip significant amounts of loosely bound material from the edges of galaxies. This material would then distribute itself with a density profile similar to that of the cluster, consistent with the observed slow fall off of cD envelopes [$r^{-1.6}$]. The argument has been continued in detail by Richstone (1975, 1976) who concluded that as much as 90% of the cluster binding mass might be stripped through tidal encounters, assuming that galaxies originally had 500 kpc dark haloes containing all

the mass needed to bind the cluster. It should be noted that tidal stripping cannot be a complete explanation of the cD galaxy phenomenon, as it only describes how a pre-existing centrally located galaxy might accrete large amounts of material. Some additional theory of the formation of galaxies [or clusters of galaxies] is needed to explain why such a central galaxy should exist [cf Merritt (1984a)]. The same qualification applies to the gas accretion mechanism described later.

An important feature of the tidal stripping mechanism is that it is not the total number of galaxies [ie the richness of the cluster] which determines the amount of stripped material, but rather the density of galaxies. The Bautz-Morgan or Oemler type sequences may then be identified as ones of density rather than richness, which accords with observation. If the stripped matter is to be identified with the envelopes of cD galaxies, then it is clear that cD galaxies must be located at the dynamical centres of their clusters, a requirement which seems quite accurately true for BMI clusters.

The evidence for tidal reduction of the visible radii of cluster galaxies is ambiguous. Oemler (1976) admitted considerable uncertainty in his estimates of "cut-off" radii, but found no evidence that elliptical galaxies in the outer regions of Coma have larger radii than those in the centre. However, Strom & Strom (1978) found quite strong radius segregation of ellipticals in spiral-poor and cD clusters [including Coma], whereas the radii of ellipticals in spiral-rich clusters were found to be systematically larger and in good agreement within

each cluster. They tested their result by correlating central surface-brightness with absolute magnitude, and found that though the range of central surface-brightness was the same for galaxies with larger and smaller radii, the galaxies with smaller radii [which had presumably undergone a number of tidal encounters] were on average $0^m.5$ fainter. This qualitative behaviour would be expected from a mechanism which preferentially removed the outer stars from a galaxy.

Estimates of the amount of diffuse emission in clusters are very hard to make. Oemler (1973) comments that if the profile of the cD galaxy in A2670 is extended throughout the cluster, whose profile it matches well, then as much as 35% of the total cluster luminosity might be attributable to the envelope. Melnick, White & Hoessel (1977) looked in detail at diffuse emission from Coma and found the two supergiant galaxies to share a common envelope, but put an upper limit of 25% on the total diffuse emission.

Richstone admitted a difficulty for the tidal stripping mechanism in accounting for the supergiant galaxies found in poor clusters [MKW and AWM], as the presence of spiral galaxies in these clusters suggests that tidal encounters have been limited. However, the envelopes of D galaxies show a marked correlation with richness [van den Bergh (1977), Oemler (1976), Thuan & Romanishin (1981)], and it seems likely that the mechanisms determining the body and envelope of cD galaxies may be different.

1.2.3.2 Galactic Cannibalism

The theory of galactic cannibalism has been described in a series of three papers: Ostriker & Tremaine (1975), Ostriker & Hausman (1977) and Hausman & Ostriker (1978) [OT, OH, HO].

If a large extensive galaxy has an envelope that includes galaxies passing nearby, then there will be a tendency for the passing galaxy to lose energy to the envelope by dynamical friction [see eg Tremaine (1976) for the method as applied to globular clusters]. If the passing galaxy is moving slowly enough it will eventually spiral into the core of the large galaxy, being disrupted gradually as it falls in. OT found that, using the observed parameters of clusters of galaxies, a central galaxy accreting by this mechanism will soon become the most luminous galaxy in its cluster.

OT remark that there are two competing effects which determine the appearance of the merger product, and it is this balance that makes their formation mechanism "special", because it allows the luminosity within a metric aperture to change only weakly with each galaxy cannibalised. One effect is the tendency of a galaxy to shrink when mass is added to it, since individual stellar orbits will have to contract to maintain equilibrium if the mass inside the orbit is increased. The opposing effect is the redistribution of the orbital energy of the accreted galaxy, which tends to inflate both cannibal and victim [ie the collision is inelastic Ostriker (1978)].

The problem of the size [and sign] of the correction to the luminosity of such an accreting first-ranked galaxy viewed through a metric aperture is dealt with by Gunn & Tinsley (1976). They found a very sensitive dependence on the details of the structures of the merging galaxies and thought the correction might be of either sign but, in any case, would be a small proportion of the fractional mass accreted. OH comment that for the large metric apertures of observers such as Sandage [43 kpc] the evolution will always be in the sense of brightening as time progresses.

The accretion of less massive, and therefore bluer, galaxies [by the colour-magnitude effect, Sandage (1972b), Sandage & Visvanathan (1978)] will mean that a composite object such as a cD galaxy should be bluer than an elliptical galaxy of the same absolute magnitude. Such a comparison is possible with the MKW D galaxies since they have magnitudes comparable to those of "normal" first-ranked cluster galaxies [$\langle M_V \rangle = -23^m.20$, Schild & Davis (1979)] and Lugger (1979) found that the MKW galaxies observed by Schild & Davis are indeed $0^m.07$ bluer in (U-B) than ellipticals and S0 galaxies in Coma and Virgo.

OH give a simple example which defines qualitatively the effect of merging N identical galaxies, each of mass M_O and gravitational radius R_O. The total energy of each galaxy is:

$$E_O = - \frac{G M_O^2}{2 R_O}$$

Ignoring the orbital energy, the final merger product will have mass $M_m = N.M_o$, and total energy:

$$E_m = N E_o = - \frac{N G M_o^2}{2 R_o}$$

and if the new galaxy is merely a scaled version of the old [ie the merger is homologous] then:

$$E_m = - \frac{G (N M_o)^2}{2 R_m}$$

If surface-brightness is defined $S_m \alpha (N.M_o)/R^2$ then we have:

$$R_m = N R_o \qquad S_m = \frac{S_o}{N}$$

The effect of [homologous] mergers is therefore to increase the size and mass of the accreting galaxy but to decrease the surface-brightness. When the central density of the cannibal becomes lower than the central density of the galaxies being accreted, the nuclei of the accreted galaxies may survive disruption to sink right in to the centre of the cannibal to form a multiple nucleus galaxy. Note that more detailed numerical simulations by other authors can produce non-homologous merger products [Farouki et al (1983), Duncan et al (1983)].

HO performed rather more detailed merger simulations and made predictions for the changes in merger remnant luminosity [for various apertures] and, more usefully, the expected form of the correlation of the luminosity growth curve slope, α, [Gunn & Oke

(1975)] with total magnitude. The predictions of HO are successful in describing the data obtained by Hoessel (1980), who found the correlation of α and absolute magnitude to be very well reproduced by an HO model describing the mergers of objects of similar size [also see Schneider, Gunn & Hoessel (1983a,b)]. This is consistent with the results of Sandage & Hardy (1973), and Struble & Rood (1982), who suggested that the most likely victim of a cannibal is the next brightest galaxy.

Recent simulations have attempted to combine the effects of dynamical friction and tidal stripping to provide composite models of the formation of cD galaxy clusters. These include Richstone & Malumuth (1983) and Malumuth & Richstone (1984), who have had conspicuous success in building objects which have many of the properties observed in cD galaxies. Other attempts include Merritt (1983, 1984a), Miller (1983), Farouki et al (1983) and Duncan et al (1983).

The theory of galactic cannibalism also makes predictions about cluster luminosity function evolution [Ostriker & Hausman (1977)]. Because bright galaxies are preferentially disrupted, the position of the "knee" in observed luminosity functions should move progressively faintwards in clusters which have experienced more cannibalism [ie BMI clusters].

1.2.3.3 Gas Accretion

The third proposed explanation of the existence of cD galaxies relies on the interpretation of X-ray observations.

Most extragalactic X-ray sources are clusters of galaxies. Such cluster X-ray emission is generally found to correlate with form types, such as those defined by the BM and RS schemes. Bahcall (1977) found that some 33% of RS type cD - B clusters were X-ray emitters [and strong ones] whereas only 8% of irregular I clusters were emitters [and weak ones]. When the identification with an optical cluster is good and the X-ray luminosity is large enough, the emission is often found to be distributed about the cluster core, usually about a cD or active radio galaxy [Jones et al (1979), Bahcall (1977)]. X-ray luminosity profiles require models to determine the distribution of emitting gas but, assuming thermal bremsstrahlen, the characteristic scale of the gas distribution is typically of the order 0.2 - 0.5 Mpc [Kellog & Murray (1974), Jones & Forman (1984)]. This is about the same as [or larger than] estimates of rich cluster core radii [Bahcall (1975), Dressler (1978), Semeniuk (1982)].

Accretion rates of tens to hundreds of solar masses per year [Stewart et al (1984)] might form a cD galaxy over a Hubble time. However, it is then rather difficult to account for the similarity of the stellar compositions [and M/L ratios] of cD and normal elliptical galaxies, if the accretion process has been creating stars over some 10^{10} years. More observations and modelling are required.

1.2.4 Kinematics of First-ranked Galaxies

Recent work on the kinematical properties of normal elliptical galaxies [Binney (1982)] has revealed a number of interesting connections between the dynamically important properties of elliptical galaxies [rotation and velocity dispersion] and their other properties [luminosity and shape, for example]. This suggests that a quite new approach to the study of first-ranked cluster galaxies might be possible, through examination of their kinematical, rather than their morphological or photometric properties.

The discovery by Bertola & Capaccioli (1975) that elliptical galaxies rotate too slowly to maintain their shapes [interpreted as oblate spheroids] has profoundly altered the view of elliptical galaxy formation [Binney (1982)]. This result has been confirmed by many subsequent observations [Illingworth (1977), Schechter & Gunn (1979), Davies et al (1983)] but hardly any attention has been directed towards the rotational properties of first-ranked cluster galaxies. Since these objects are more flattened than the norm for field ellipticals [Leir & van den Bergh (1977)], it is clearly of considerable interest to do so.

The study of stellar velocity dispersion profiles can give valuable information [if model-dependent] concerning the distribution of matter in elliptical galaxies [Efstathiou et al (1982), Davies et al (1983)]. While such studies are important for establishing the properties of normal elliptical galaxies, they are potentially even more important

when applied to the extremely large and luminous cD galaxies, where the concurrence of materials of widely differing M/L is expected [the central cD, its envelope and possibly a background of cluster binding material].

Dressler (1979, 1981) has performed the only detailed investigation of the relationship between the dynamics of a cD galaxy and its cluster environment. He found that the velocity dispersion in the envelope of the cD galaxy in A2029 rose from 375 kms^{-1} in the centre to over 500 kms^{-1} at 100 kpc from the nucleus. His interpretation of this result was that the M/L ratio must rise significantly in that distance, indicating the presence of a number of additional mass components. Dressler used a three-component dynamical model, identifying the components as an [inflated] elliptical galaxy, surrounded by an envelope of material of M/L intermediate between an elliptical galaxy and a cluster; the third component consisted of dark material assumed to provide the mass necessary to bind the cluster. While Dressler's model will stand or fall as further results are obtained, it is clearly essential to make new observations in order to establish whether these results are general characteristics of cD galaxies. Tonry (1984) has also looked at the velocity dispersion profiles of the inner regions of two multiple nuclei galaxies.

Another dynamical approach relies upon the observed correlation between the central velocity dispersions of elliptical galaxies and their luminosities, [Faber & Jackson (1976), Tonry & Davis (1981), Tonry (1981), Terlevich et al (1981), Davies et al

(1983)]. The form of the relation is parameterised $L \propto \sigma^n$, where n is generally found to be about four. If n is exactly four, an explanation can be found by application of the Virial Theorem to similar systems of identical M/L and central surface-brightness [Fish (1964), Aaronson, Huchra & Mould (1979)]. If this relation is established sufficiently well for normal elliptical galaxies then observations of first-ranked cluster ellipticals should reveal whether their extreme luminosities are matched by correspondingly high stellar velocity dispersions. If cD galaxies are produced by mergers [homologous or not], they should have significant excess luminosities for their central velocity dispersions, in terms of the L-σ relation defined for normal elliptical galaxies. Hausman & Ostriker (1978) and Duncan et al (1983) provide theoretical predictions of the relationship between L and σ.

The dynamics of luminous elliptical galaxies have been discussed by Malumuth & Kirshner (1981, 1985). They found that their sample of 31 BCM [brightest cluster member] galaxies were substantially brighter than predicted by the normal galaxy L-σ relation. Where there was a velocity dispersion overlap between their samples of BCM and normal elliptical galaxies, the BCM galaxies averaged $1^m.22$ [in V] too bright for their velocity dispersions. Their results are generally consistent with predictions made by simple merger models, but examination of the surface-brightness profiles suggests that cD galaxy mergers may not be exactly homologous [cf Morbey & Morris (1983), who found that $I_e \propto r_e^{-1.12}$, rather than the $I_e \propto r_e^{-1}$ required for homologous mergers].

Attention has recently begun to focus on the detailed properties of multiple nuclei systems. Hoessel (1980) found that 28% of the first-ranked cluster galaxies in his sample had multiple nuclei - far too many to be the result of a simple projection effect [Schneider, Gunn & Hoessel (1983b)]. Since the merger time scale is approximately one orbit [Rood & Leir (1979), Tremaine (1981)], 2.5×10^8 years, with a probable time between collisions of 10^9 years, the fraction is reasonable if all mergers produce multiple nuclei. Other authors accept that the frequent occurence of multiple nuclei is related to the presence of a central galaxy, but argue that the associations are transient and will not generally lead to mergers [Merritt (1984b), Tonry (1984, 1985), Smith et al (1985)]. The actual situation is probably intermediate, with some systems being real associations which will lead to mergers [30% - Tonry (1985), Hoessel et al (1985)] and others being merely transient. This interest in the kinematical properties of multiple nuclei galaxies opens up another area where spectroscopic observations are appropriate.

1.3 ARRANGEMENT OF THESIS

The aim of this investigation is to make detailed observations of the rotation curves and velocity dispersion profiles of a sample of first-ranked cluster ellipticals - to help establish their general dynamical characteristics. Spectroscopic observations are reported of four galaxies: two dumb-bell galaxies [IC2082 and Sersic40/6 cD] and two single D/cD galaxies [0559-40 and Pks2354-35].

Chapter 2 provides a very brief indication of some of the preliminary data processing that is required to prepare the spectroscopic data for astronomical analysis. The approach adopted is that this part of the data reduction procedure is well understood [and well documented in various software data reduction packages] and only those procedures are described which were conducted in a novel or non-standard way.

The statistical procedures used to extract the velocities and velocity dispersions from the galaxy spectra are derived and tested in chapter 3. New observations of 11 first-ranked and field elliptical galaxies are reported in chapter 4. These observations do not form part of the astronomical analysis of this study, but are included to allow validation of the data reduction procedures against published data.

Observations of the giant dumb-bell galaxy IC2082 are reported in chapter 5. The analysis includes: photometry; estimates of cluster velocity dispersion and core radius; discussion of the dumb-bell motion of the system and dynamical modelling of the velocity dispersion profile. Results from the three other galaxies are reported in chapter 6, and discussed within the same framework as IC2082.

Chapter 7 contains a summary of the main conclusions of the study. The work described in this thesis has been substantially reported in two publications: Carter et al (1981, 1985).

1.4 NUMERICAL CONSTANTS

$H_o = 50\ kms^{-1}Mpc^{-1}$

$q_o = +1$

$c = 3 \times 10^5\ kms^{-1}$

$1pc = 3.0856 \times 10^{16}\ m$

$G = 6.673 \times 10^{-11}\ Nm^2kg^{-2}$

$M_\odot = 1.989 \times 10^{30}\ kg$

$M_{B\odot} = 5^m.48$

$M_{V\odot} = 4^m.83$ [Allen (1973)]

$M_{R\odot} = 4^m.31$

$A_B = 0.123\ [\mathrm{cosec}(b) - 1]$ for $b < 50°$

$A_B = 0$ for $b \geq 50°$

$A_B/A_V = 4/3$

$A_R/A_V = 0.72$ [Sandage (1973a, 1975)]

To convert linear distances to angular measures [Sandage (1972a)]:

$$\theta = \frac{r\ H_0\ q_0^2\ (1+z)^2}{c\{q_0 z + (q_0-1)[(1+2q_0 z)^{\frac{1}{2}} - 1]\}}$$

For $q_0=+1$ this reduces to:

$$\theta = \frac{r\ H_0\ (1+z)^2}{cz}$$

To convert seconds of arc to kpc [$H_0=50\ kms^{-1}Mpc^{-1}$]:

$$\text{secs/kpc} = 0.0343774\ \frac{(1+z)^2}{z}$$

The "Second Reference Catalogue of Bright Galaxies", [de Vaucouleurs, de Vaucouleurs & Corwin (1976)] is referred to throughout the text as the "Reference Catalogue". Similarly, Abell clusters [Abell (1958)] are referred to by the prefix "A": thus, A1413.

2 CHAPTER TWO : PRELIMINARY DATA REDUCTION

2.1 INTRODUCTION

There are a number of corrections which must be applied to "raw" spectra before they are suitable for quantitative analysis. The spectral data in this study comes from two different photon-counting detectors, but the reduction procedures were broadly similar and are discussed together. The author performed the complete reduction only for the SAAO data [South African Astronomical Observatory - chapter 4] and examples of reduction techniques and numerical quantities are, therefore, taken from experience with SAAO data rather than AAT data [Anglo-Australian Telescope - chapters 5 and 6]. Comparisons between the two types of data are made where observational points can usefully be made.

The Image Photon Counting System [IPCS] attached to the RGO spectrograph at the AAT provided long slit spectra divided into 40 [5 arcsec] increments of 2048 pixels each. The Reticon Photon Counting System [RPCS] mounted on the Image Tube Spectrograph [ITS] at SAAO provided spectra from two apertures separated by 25 arcsec on the sky, each spectrum having 1872 pixels. The reduction was performed using standard software packages - the IPCS data was reduced using the AAT SDRSYS package and the RPCS data was reduced using the ESP package produced by the Royal Observatory, Edinburgh. The documentation provided with these packages provides a detailed description of the procedures available.

2.2 FLAT FIELDING

The first stage of the reduction process is to remove the effects of variations in sensitivity of the detector. Uniform illumination of the detecting surface by a source of continuum light, such as a tungsten filament lamp, provides a "flat-field" spectrum. The pixel-to-pixel variations in this spectrum are caused by variations in detector sensitivity, whereas the large scale features are principally determined by the spectrograph optics. The optics used for viewing astronomical objects are not generally the same as the optics used for viewing the flat-field calibration lamp, so the large scale features are removed. For the RPCS data, continuum division using the ESP digital Martin filter proved very successful. Spectra may then be corrected by dividing the detected spectrum by such a continuum-divided flat-field [normalised to conserve counts].

As illustrated in figure 2.2.1, the flat-field characteristics of the two detectors differ markedly. The RPCS consists of a fixed array of 936 diodes, and cascades of photo-electrons from the stacked Varo tubes in the image intensifier are located to half a diode, giving the 1872 pixels of recorded data. The odd-even effect of such an event-location procedure is apparent.

In contrast, the IPCS has an event-location logic which assigns events to hypothetical pixels, whose size and position depends upon the instrument set-up. Pixels may therefore move across the surface of the detector. For this reason, the IPCS

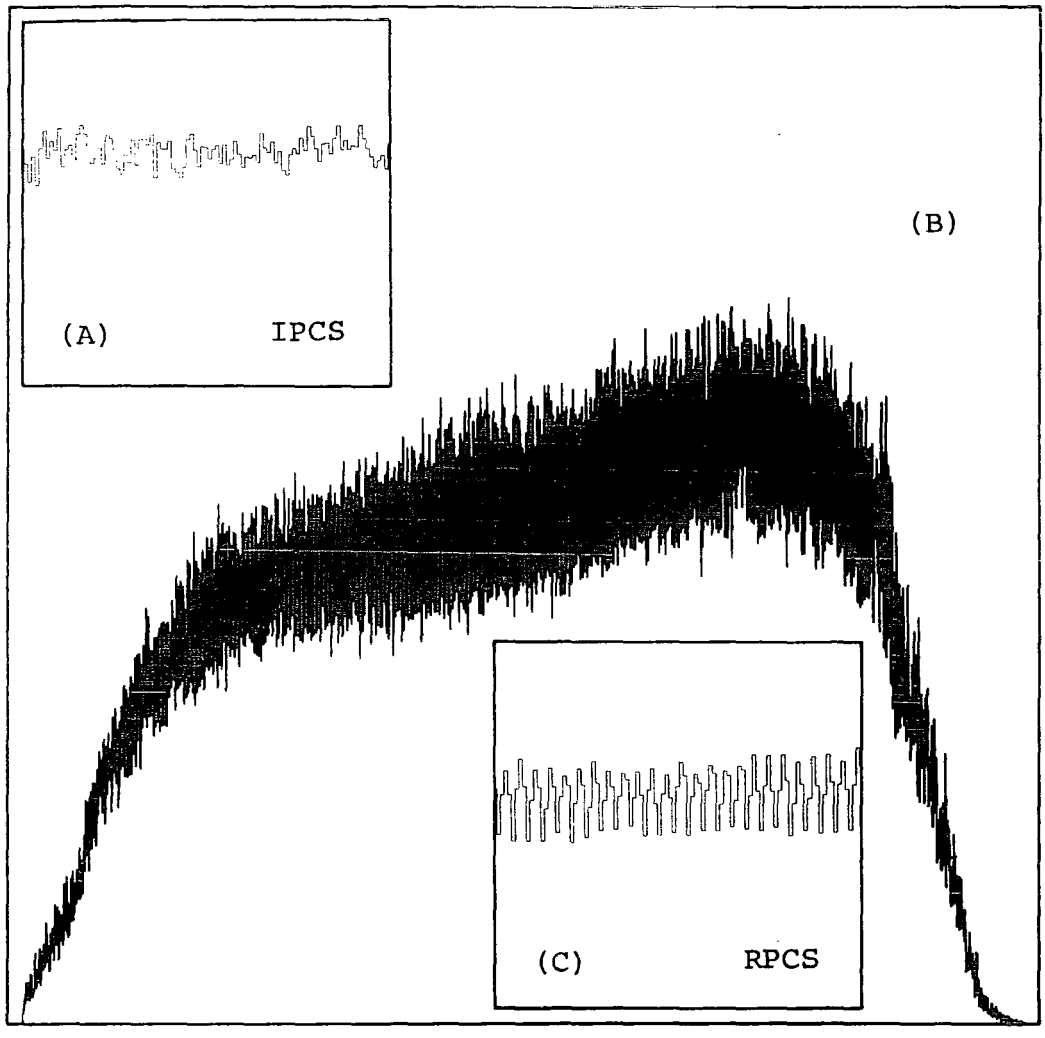

Figure 2.2.1

(A). Detail of IPCS flat-field
(B). RPCS flat-field
(C). Detail of RPCS flat-field

flat-fields are time-dependent and irregular. Comparisons of IPCS flat-fields taken at the start and finish of a night's observation show that variations with time are significant, whereas RPCS falt-fields show remarkably good reproducibility [as judged by division of two normalised flat-fields].

The effect of flat-fielding is shown in figure 2.2.2 for an example RPCS spectrum, showing the dramatic improvement in S/N.

2.3 WAVELENGTH CALIBRATION

When converted to wavelength units the sizes of the detector pixels will not in general be equal, because of geometrical and other distortions in the spectrograph and image tubes. A procedure must be used to correct for such distortions - and is often called "scrunching".

Ultimately the spectra must be defined on a scale in which pixels have equal size in log wavelength and some reduction programs reduce spectra directly to such a scale. The data used in this study was, however, first reduced to a linear wavelength scale and was re-binned to a logarithmic scale in a separate operation.

RPCS data was taken as 1500 second object exposures sandwiched between 150 second arc exposures [He-Ar-Ne-Cu]. The ITS at SAAO is normally used with a $CuSO_4$ filter to mask the red end of the arc spectrum. This filter was removed to increase the

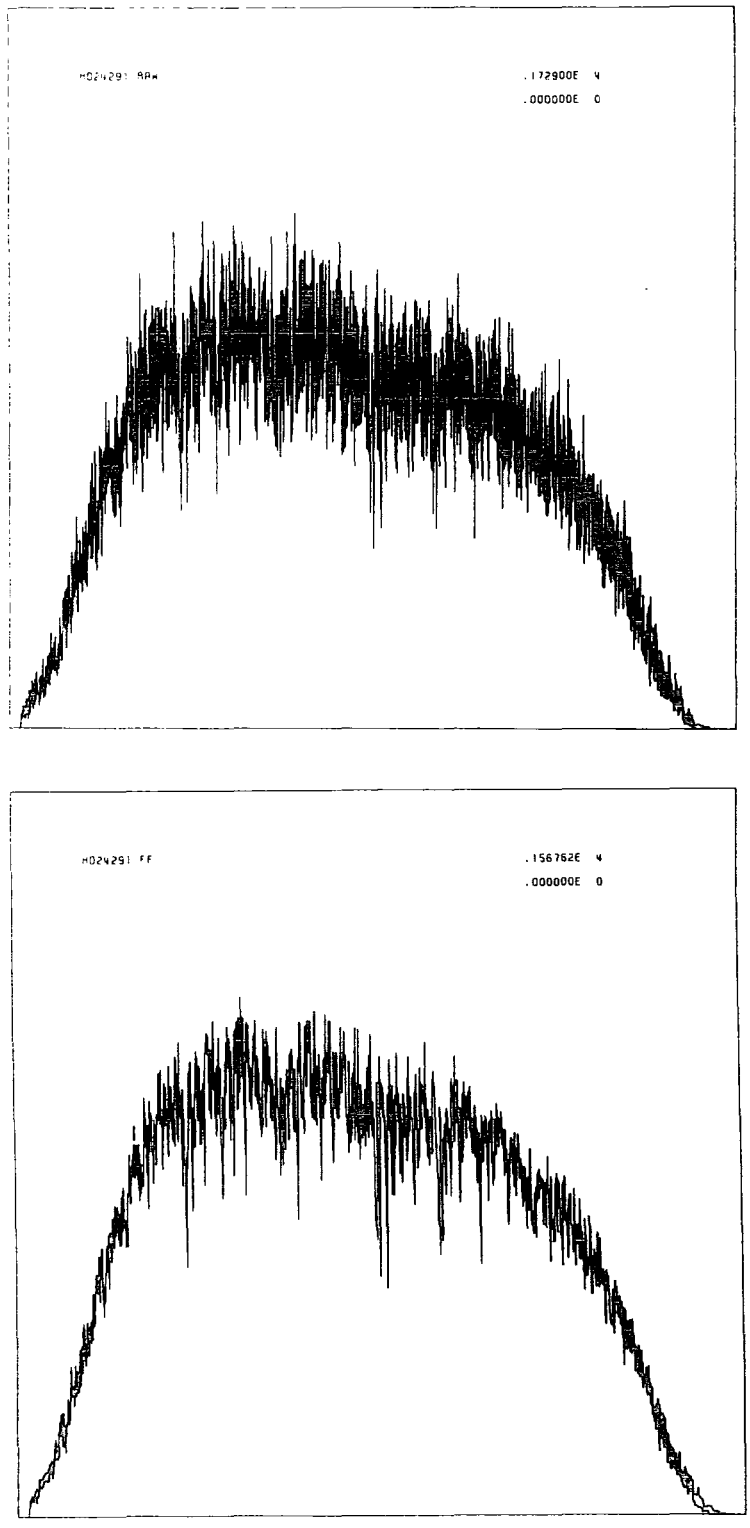

Figure 2.2.2

Raw and flat-fielded RPCS star spectrum

strength of the rather sparse red arc lines. Identification of emission lines by a combination of interactive and automatic algorithms then enables the construction of a table of [accurately known] arc line wavelength against pixel number. A low order polynomial fit to this table defines the transformations to a linear wavelength scale. Each exposure of an object was reduced using the sum of the adjacent arc exposures [in time]. However, no attempt was made to combine arcs from different apertures, as there was a two pixel offset between the two apertures.

Figure 2.3.1 shows a typical plot of wavelength against pixel number [channel] for some RPCS arc data. The high dispersion grating [50 Å/mm] and fixed pixel array give an impressively linear relationship.

Uncertainties in the wavelength calibration introduce errors into the determinations of radial velocities and velocity dispersions. Tests carried out with sky-lines [for which the wavelengths are precisely known] and repeated observations of objects show that absolute velocities [given a perfect estimation procedure] should be accurate to 20 kms^{-1}. Velocity dispersions are rather less sensitive due to correlations between scrunching errors.

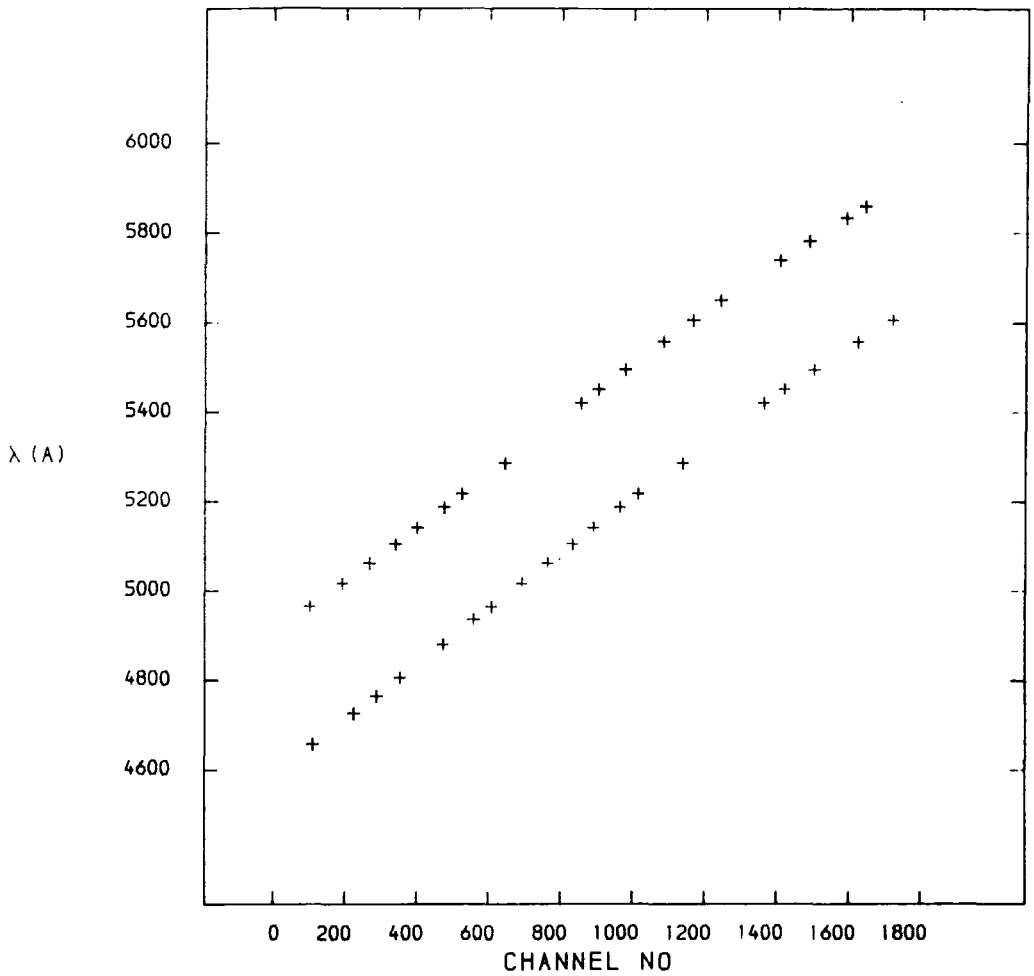

Figure 2.3.1 Wavelength-Channel Number

Plot of arc-line wavelength against detector channel number for the RPCS diode array. The two sets of points result from the different grating angles used to observe objects with a range of redshifts.

2.4 S-DISTORTION

The focusing of photo-electrons in the image-intensification stage of two-dimensional spectral detectors, such as the IPCS and the RPCS, causes the spectrum of a point source object to have a characteristic "S" shape on the detector surface. For an extended source of emission this causes degradation of the spatial resolution.

The IPCS has a real-time facility for removing a constant S-distortion from all increments in a frame of data. Since, in practice, S-distortion varies across the face of the photo-cathode the "scan-corrections" will eliminate S-distortion only in one region of a frame - usually chosen to be the central few increments. It may, therefore, be necessary to remove residual S-distortion as part of the data reduction process. IPCS data taken for this study which suffered badly from S-distortion was not included in the analysis.

The coarseness of the spatial resolution of the RPCS, and the choice of dekker and slit widths, prevented any significant fraction of light from one aperture being detected by the other diode array. The two spectra may thus be treated independently.

2.5 SKY SUBTRACTION

The galaxies observed in this study have a range of galaxy/sky photon counts from better than 10, to less than 1 [for the long slit data]. Allowance must therefore be made for the contribution of the night sky to the detected spectra.

2.5.1 IPCS Sky-Subtraction

The IPCS data was sky-subtracted using the following procedure. The observations included frames of blank sky from which "vignetting functions" were calculated. If the j^{th} pixel [of N] of the i^{th} increment [of I] within a frame is $a_i(j)$, the vignetting function may be defined:

$$v(i) = \frac{\sum_{j=1}^{N} a_i(j)}{1/I \sum_{i=1}^{I} \sum_{j=1}^{N} a_i(j)} \qquad 2.5.1$$

A few spectra from the ends of the slit were de-vignetted [divided by v(i)] and averaged to form a mean sky. For each increment of an object frame this mean sky was re-vignetted [multiplied by the appropriate v(i)] and subtracted. Any sky-line residuals were then replaced by linear interpolation between two adjacent featureless regions. Sky-line residuals were $\leq$2%, which is the estimated accuracy of the whole procedure.

The advantage of this method over sky-subtraction using the observed sky frame with a correction factor [for exposure time differences: typically 10/1] is that it makes use of the higher S/N sky spectra available from the long object exposures. The method assumes, of course, that there is no significant object signal in the outer increments.

For nuclear spectra, no dependence was found of the radial velocity or velocity dispersion on the sky-subtraction procedure. However, uncertainties in sky-subtraction become a significant source of error for spectra as faint as the sky itself. This was taken into account in the error estimates for the derived parameters.

2.5.2 RPCS Sky-Subtraction

The faintest objects were sky-subtracted by direct differencing of the spectra from the A and B apertures [object & sky]. Since the objects were observed for equal periods in both apertures, any differences in vignetting or sensitivity cancel out. Offset skies were used for objects so bright that the "sky" aperture was contaminated with object signal. No dependence was found between the derived parameters and the method of sky-subtraction. This is because the narrow spectral region observed contained no very prominent sky-lines.

2.6 CONTINUUM REMOVAL

The continua of stellar and galactic spectra allow the expected photon noise to be estimated, but contribute no other information to help determine radial velocities and velocity dispersions - they may be removed either by subtraction or division.

Because it preserves line-strengths, continuum division is the more natural method of removing the continuum for a study involving absorption lines. However, continuum subtraction was found to be the most satisfactory procedure for the particular data under study here, because of the steep slopes in the detected continua [caused by vignetting] - continuum division effectively emphasises those regions with the poorest signal-to-noise in a spectrum with a wide dynamic range, whereas in this study only the highest S/N lines should be emphasised.

The method of fitting the continuum had no significant effect on the results [velocity errors were always ≤ 2 kms^{-1}]. A third order least-squares polynomial fit was used in the reductions. Tests were made using higher order polynomials and interactively fitted cubic spline functions, but no improvement was found. The insensitivity to continuum removal is due to the use of filters in the parameter estimation procedures [a Fourier filter in the CCF and wavenumber cut-offs in the Fourier Difference and Quotient methods - see chapter 3].

3 CHAPTER THREE : SPECTRAL DATA REDUCTION

3.1 INTRODUCTION

3.1.1 Motivation

The agreement between velocity dispersions measured by different authors is improving [see de Vaucouleurs & Olson (1982), Capaccioli (1979)]. However, there is further scope for improvement and some ambiguities in the methods currently used might be resolved by a detailed re-evaluation.

The purpose of the account given in this chapter is, therefore, to describe the methods currently used to determine redshifts and velocity dispersions from the absorption line spectra of elliptical galaxies; to suggest why improvements might be possible and, in conclusion, to propose a new method which is to be adopted in the analysis of the data used in this study.

A brief history of attempts to measure velocity dispersions is given in section 3.2 and is followed in sections 3.3-3.6 by a detailed derivation of the "objective" statistical techniques found to work best for estimation of velocity dispersions and radial velocities. An extensive series of tests is described throughout the text and particularly in section 3.7.

Having gone through all the procedures described in chapter 2 the spectra are now suitable for analysis. They consist of some number of channels [1024 or 2048, in this study], with photon counts in each equally sized wavelength channel; sky background and continuum trends have been removed.

3.1.2 Logging

There is one final transformation to be applied to the data before analysis. The spectra must be re-binned to a scale for which channels have equal size in $\ln(\lambda)$.

A definition of redshift is:

$$z = \frac{\lambda_{observed} - \lambda_{rest}}{\lambda_{rest}} = \frac{\Delta\lambda}{\lambda} \qquad 3.1.1$$

The problem with using wavelength measures of redshift is illustrated by the following example. Suppose the observed wavelength of a redshifted line, at λ_1, is measured and compared with the corresponding rest wavelength to give $\Delta\lambda_1$. The wavelength of a second line, at λ_2, is then measured to give $\Delta\lambda_2$. If λ_1 is different from λ_2, then $\Delta\lambda_1$ is different from $\Delta\lambda_2$. The techniques described later in this chapter compare <u>many</u> lines in an "object" spectrum with corresponding lines in a standard "template" spectrum. This comparison is to be done simultaneously, and it is therefore necessary to define a scale for which differences in line positions do <u>not</u> depend on rest wavelength.

Clearly,

$$\ln(1+z) = \ln(\lambda_{observed}) - \ln(\lambda_{rest}) \qquad 3.1.2$$

So, if the spectra are re-binned into channels of equal size in $\ln(\lambda)$, then the differences in line positions are independent of rest wavelength.

Define λ_{start} as the wavelength of the start of the first channel, and λ_{end} as the end of the last channel. If this spectrum is re-binned into N new logarithmic channels, then the size of these new channels will be [in units of $\ln(\lambda)$]:

$$\Delta = \frac{\ln(\lambda_{end}) - \ln(\lambda_{start})}{N} \qquad 3.1.3$$

If the difference in the positions of corresponding lines in the object and template spectra is δ of these logged channels, each of size Δ, then the redshift, z [and the representative velocity cz] is calculated from:

$$cz = c \cdot \left[e^{\delta\Delta} - 1 \right] \qquad 3.1.4$$

If the template and object spectra do not start at the same wavelength, and there is a difference of δ channels between corresponding line positions, then:

$$c\,z \;=\; c \cdot \left[\frac{\lambda_{start}^{object}}{\lambda_{start}^{template}}\, e^{\delta\Delta} \;-\; 1 \right] \qquad 3.1.5$$

Care should be taken always to use the full form of 3.1.5 to find redshifts. Note that cz is only approximated by $c\delta\Delta$ [ie c.ln(1+z)] for $z \ll 1$.

The redshift is related to the relativistic Doppler velocity by the relation:

$$V_{rel.} \;=\; c \cdot \left[\frac{(1+z)^2 \;-\; 1}{(1+z)^2 \;+\; 1} \right] \qquad 3.1.6$$

3.2 HISTORICAL METHODS

3.2.1 "Subjective"

The history of attempts to estimate velocity dispersions from the absorption-line spectra of elliptical galaxies, lenticulars and spiral bulges stretches over some three decades. Work in the 1950's and early 1960's established the basis of the methods that are now used. Activity declined as observations rapidly came up against practical limits set by the detectors being used. However, progress was made in the understanding of the stellar dynamics which motivated the studies [Michie (1963), King (1962, 1966), Lynden-Bell (1967)]. Eventually, the improved sensitivity and linearity of photon-counting detectors allowed the continuous development seen in the last ten years.

A general, if invidious, categorisation may be made of the methods by which velocity dispersions are estimated: either as "subjective" or as "objective". Preference now inclines toward the objective methods, though there remain valid criticisms even of these.

The usual method for finding subjective velocity dispersions consists of some, or all, of the following stages: a star [template] and a galaxy [object] are observed and their spectra converted to a linear scale of intensity; the template spectrum is broadened; the object spectrum is [blue-] shifted to the rest frame of the template; the spectra are filtered and, finally, the template spectrum is

compared with the object spectrum. The aim is to find the broadening for which the broadened template spectrum best matches the object spectrum, according to a set of criteria fixed by each investigator.

Minkowski (1962) reported on observations which had been made some time earlier. An analogue technique was used to broaden photographically recorded star spectrograms. These spectra were broadened either by using a mask with a Gaussian transmission profile [placed over the spectrograph slit], or by efforts subsequent to observation in the dark-room. Later work used numerical computation to broaden the template. This was possible after conversion of the spectrum to an appropriate scale of intensity [Burbidge, Burbidge & Fish (196la,b,c), Richstone & Sargent (1972)], or by using observations from electronic detectors with good intrinsic linearity [Morton & co-workers (1972,1973,1976), Illingworth (1976), Williams (1977)]. Brault & White (1971) introduced optical astronomers to the techniques of power spectrum analysis, and described the use of an optimal filter for Fourier filtering and restoration of data. Filters of this type can significantly improve the comparison of object and template spectra.

The method of visual comparison has problems: the implied relative weights assigned to individual spectral features in the fitting procedure are not derived by any formal procedure, and are therefore unlikely to be optimal. Morton & Elmergreen (1976) give a thorough account of the problems. In their famous paper, Faber & Jackson (1976) preferred visual comparison to a Fourier method developed by

Illingworth & Freeman (1974). However, they do mention that the dependence of line depth on metallicity may be particularly important in affecting velocity dispersion estimates from visual fitting - possibly biassing previous work. Faber & Jackson therefore chose features whose strengths do not change greatly with metallicity or spectral type.

Improvements made by Morton et al (1977) and Illingworth (1976) included the addition of continuum light to the template to increase the wavelength range over which the fit was acceptable. Also suggested was the use of a composite template to match the composite nature of the objects. Williams (1977) took the idea of a composite template further, by using spectro-photometry of elliptical galaxies to determine a population model, which could then be used to construct a template. A similar technique was used by Pritchet (1978) with a Fourier method. However, such composite templates suffer from the defect of all stellar templates: it is not possible to observe Galactic stars with metallicities as high as stars typical of giant elliptical galaxies. The advantage of extra sophistication in template construction is therefore somewhat mitigated.

Not all workers used fitting by eye to find the best estimate of velocity dispersion: Richstone & Sargent (1972), for example, used least-squares matching of spectra and their observations of M32 showed agreement with visual fitting. Morton & Elmergreen suggested that, in general, the least-squares fitting gives too much weight to line depths, which

might not match because of differences of spectral type or metallicity between the object and template. In contrast, visual fitting emphasises the matching of line widths.

The agreement between different authors was not good. Even excluding Minkowski (1962), and some Faber & Jackson (1976) data, the estimates show a scatter of at least 50 kms^{-1}. A number of alternative suggestions for calculating velocity dispersions were made, based on the use of the Fourier Transform, through which a measure of agreement in estimation has been achieved.

3.2.2 "Objective"

There are a number of reasons for preferring an objective method. In particular, the methods use the whole of the spectral region observed, rather than just a few strong lines. They therefore include a large number of weaker lines in the comparison - lines which would be unusable in the direct visual comparison method. Simple filtering of the unwanted low and high frequency components of the spectrum is also possible, without tackling the problem of optimal restoration. The objective methods perform excellently in such tests as have been devised, and comparisons have been made between the subjective and objective methods by a number of authors [Faber & Jackson (1976), Illingworth (1976), Davies (1981)].

The Fourier methods rely for their simplicity on the Convolution and Shift Theorems for Fourier Transforms. It is assumed that the object spectrum may be represented as the result of convolving the template spectrum with a distribution of velocities thought to represent that of the stars in an elliptical galaxy - generally assumed to be Maxwellian [Lynden-Bell (1967)]. There is also a shift between the broadened template and the galaxy. Some methods make an additional assumption about the form of the instrumental profile, usually Gaussian.

The Convolution Theorem states that the Fourier Transform [FT] of the convolution of two functions [ie the object spectrum], is given by the product of the FT's of each of these two functions [ie the template spectrum and the broadening function]. The Shift Theorem then accounts for the relative shift between the object and template as a simple phase factor. Allowances must be made for the discreteness and finite length of data, but, nevertheless, these theorems allow a tremendous simplification. Particularly helpful is the fact that the FT of a Gaussian function is itself a Gaussian - a formal treatment then becomes rather simple.

Illingworth & Freeman (1974) produced the first widely used Fourier technique: the power spectrum of a broadened template is matched with the power spectrum of an object to produce an estimate of the velocity dispersion. Because a power spectrum is calculated, all phase information is lost, and the velocity must be found by other means. Illingworth applied his method with great success to a number of

narrow-lined globular clusters [Illingworth & Freeman (1974), Illingworth (1976)]. The method was also applied successfully by Pritchet (1978). Faber & Jackson found that, for broad-lined elliptical galaxies, the method was overly sensitive to noise, which illustrates a problem inherent in the use of power spectra: the noise power will generally fluctuate about some varying non-zero value. The FT itself may have a varying noise amplitude with wavenumber, but the mean noise amplitude at any particular wavenumber should be zero. The FT is therefore likely to produce a better estimation technique.

The Fourier Quotient method was introduced by Simkin (1974) and avoids the use of power spectra. The method was brought to the state of popularity it now enjoys by Sargent, Schechter, Boksenberg & Shortridge (1977) [SSBS]. The object FT is divided by the template FT to give a complex function. Ideally, this quotient is the complex conjugate of the broadening function FT, multiplied by a "line-strength" scale parameter. The overall phase as a function of wavenumber is determined by the relative shift. Discussion of this successful technique is held over until section 3.5. A comparable method, using the difference between the FT's of a broadened template and an object, was introduced by Dressler (1979). A Fourier Difference method is suggested in section 3.6 as the best overall technique.

Cross-correlation has been widely used to determine redshifts [Griffen (1967), Simkin (1974), Da Costa et al (1977)], and was adapted by Tonry & Davis (1979) to provide a direct method of estimating both redshifts and velocity dispersions. The method differs from the Fourier Quotient, in that the estimation of the parameters is done in data space rather than Fourier space. However, Fourier filters are used and application of the Convolution Theorem speeds up an otherwise very tedious calculation [both computationally and formally]. The method involves the cross-correlation of the object with the template spectrum. The position of the highest peak in the cross-correlation function [CCF] is determined by the relative shift between the object and the template, and the width of the peak is related to the velocity dispersion. This method has the great advantage that it is very direct, and has a scheme for calculating errors which appears to work. Cross-correlation will be discussed in section 3.4.

Velocity dispersion estimation using templates involves some problems of principle: galaxies are composite objects and the stars which comprise them are of many spectral types; in addition, the stars may be of different metallicity to <u>any</u> stars that can be found nearby in our Galaxy [Faber (1977)]. Attempts can be made to minimise such systematic effects [Morton & Elmergreen (1976), Faber & Jackson (1976)] and some interesting comments on the relative merits of observing at blue or visual wavelengths, as compared to near infra-red wavelengths, have been made by Pritchet (1978) and Dressler (1984a).

3.3 FORMALISM

3.3.1 Spectra

The derivations which follow in sections 3.4, 3.5 and 3.6 require the definition of a notation with which to discuss the quantitative methods. That is the purpose of this section.

A set of observed spectra will have varying line amplitudes, because of differences in exposure time and apparent magnitude. The object spectrum o(n) and the template spectrum t(n) must therefore be normalised [by a factor: f_o, f_t]. The most obvious value for the normalisation factor to take is that of the continuum of the spectrum [ie continuum division]. As discussed in chapter 2, continuum subtraction is preferred in this work, so the factors are taken to be the mean count per channel after sky subtraction [but before continuum removal].

Absorption line-strengths differ between stars and galaxies: the mean count per channel will not, therefore, be an equal fraction of the continuum level in stars and galaxies. A correction to the normalisation may be made for this effect, as in Davies (1979). However, the spectra observed for this work are not used for a detailed line-strength analysis and the correction is ignored.

As an idealisation, suppose that the template spectrum may be represented as a number of Gaussian-shaped lines centred at the positions of the absorption lines [n_{line}: where n is the channel number; n=1,N]. If the widths in logarithmic wavelength channels are τ and the fractional line amplitudes are γ_l^t [different for each line l; l=1,L] then:

$$t(n) = \sum_{l=1}^{L} \gamma_l^t \, e^{-\frac{(n-n_l)^2}{2\tau^2}} \qquad 3.3.1$$

The assumption is made that the template line widths are constant. However, the widths of template lines are a combination of the star intrinsic line widths and the instrumental width. If the instrumental width is not itself dependent on wavelength, then τ is - through the logarithmic transformation. The template line widths cannot, therefore, be exactly constant. This is particularly true if the spectra have extensive wavelength coverage. However, if both object and template are equally affected then any error tends to cancel.

It should be emphasised that the Fourier Quotient and Difference methods are mostly free from the obvious criticisms of this highly idealised representation. They only assume that the template represents the prototype of the stars in the object, no matter what the instrumental profile. The cross-correlation method is not quite so robust.

The object spectrum is formed by convolution of the template spectrum with a Maxwellian broadening function:

$$o(n) = t(n) * b(n) \qquad 3.3.2$$

Here,

$$b(n) = \frac{1}{\sqrt{2\pi}\,\sigma} e^{-\frac{(n+\delta)^2}{2\sigma^2}} \qquad 3.3.3$$

where δ is the relative shift between the template and the object, [measured in channels and positive for a red-shift]. The velocity dispersion is σ [also in channels]. The normalisation of b(n) ensures conservation of counts.

By application of the Convolution Theorem:

$$O(k) = T(k) \cdot B^*(k) \qquad 3.3.4$$

where the Fourier Transform, F(k), [k=0,N-1] of a function, f(j), [j=1,N] is defined:

$$F(k) = \sum_{j=1}^{N} f(j)\, e^{-\frac{2\pi i j k}{N}}$$

$$f(j) = \frac{1}{N} \sum_{k=0}^{N-1} F(k)\, e^{\frac{2\pi i j k}{N}} \qquad 3.3.5$$

The "*" in equation 3.3.4 indicates complex conjugation.

The form of the idealised object spectrum may now be calculated, in order to introduce the "line-strength parameter", and to see where the ideals of equations 3.3.1 and 3.3.2 may depart from reality.

The FT's of t(n) and b(n) are:

$$T(k) = \sqrt{2\pi}\,\tau\, e^{-\frac{(2\pi k)^2\tau^2}{2N^2}} \sum_{\ell=1}^{L} \gamma_\ell^t\, e^{-\frac{2\pi i k n_\ell}{N}} \qquad 3.3.6$$

$$B^*(k) = e^{-\frac{(2\pi k)^2\sigma^2}{2N^2}}\, e^{-\frac{2\pi i k\delta}{N}} \qquad 3.3.7$$

Using 3.3.4 with 3.3.6 and 3.3.7 we find:

$$O(k) = \sqrt{2\pi}\,\tau\, e^{-\frac{(2\pi k)^2(\tau^2+\sigma^2)}{2N^2}} \sum_{\ell=1}^{L} \gamma_\ell^t\, e^{-\frac{2\pi i k(n_\ell+\delta)}{N}} \qquad 3.3.8$$

The object spectrum is therefore:

$$o(n) = \frac{\tau}{\sqrt{\tau^2+\sigma^2}} \sum_{\ell=1}^{L} \gamma_\ell^t\, e^{-\frac{[n-(n_\ell+\delta)]^2}{2(\tau^2+\sigma^2)}} \qquad 3.3.9$$

In practice the object will differ from the template in "line-strength" - which is to say that γ_ℓ^o is not equal to γ_ℓ^t. To account for this, a line-strength parameter γ_ℓ is introduced for each line:

$$o(n) = \frac{\tau}{\sqrt{\tau^2 + \sigma^2}} \sum_{\ell=1}^{L} \gamma_\ell \gamma_\ell^t \, e^{-\frac{[n - (n_\ell + \delta)]^2}{2(\tau^2+\sigma^2)}} \qquad 3.3.10$$

The line-strength parameter recovered by Fourier methods is a complicated average over the γ_ℓ's, but for simplicity the γ_ℓ in 3.3.10 may be replaced by a constant γ and taken outside the summation over lines.

Real galaxy spectra differ from broadened star spectra for two important reasons. Firstly, the galaxy may have a different effective spectral type from any template and, secondly, giant elliptical galaxies have higher metallicities than the K-giant stars used as the best matching templates. These problems are collectively refered to as "mis-match" and table 3.7.1 illustrates how line-strengths differ between templates.

3.3.2 Sampled Finite Functions

The object and template spectra are functions defined at a finite number of equally spaced points. This has consequences regarding the faithfulness of the discrete FT [DFT] as a representation of the "true" continuous FT. Three effects must be

considered: aliasing, leakage and circularity [see the excellent account in Brault & White (1971)].

Aliasing may be considered as follows. Suppose the smallest important features of a function have a similar size [D]. Clearly, for a realistic representation of the function, samples [of size d] must be taken as frequently as possible [ie D/d>>1]. Re-phrased in Fourier terms this condition requires that the amplitude of the FT of the function decreases to [approximately] zero at the Nyquist wavenumber [which is half the sampling rate]. If this condition is not fulfilled then, because the DFT is symmetric about the Nyquist wavenumber, an overlap of "replicas" of the sampled true FT will occur. These replicas are called aliases, and the solution to the problem is to "oversample". For 2N samples the Nyquist Wavenumber is N-1, on a wavenumber scale 0,2N-1.

The second problem is leakage. The wavelength range of the data recorded is necessarily finite and the data may be thought of as being the result of the multiplication of an infinite length of data by a finite length box window function. Such a procedure is equivalent to the convolution of the infinite length FT by the box function FT. The FT of a box function is a sinc function, which has significant amplitude in side-lobes: the result of the operation is therefore to smear the continuous FT. The value of the true FT at k=0 is particularly important, because it may have a very different amplitude from the rest of the FT. To see why this is so, refer to 3.3.5, from which it is clear that F(0) is simply the sum of the function, f(j) [over all j].

To reduce the smearing, two procedures are recommended before proceeding with the analysis: firstly, the data [f(j)] should have the mean subtracted from all channels so there will be no peak at k=0 in the FT; secondly, some window function must be applied to the data with better side-lobe behaviour than the box function FT [ie a smoother function than the box window]. The smoothing function used in this study is the "cosine-bell", defined as follows:

$$w(j) = \left[1 - \cos\left[\frac{\pi\,(n_{bell} + 1 - j)}{2\,n_{bell}} \right] \right] \qquad j = 1, n_{bell} \qquad 3.3.11$$

$$w(j) = 1 \qquad j = n_{bell}, N - n_{bell}$$

$$w(j) = \left[1 - \cos\left[\frac{\pi\,(N - j)}{2\,n_{bell}} \right] \right] \qquad j = N - n_{bell}, N$$

Lastly, there is the problem of "circularity" or "wrap-around". Because the spectra are represented as periodic functions, care must be taken when applying the results of the Convolution Theorem. The two ends of the spectra being analysed are unlikely to match very well and the cosine-bell is used to taper off the ends of the spectra, reducing this spurious contribution to the CCF.

When transforming the spectra to a logarithmic scale a useful procedure is to match the spectral regions of the template and object. In their data reduction, Da Costa et al (1977) first determined an initial redshift and then iterated the spectral region matched until the relative shift of object and template was close to zero - this then ensured that no unmatched data could bias the comparison of object and template. In addition, this procedure has been adopted as standard in this work because the Fourier methods require accurate matching for computational reasons: the χ^2 minimisation algorithms can have difficulty finding global minima if started with very uncertain initial parameter estimates - especially velocity.

3.4 CROSS-CORRELATION

3.4.1 The Function

For an object spectrum o(j) and a template spectrum t(j) the CCF is defined:

$$c(d) = \sum_{j=1}^{N} \frac{o(j)\ t(j-d)}{N\ \sigma_o\ \sigma_t} \qquad d = 0, N-1 \qquad 3.4.1$$

where,

$$\sigma_o^2 = \frac{1}{N} \sum_{j=1}^{N} [o(j)]^2 \qquad 3.4.2$$

$$\sigma_t^2 = \frac{1}{N} \sum_{j=1}^{N} [t(j)]^2 \qquad 3.4.3$$

and "d" is the lag between object and template. The normalisation of the CCF ensures that c(0)=1 for auto-correlation [ie o(j)=t(j); j=1,N]. From the Convolution Theorem:

$$C(k) = \frac{O(k)\ .\ T^*(k)}{N\ \sigma_o\ \sigma_t} \qquad 3.4.4$$

and from 3.3.6 and 3.3.8:

$$C(k) = \beta . \, 2\pi\tau^2 . \, e^{-\frac{(2\pi k)^2 (2\tau^2 + \sigma^2)}{2N^2}} . \left[\sum_{\ell=1}^{L} Y_\ell Y_\ell^t \, e^{-\frac{2\pi i k (n_\ell + \delta)}{N}}\right]\left[\sum_{\ell'=1}^{L} Y_{\ell'}^t \, e^{-\frac{2\pi i k n_{\ell'}}{N}}\right] \qquad 3.4.5$$

$$= \beta . \, 2\pi\tau^2 . \, e^{-\frac{(2\pi k)^2 (2\tau^2 + \sigma^2)}{2N^2}} . \left[e^{-\frac{2\pi i k \delta}{N}}\right]\left[\sum_{\ell=1}^{L} (Y_\ell^t)^2 Y_\ell + O(1/L)\right] \qquad 3.4.6$$

where $\beta = 1/(N . \sigma_o \, \sigma_t)$ and L is the number of lines in a spectrum.

When transformed to data space, the term in square brackets in 3.4.6 will give a large peak at δ, corresponding to the best match of object and template. Numerous smaller peaks are symmetrically distributed about δ [ie the overall phase of the term is $-2\pi k\delta/N$]. These subsidiary peaks are about 1/L of the size of the large peak, and are caused by matching of lines with different rest wavelengths. Figure 3.4.1 shows the CCF of a galaxy object with a star template. Figure 3.4.2 shows a galaxy auto-correlation function, and the smaller peaks are clearly symmetric about zero lag. The highest peak is also correctly normalised to unity.

The normalisation constant, β, must now be calculated so that the [idealised] form of the main peak may be derived.

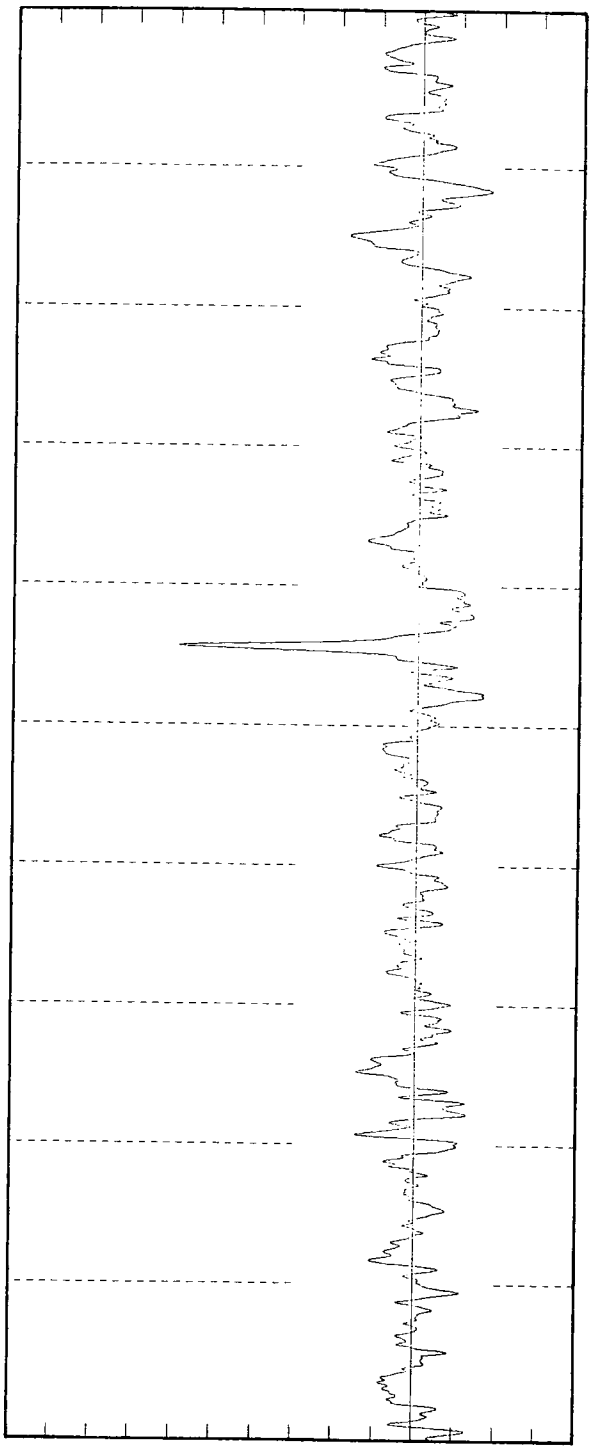

Galaxy-Star Cross-correlation Function

Figure 3.4.1

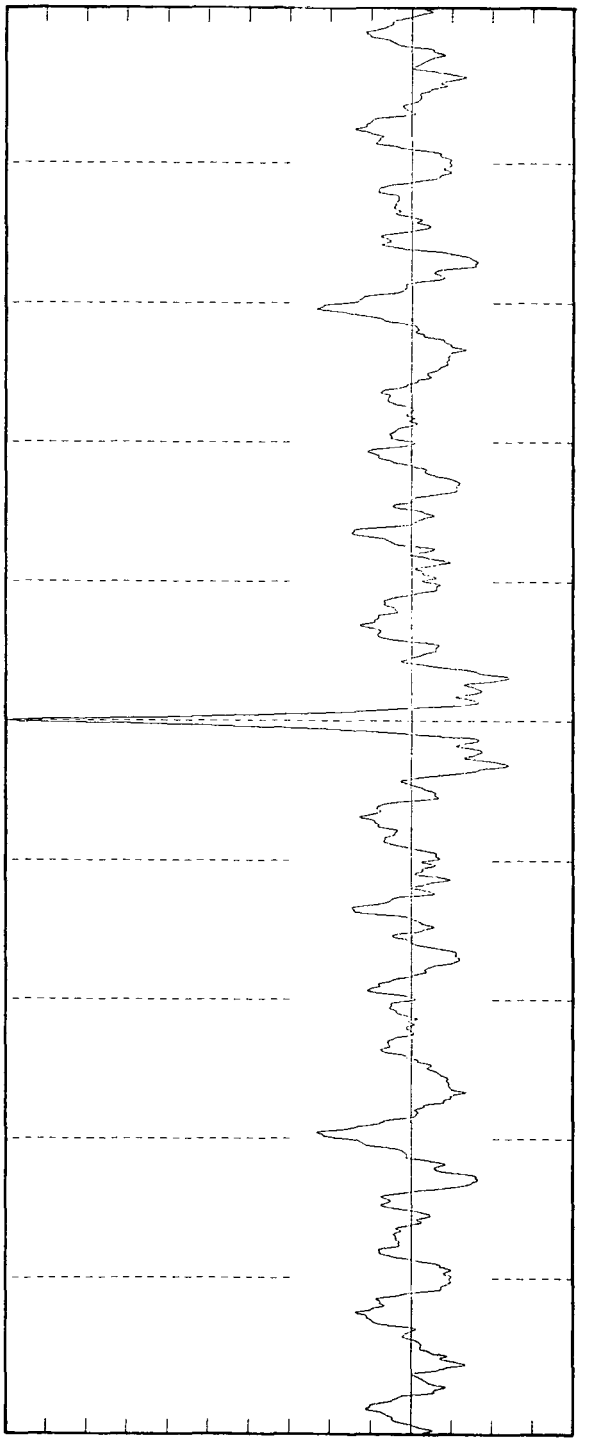

Figure 3.4.2 Galaxy-Galaxy Auto-correlation Function

Suppose we have a spectrum:

$$f(j) = \alpha \sum_{\ell=1}^{L} \gamma_\ell \gamma_\ell^t \, e^{-\frac{(j-n_\ell)^2}{2w^2}} \qquad 3.4.7$$

then,

$$\sigma_f^2 = \frac{1}{N} \sum_{j=1}^{N} [f(j)]^2$$

$$= \frac{1}{N} \alpha^2 \sum_{j=1}^{N} \left[\sum_{\ell=1}^{L} \gamma_\ell \gamma_\ell^t \, e^{-\frac{(j-n_\ell)^2}{2w^2}} \right]$$

If line overlaps are neglected and the summation over j is approximated by an integral, then:

$$\sigma_f^2 = \frac{\alpha^2}{N} \sqrt{\pi}\, w \sum_{\ell=1}^{L} [\gamma_\ell \gamma_\ell^t]^2 \qquad 3.4.8$$

Using the definitions of the template and object spectra in equations 3.3.1 and 3.3.10 with 3.4.8, we find:

$$\frac{1}{\beta} = \sqrt{2}\tau \sqrt{\frac{\tau}{\sqrt{\tau^2+\sigma^2}} \sum_{\ell=1}^{L} (\gamma_\ell \gamma_\ell^t)^2 \sum_{\ell'=1}^{L} (\gamma_{\ell'}^t)^2} \qquad 3.4.9$$

If the FT of the CCF, C(k), is transformed back to data space and ε is defined as the deviation from the position of the main peak [δ] then, substituting 3.4.9 we find:

$$c(\varepsilon) = \sqrt{\frac{2\tau\sqrt{\tau^2+\sigma^2}}{2\tau^2+\sigma^2}}\; e^{-\frac{\varepsilon^2}{2(2\tau^2+\sigma^2)}} \cdot \left[\frac{\sum_{\ell=1}^{L}(\gamma_\ell^t)^2\gamma_\ell}{\sqrt{\sum_{\ell=1}^{L}(\gamma_\ell\gamma_\ell^t)^2\;\sum_{\ell=1}^{L}(\gamma_\ell^t)^2}}\right] \qquad 3.4.10$$

The expression has a number of features which suggest it has a form consistent with the assumptions made. Firstly, if γ_ℓ is a constant for all lines, the term in square brackets becomes equal to unity. If σ is then put to zero, c(0) is equal to unity, as required for auto-correlation.

Equation 3.4.10 can be written:

$$c(\varepsilon) = \frac{\sqrt{2}\,\tau}{\sqrt{2\tau^2+\sigma^2}} \cdot \frac{\sigma_t}{\sigma_o} \cdot e^{-\frac{\varepsilon^2}{2(2\tau^2+\sigma^2)}} \cdot \frac{\sum_{\ell=1}^{L}(\gamma_\ell^t)^2\gamma_\ell}{\sum_{\ell=1}^{L}(\gamma_\ell^t)^2} \qquad 3.4.11$$

or, if γ_ℓ is a constant for all lines:

$$c(\varepsilon) = \frac{\sqrt{2}\,\tau\,\gamma}{\sqrt{2\tau^2+\sigma^2}} \cdot \frac{\sigma_t}{\sigma_o} \cdot e^{-\frac{\varepsilon^2}{2(2\tau^2+\sigma^2)}} \qquad 3.4.12$$

The width of the cross-correlation peak is $(2\tau^2+\sigma^2)$ and, if τ is known, the velocity dispersion may be found. Equation 3.4.10 indicates that the height of the peak is fixed by the ratio of the velocity dispersion σ to the template width τ [with a complicated dependence on the line-strength]. The height does not, however, provide a good method of determining velocity dispersion, as σ_o includes the variance of any noise present. For poor S/N spectra, σ_o will be greatly increased over the ideal estimate of 3.4.8. As S/N decreases, the height of the main peak will be reduced by σ_o until eventually it disappears among the secondary peaks.

3.4.2 Filters

Figures 3.4.1 and 3.4.2 show clearly that a CCF calculated from real spectra deviates significantly from the ideal of equation 3.4.6. There are a number of problems associated with the assumptions used to derive the shape of the peak: lines are not Gaussian in profile and are often blended, and spectra have features not attributable to lines - filtering is required to remove such unwanted features.

By a suitable choice of filter, residual continuum trends may be removed, and noise suppressed. The problem of optimal restoration has been dealt with by Brault & White (1971) and a brief description is given here to illustrate the problems involved in filtering.

Suppose there is a observed spectrum, s(n), whose FT is S(k). This spectrum, s(n), may be represented as the convolution of a function, t(n), with an apparatus function, a(n).

$$S(k) = T(k) \,.\, A(k) \qquad 3.4.13$$

In the absence of noise, a restoration may be attempted as follows:

$$R(k) = S(k)/A(k) = T(k) \qquad 3.4.14$$

Transformation of R(k) gives r(n), the restored spectrum. If there is noise, N(k), associated with the detection procedure, then:

$$S(k) = T(k).A(k) + N(k) \qquad 3.4.15$$

and the attempt at restoration would be:

$$R(k) = S(k)/A(k) = T(k) + N(k)/A(k) \qquad 3.4.16$$

If A(k) is small at high wavenumbers, any high wavenumber noise will be amplified by the division in 3.4.16 and the restoration will possibly fail.

Brault & White describe how to find a transfer function $\varphi(k)$ so that the restoration most nearly equals T(k).

$$R(k) = [S(k)/A(k)] \cdot \varphi(k)$$

such that both $\sum[R(k)-T(k)]^2$ and $\sum[r(n)-t(n)]^2$ are a minimum. The problem is solved using variational calculus to give the appropriate function:

$$\varphi(k) = \frac{|T(k).A(k)|^2}{|T(k).A(k)|^2 + |N(k)|^2} \qquad 3.4.17$$

$$= \frac{P_{signal}}{P_{signal} + P_{noise}}$$

where P_{signal} is the signal power and P_{noise} is the noise power. This filter is designed to deal with high wavenumber noise and approximations to it are widely used in the literature.

Experience indicates that such sophisticated filters are not needed. However, an approximation to 3.4.17 is adequate, if filtering of low wavenumbers is also included.

The transfer functions used for cross-correlation in this study are of the form:

$$\begin{aligned} \varphi(k) &= 0 && k<k_1, k>k_4 \\ \varphi(k) &= (k-k_1)/(k_2-k_1) && k_1 \leq k \leq k_2 \\ \varphi(k) &= 1.0 && k_2 \leq k \leq k_3 \\ \varphi(k) &= (k_4-k)/(k_4-k_3) && k_3 \leq k \leq k_4 \end{aligned} \qquad 3.4.18$$

The filter corresponding to this transfer function [ie the inverse FT of the transfer function] is shown in figure 3.4.3. The characteristic side-lobes of this filter produce the negative CCF values near the peak. Da Costa et al (1977) use a rather smoother "bi-Gaussian" transfer function, but tests indicate that the exact form of the filter is not crucial: redshifts are almost entirely unaffected, and a calibration procedure removes the effect of filtering from velocity dispersions.

As just mentioned, a calibration procedure is required to extract the true dispersion from a measured cross-correlation peak width. There are two principal reasons for this: the template line width, τ, must be calibrated, and the effects of filtering [cosine-bell, linear filter, zero-mean] must be removed. The relationship between the true widths [σ] in terms of measured widths [w] is generally referred to as the "σ-w relation". Two calibration methods were examined.

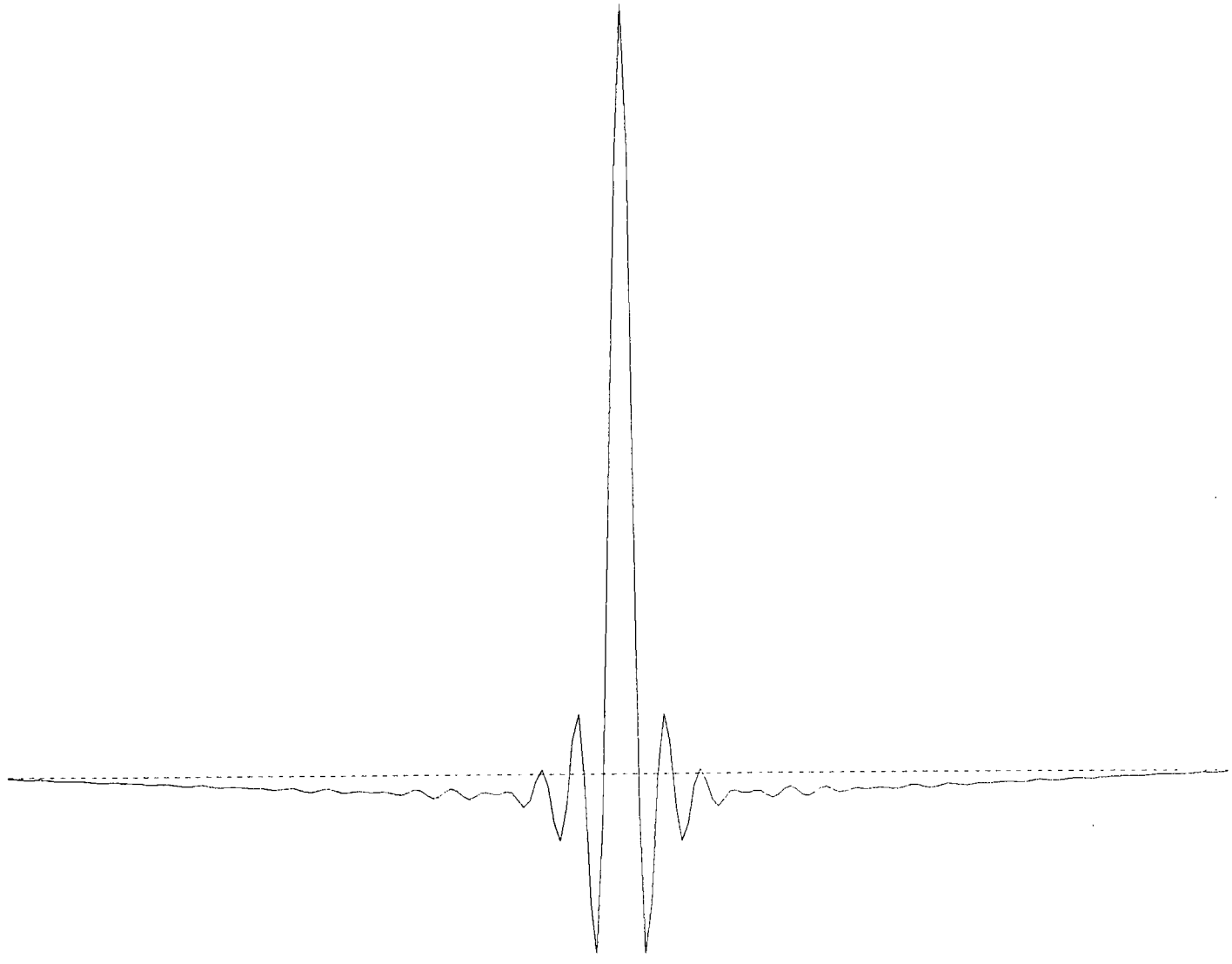

Figure 3.4.3 Filter derived from linear transfer function

The first method simulated Gaussian CCF peaks with varying known true widths [σ_{in}, or σ]. These peaks were then filtered and fit by the cross-correlation program, to produce a measured width [σ_{out}, or w]. A polynomial fit to true width against measured width then provides the first part of the calibration - removing the effects of the particular fitting procedure used by the cross-correlation program [in general, a parabolic fit was used]. However, to calculate a velocity dispersion for a galaxy τ must also be determined. To do this, a number of templates were broadened to have dispersions spanning the range expected from the galaxies under study. τ was then iteratively adjusted until the calculated dispersions matched the known template broadenings.

The second method proved less arduous and more accurate - and was adopted for most of the cross-correlation analysis to be described in subsequent chapters. The technique combines the two parts of the previous method into one operation, so that τ is never explicitly determined. A template was broadened by varying known amounts [σ] to cover the range of the calibration needed. The cross-correlation program, with no built-in peak σ-w relation, was then used to determine the measured CCF peak width [w]. A cubic polynomial for σ=f(w) is then adequate to represent the overall σ-w relation for the filters and instrumental set-ups used in this study. Two σ-w curves from the second calibration method are shown in figure 3.4.4, representing different filters and instrumental set-ups.

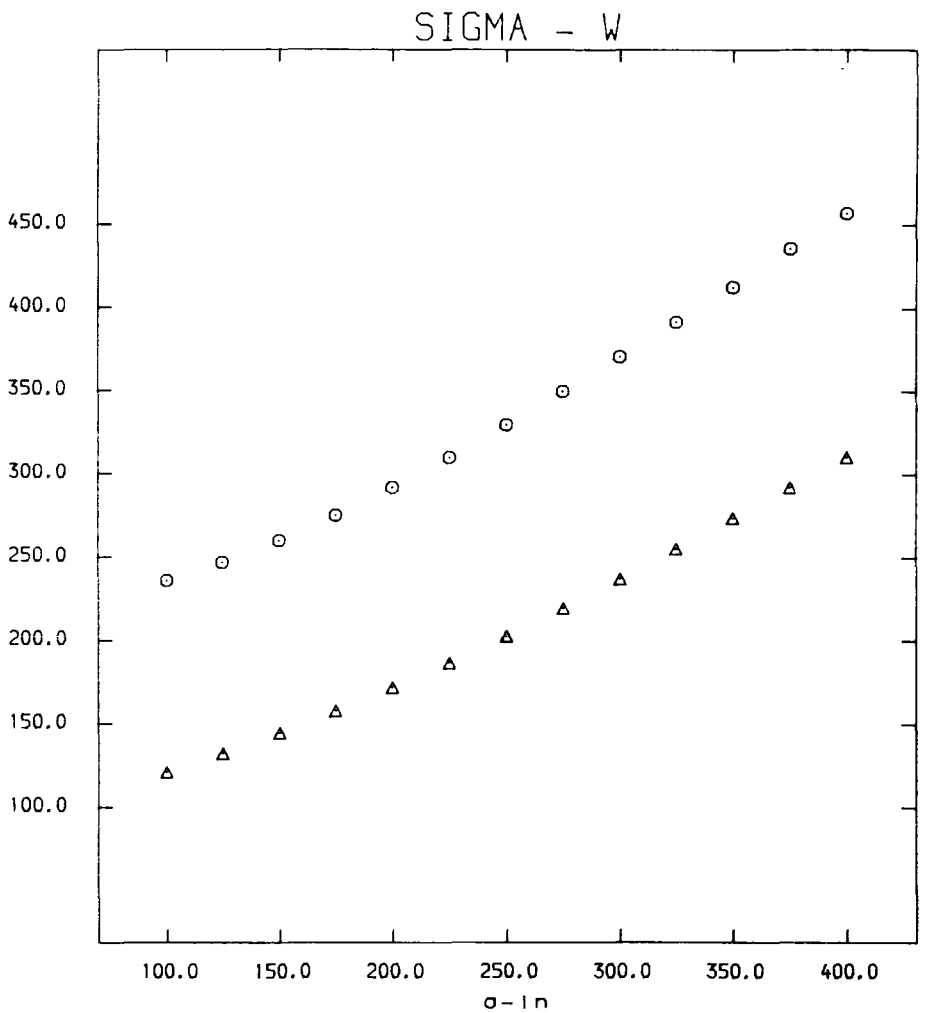

Figure 3.4.4 σ-w Relation

SAAO (Chapter 4) : △

AAT (Chapter 6) : ⊙

3.4.3 Error Estimation

Tonry & Davis (1979) proposed a procedure for finding the error in the position and width of the cross-correlation peak. They pointed out that, since the CCF should be symmetric about the main peak, the anti-symmetric component of the CCF must be the result of noise and mis-match, and might be used to estimate errors.

If the variance of the anti-symmetric part is:

$$\sigma_a^2 = \frac{1}{N} \sum_{j=1}^{N} [c(\delta+j) + c(\delta-j)]^2 \qquad 3.4.19$$

then the "noise" will have half this variance, $\sigma_n^2 = \frac{1}{2}\sigma_a^2$. A statistic may then be defined to measure how far the peak is above the "noise":

$$R = \frac{h}{\sqrt{2}\ \sigma_n} \qquad 3.4.20$$

where "h" is the height of the peak. The error in the position of the peak is then:

$$\varepsilon = \frac{N}{8.B} \frac{1}{1+R} \qquad 3.4.21$$

Tonry & Davis suggest the value of B is taken to be the wavenumber at which the FT of the CCF falls to half its maximum value. If "w" is the width of the measured peak, then:

$$\varepsilon = \frac{\pi}{4\sqrt{\ln 4}} \frac{w}{1+R} = \frac{2}{3} \frac{w}{1+R} \text{ channels} \qquad 3.4.22$$

The error depends on the width of the peak because the noise peaks are assumed to have a similar power spectrum to the CCF itself. Tonry & Davis were able to test this formula against independent estimates of velocity [21 cm] and found 3.4.21 to be a good representation of the errors. In practice, the factor N/8B is adjusted to fit the observed error distribution, if this is possible.

A similar expression is found for the error in the <u>width</u> of the peak. The error in the measured width must be propagated through the σ-w relation to obtain a calibrated error:

$$\Delta w = \varepsilon \qquad 3.4.23$$

$$\Delta\mu = \frac{d\mu}{dw} \cdot \Delta w \qquad 3.4.24$$

where Δw is the error in the measured peak width, $\Delta\mu$ is the error in the calibrated peak width. $d\mu/dw$ is the gradient of the σ-w relation.

The error in velocity dispersion depends upon the error both in the width of the peak and in the value of τ. If μ is the width of the galaxy-star peak and τ is the star width, then:

$$\mu^2 = 2\tau^2 + \sigma^2 \qquad 3.4.25$$

$$(\Delta\sigma)^2 = 2\sqrt{\mu^2\Delta\mu^2 + 4\tau^2\Delta\tau^2 + \sigma^4} - 2\sigma^2 \qquad 3.4.26$$

Tonry & Davis (1981) make some further comments about errors in velocity dispersions.

By comparison of their large set of data with external sources Tonry & Davis were able to adjust their error calculation procedure to reproduce the observed distribution of derived parameter values; this is not possible in this study, which involves only a few objects. The uncertainty in estimating errors is such that 3.4.26 may be simplified by assuming $\Delta\tau=0$:

$$\Delta\sigma = \frac{\mu}{\sigma}\Delta\mu \qquad 3.4.27$$

The filters used in this study produced almost linear σ-w relations. The slopes were 1.2 [AAT] and 1.4 [SAAO], giving μ/σ of 1.2 [AAT] and 1.0 [SAAO]. We may therefore write:

$$\Delta\sigma = \left[\frac{\mu}{\sigma}\frac{d\mu}{dw}\right]\frac{2}{3}\frac{w}{1+R} = \frac{2}{3}\cdot\frac{w^{rep}}{1+R}\cdot 1.4 \qquad 3.4.28$$

For consistency, a "representative" value of w was chosen, w^{rep} - equivalent to choosing a "B" in 3.4.21. This value was then used for all galaxy data from the same observing run. In order to find w^{rep} and to check the form of 3.4.28, noise tests were used. Mean-subtracted Poisson noise was added to high quality spectra to degrade the S/N to a known value; the scatter in the derived parameters was then noted for a large number of tests [100]. R-values from spectra degraded in these tests were found to be unusually high for the calculated S/N, as compared with real data. An empirical relationship to convert S/N values to R values was therefore derived from actual data - R-values derived from the known noise test S/N were then used in the error model, rather than R-values calculated from the noisy spectra themselves. This procedure enabled a direct comparison between the observed scatter in noise test parameter values and the "formal" predictions of 3.4.28. The results of such tests are illustrated in figure 3.4.5. The errors derived from the noise tests are less than the formal errors at high S/N. For poor S/N the noise test errors exceed the formal prediction.

For the noise tests, the ratio of dispersion to velocity error was found to be 1.25, which should be compared with a value of 1.2 found by Tonry & Davis (1981), and the predicted value of 1.4 given in equation 3.4.28. The error in velocity dispersion is then:

$$\Delta\sigma = \frac{2}{3} \cdot \frac{w^{rep}}{1+R} \cdot 1.25 = 1.25\,\Delta v \qquad 3.4.29$$

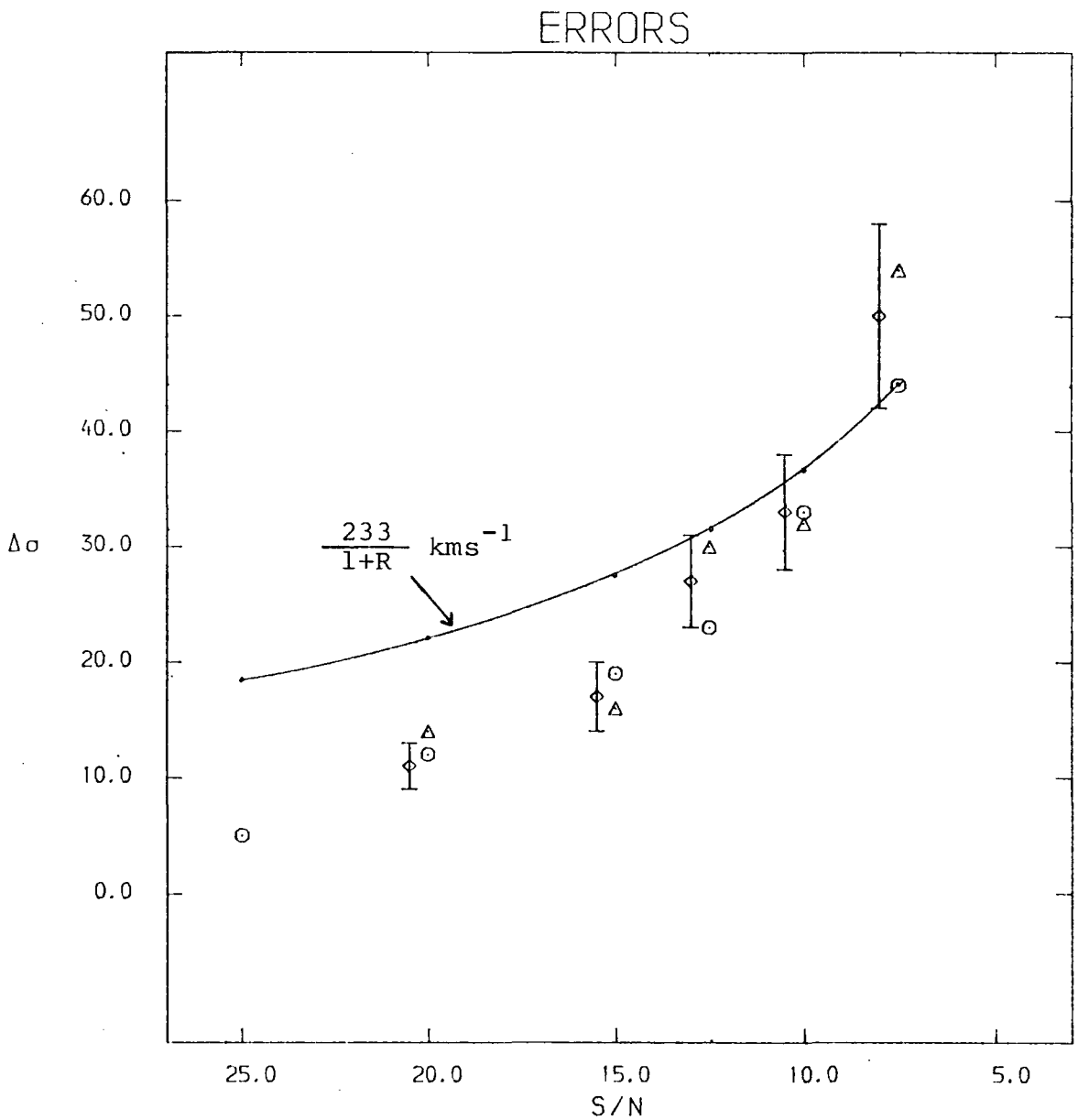

Figure 3.4.5

Noise test errors vs Tonry & Davis error model

Tonry & Davis used independent estimates of errors to fix the parameter "B" in 3.4.21. B may be estimated directly from plots of FT amplitudes, but this is a very uncertain procedure - the B and w^{rep} values do, however, appear to be broadly consistent. A representative value of 280 kms^{-1} has been used in figure 3.4.5, so $\Delta\sigma$=233/(1+R) kms^{-1} or $\Delta\sigma$=3.9/(1+R) channels [corresponding to a B of 66].

Table 3.7.2 shows that the scatter in derived parameters induced by the addition of noise is the same for cross-correlation, the Fourier Quotient and the Fourier Difference. This result is the justification for the use, in this work, of the Tonry & Davis error scheme for calculation of the errors quoted for the Fourier methods.

3.4.4 Comments

The chief advantage of the CCF over the Fourier methods is its directness. If anomalous results are produced, anything awry in the CCF is rather more obvious than in the quantities dealt with by the Fourier techniques. The cross-correlation method is computationally very quick, though it does need some initial calibration; the results are independent of filter, and a reliable procedure is available for finding errors.

However, when estimating velocity dispersions the procedure is rather assumption laden and does require calibration. As will be seen in sections 3.5 and 3.6, the Fourier methods are not as sensitive to these assumptions and might therefore

be expected to provide better estimates of velocity dispersion. A significant difference between the cross-correlation and Fourier methods is the ability of the Fourier methods to estimate a line-strength parameter. A comparison of the three methods is given in section 3.7.

One advantage, already mentioned, which the objective methods have over the subjective visual comparisons is that all of the observed spectral region is used. With the cross-correlation procedure, it is possible to estimate how much of the main CCF peak is contributed by any region of the spectrum. As a typical example, two templates from the SAAO data described in chapter 2 were cross-correlated, and it was found that the five strongest groups of lines contributed only 40% of the height of the peak. An example of the product [at zero lag] of the two template spectra is shown in figure 3.4.6. The value of the CCF is the integral over all channels of this product.

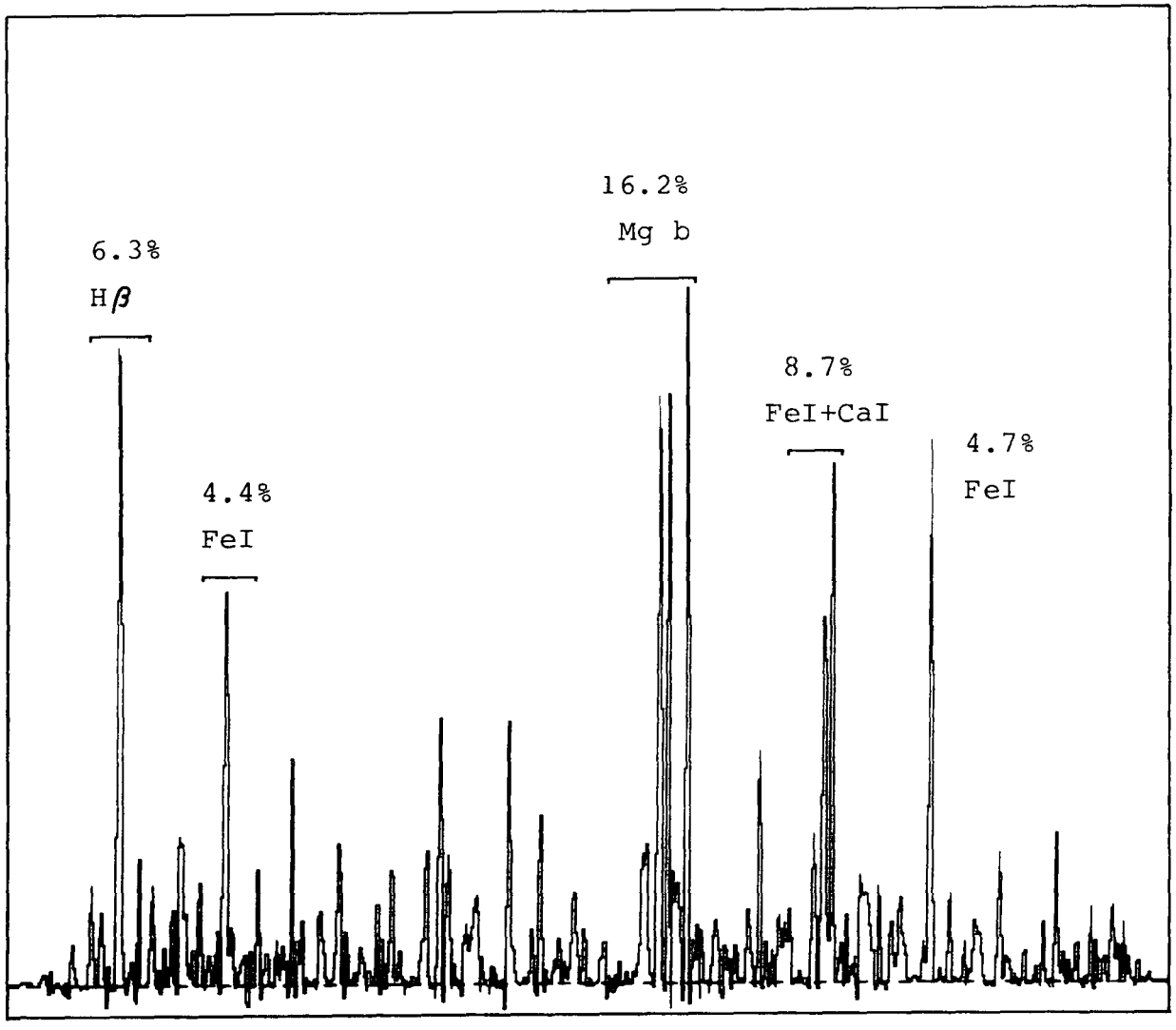

Figure 3.4.6 Contributions to the CCF

3.5 THE FOURIER QUOTIENT

3.5.1 The Quotient

From the Convolution Theorem [equation 3.3.4] and the definitions of T(k) and O(k) in equations 3.3.6 and 3.3.8, it is clear that an estimate of the FT of the broadening function, B(k), may be made as follows:

$$Q(k) = \frac{O(k)}{T(k)} \qquad 3.5.1$$

$$= e^{-\frac{(2\pi k)^2\sigma^2}{2N^2}} e^{-\frac{2\pi i k\delta}{N}} \left[\frac{\sum_{\ell=1}^{L} \gamma_\ell \gamma_\ell^t e^{-\frac{2\pi i k n_\ell}{N}}}{\sum_{\ell=1}^{L} \gamma_\ell^t e^{-\frac{2\pi i k n_\ell}{N}}} \right]$$

and if all the γ_ℓ are taken to be equal:

$$Q(k) = \gamma\, e^{-\frac{(2\pi k)^2\sigma^2}{2N^2}} e^{-\frac{2\pi i k\delta}{N}} = \gamma . B^*(k) \qquad 3.5.2$$

Equation 3.5.2 suffers from the sensitivity to noise seen in the restoration of equation 3.4.15. Simkin (1974) tried the full restoration using an optimal transfer function and a complicated system for the elimination of aberrant points in the Quotient. The approach of SSBS and subsequent workers has been to abandon the restoration to data space and to fit the

broadening function in Fourier space. A weighting function is then used to estimate the expected fluctuations in the quotient O(k)/T(k). An understanding of the weighting to be applied to the fit is clearly essential.

3.5.2 Weighting

Suppose the FT of a set of data, d(n), is D(k). If a fit, F(k), is made to D(k), to be judged by a least-squares quantity for goodness of fit, then a function $\Delta(k)$ must be found, which estimates the expected error in D(k)-F(k).

$$\chi^2 = \sum_{k=0}^{N-1} \left| \frac{D(k) - F(k)}{\Delta(k)} \right|^2 \qquad 3.5.3$$

The weighting function is $\sqrt{|1/\Delta(k)|^2}$. Regions of low noise are favoured by such a function [ie there is little expected error in the numerator where $\Delta(k)$ is small, and the weight given to such points is high]. It is not the purpose of the weighting function to weight highly regions of the fit with high signal-to-noise: the signal is taken out in the comparison D(k)-F(k). There seems to be some ambiguity in the literature on this point [Williams (1981)].

The general arguments of SSBS shall now be followed, to calculate the expected fluctuations in the FT of a spectrum assumed to have Poisson noise.

Suppose an "observed" spectrum, $f^o(j)$, [ie not normalised by the mean count per channel] has a noiseless part, $n^o(j)$, and a noise component, $\nu^o(j)$, then:

$$f^o(j) = n^o(j) + \nu^o(j) \qquad 3.5.4$$

$$F^o(k) = N^o(k) + \sum_{j=1}^{N} \nu^o(j)\, e^{-\frac{2\pi i j k}{N}} \qquad 3.5.5$$

We wish to find the expected square deviation of the observed $F^o(k)$ about the true $N^o(k)$:

$$|\Delta F^o(k)|^2 = \langle |F^o(k) - N^o(k)|^2 \rangle \qquad 3.5.6$$

$$= \left\langle \sum_{j=1}^{N} \nu^o(j)\, e^{-\frac{2\pi i j k}{N}} \cdot \sum_{j=1}^{N} \nu^o(j)\, e^{-\frac{2\pi i j k}{N}} \right\rangle$$

$$= \sum_{j=1}^{N} \langle [\nu^o(j)]^2 \rangle$$

where angle brackets indicate an expectation value, the noise $\nu^o(j)$ is required to be uncorrelated [channel to channel] and $\langle \nu^o(j) \rangle = 0$.

For noise which is Poisson distributed:

$$\langle [\nu^{o}(j)]^{2} \rangle = n^{o}(j) = \langle f^{o}(j) \rangle \qquad 3.5.7$$

So,

$$|\Delta F^{o}(k)|^{2} = \sum_{j=1}^{N} f^{o}(j) \qquad 3.5.8$$

Equation 3.5.8 is effectively equation 3 of the SSBS paper. In practice, the data is manipulated before calculating the FT: the data is end-masked with a function w(j) [a cosine-bell in this study] and the spectra are divided by the mean count per channel, to get f(j) from $f^{o}(j)$.

$$f(j) = \frac{f^{o}(j)\, w(j)}{f_{s}} \qquad 3.5.9$$

Repeating the previous analysis, equation 4 of SSBS is obtained:

$$|\Delta F^{o}(k)|^{2} = \frac{N^{2} \sum_{j=1}^{N} [w(j)]^{2} f^{o}(j)}{\left[\sum_{j=1}^{N} f^{o}(j) \right]^{2}} \qquad 3.5.10$$

However, there is an error in this analysis - the fluctuations in F(k) are indeed determined by the noise in f(j), but the noise in any particular data channel is fixed by the Poisson fluctuations about the mean photon count in that channel <u>before the sky is subtracted</u>. This error may account for the high values of χ^2 found by some authors [Davies (1981)]. If a(j) is the photon count in the sky*, then:

$$|\Delta F^{o}(k)|^2 = \frac{N^2 \sum_{j=1}^{N} [w(j)]^2 \, [f^{o}(j) + a(j)]}{\left[\sum_{j=1}^{N} f^{o}(j) \right]^2} \qquad 3.5.11$$

If 3.5.11 is used in a practical calculation, then mean counts per channel are used:

$$f_o = \frac{1}{N} \sum_{j=1}^{N} o^{o}(j) \qquad 3.5.12$$

and,

$$|\Delta O(k)|^2 = \frac{N (f_o + f_{sky})}{f_o^2} \qquad 3.5.13$$

Equations 3.5.12 and 3.5.13 show how to calculate the expected fluctuations in O(k), using the mean count per channel before [f_o+f_{sky}] and after [f_o] sky-subtraction. Equation 3.5.13 indicates that the expected fluctuations are independent of wavenumber, k, as should be the case for "white" noise.

* where a(j) includes any contribution from the sky frame used for sky subtraction.

SSBS now estimate the quantities σ, δ and γ by minimisation of:

$$\chi^2 = \sum_{k_{low}}^{k_{high}} \left| \frac{Q(k) - \gamma B^*(k)}{\Delta Q(k)} \right|^2 \qquad 3.5.14$$

where,

$$Q(k) = \frac{O(k)}{T(k)} \qquad 3.5.15$$

and,

$$\frac{\Delta Q(k)}{Q(k)} = \sqrt{\left| \frac{\Delta T(k)}{T(k)} \right|^2 + \left| \frac{\Delta O(k)}{O(k)} \right|^2} \qquad 3.5.16$$

The wavenumber limits between which the χ^2 quantity in 3.5.14 is evaluated are fixed by practical considerations. The low wavenumber limit, k_{low}, is chosen to eliminate residual continuum trends remaining in the spectra after continuum removal. The high wavenumber limit, k_{high}, is fixed at the lowest value possible, such that the values of σ, δ and γ are unchanged as k_{high} is decreased. Computation time is reduced by choosing the lowest k_{high} possible.

The SSBS method has been used by many authors and numerous tests have been applied to the method to check its accuracy. SSBS themselves and Sargent et al (1978) give full accounts of the tests and the remaining problems with the method. A test often quoted is the "broadening test", whereby a template is broadened by a known amount and noise is added; application of the Fourier Quotient method using another template should then recover the original dispersion.

Except for velocity dispersions of the order of the instrumental width, the method produces errors of only a few percent. Tests have also shown that dispersions are the same when derived from different wavelength regions [but see Kormendy & Illingworth (1982) for comments on the CaII H and K lines], or using templates of differing spectral type. Adding noise to object spectra has not been found to bias the values of any of the derived parameters. A discussion of the results of such tests is given in section 3.7.

However, three problems remain: velocity dispersions of the same order as the instrumental width are overestimated [Schechter & Gunn (1979); Whitmore, Kirshner & Schechter (1979); Kormendy & Illingworth (1982)]; secondly, there is a marked correlation between derived values of σ and γ, in the sense that where σ is large so too is γ [Schechter & Gunn (1979), Sargent et al (1978)]; lastly, there are a number of authors who are concerned at the process of taking the Fourier Quotient at all, or criticise the weighting function [Morton & Elmergreen (1976), Dressler (1979), Davies (1981)].

Schechter & Gunn comment that velocity dispersions of the order of approximately one pixel are overestimated, which they attribute to mis-match between template and object. Whitmore, Kirshner & Schechter in 1979 and in subsequent papers [eg Whitmore & Kirshner (1981)], correct for two possible sources of spurious dispersion: drift in arc line positions during an exposure, [D], and the low σ overestimation [W]. This empirical correction is important only for small velocity dispersions.

$$\sigma^2_{true} = \sigma^2_{obs} - k.D^2 - W^2$$

$$k = \text{constant}$$

An explanation of this spurious "resolution width" may be made by reference to misgivings about Fourier Quotients expressed by Morton & Elmergreen (1976) [they tested Simkin's method]. Though not interested in this particular problem, they comment that there are three regimes in the estimation of a Fourier Quotient: at low wavenumbers object signal is divided by template signal; at higher wavenumbers object noise is divided by template signal and at the highest wavenumbers object noise is divided by template noise. Under the first regime the value of the quotient should be approximately γ, the line-strength, and at high wavenumbers the quotient will be some extremely noisy function distributed about zero. A procedure fitting such a quotient will find a spuriously high σ. Clearly, if a template and object matched exactly, the quotient would have the value γ for <u>all</u> wavenumbers. An example is illustrated in figure 3.5.1, where the

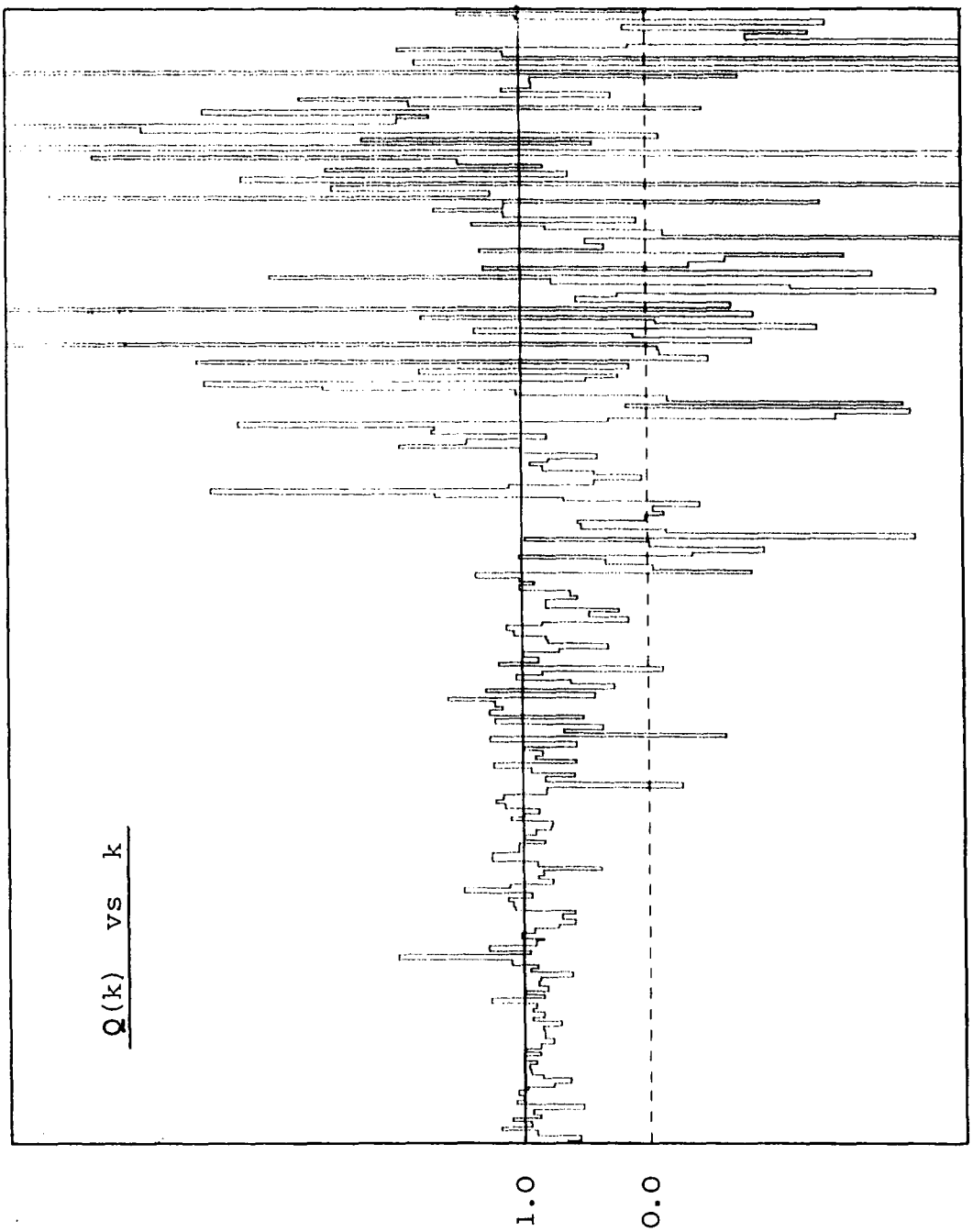

Figure 3.5.1 Fourier Quotient of two template spectra

quotient has been formed from two stellar spectra. Note that if the two spectra had been swapped around, so that the old template became the new object, a similar spurious dispersion would be found [the velocity shift would be reversed and the line-strength should be inverted].

The second of the three problems is probably insoluble. A correlation between σ and γ is built into the χ^2 quantity being minimised. If, for example, a low wavenumber value of the quotient is unusually high then the fitted curve will be dragged upward, resulting in a higher and narrower peak [ie a higher γ and a larger σ]. The correlation is illustrated in figure 3.6.2, where the uncorrelated nature of the other two combinations of parameters is apparent. Though adding noise to galaxy spectra might produce correlated values of σ and γ, these noise tests show that, on average, parameter values are unbiassed. Attempts have been made to reduce the correlation between σ and γ by weighting schemes [Williams (1981)].

Analysis of long slit spectra often shows the line-strength parameter decreasing with distance from the nucleus. This effect is due either to real gradients in line-strength, or possibly to scattered light in the spectrograph [light scattered from the brightest part of an image may re-appear as a featureless continuum contaminating the rest of the image]. It should be emphasised that this sort of behaviour of the line-strength parameter is not correlated with changes in the velocity dispersion [unless through some systematic error].

Lastly, there are the problems associated with the Fourier Quotient itself. Though the template should be of as high quality as possible [and this is a prerequisite for good dispersions], it is inevitable that the FT of the template will have noise. The division of the even noisier object FT by this template may result in a highly irregular quotient. Some authors remove highly aberrant points from the fit to reduce the uncertainty [Simkin (1974), Davies (1981)]. Dressler (1979) suggested a Fourier Difference method, which completely avoids the problem of forming the quotient - and a new method is proposed in section 3.6 which unites the SSBS formalism with the Fourier Difference resistance to noise.

The second problem with quotients, as discussed at length by Davies (1979), is the fact that it is not possible to derive a formal weighting function for the quotient of two functions each of which have Poisson noise. Equation 3.5.16 is appropriate to the combination of errors from the product, not the quotient, of two functions. The quotient of two functions with Poisson errors has a resultant distribution of errors defined by the Cauchy distribution. Moreover, since it is not possible to define a variance for a Cauchy distribution it is not possible to derive an error function for a classical χ^2. This makes the SSBS weighting scheme formally untenable.

Despite the apparent success of the Fourier Quotient it is clear that, as stated by SSBS, the method is not completely consistent. An attempt is made in section 3.6 to find a more consistent method.

3.5.3 Errors

The model, B(k), fit to the data, Q(k), is not a linear function of the solved-for parameters σ, δ and γ: the analysis therefore uses non-linear least-squares. In general, errors may be derived for the Fourier Quotient method only rather indirectly. The prescription of Lampton et al (1976) is typical and is described in this section.

First, a significance level is chosen [where the significance at which a hypothesis is rejected is the probability that the hypothesis has been wrongly rejected]. A region in parameter space is then constructed, bounded by parameter values at which the critical χ^2 appropriate to that significance level is obtained. The boundary parameter values are calculated by holding all but one of the parameters fixed, and then incrementing the remaining parameter until χ^2 reaches the critical value. The error is then simply the difference between the parameter value at the critical χ^2 and the parameter value at the minimum χ^2. The Lampton et al method relies on the difference between the perturbed χ^2 and the minimum χ^2 being distributed as a true χ^2 quantity - the χ^2 itself may not be strictly a true χ^2.

Suppose a parameter is incremented from its value at the best fit, to produce a perturbed χ^2 [χ^2_{per}] greater than the best fit χ^2 [χ^2_{min}], then:

$$\Delta S = \chi^2_{per} - \chi^2_{min} \qquad 3.5.17$$

and it is then true that ΔS is distributed as the χ^2 for the number of parameters, N_p.

$$\Delta S \sim \chi^2_{Np} \qquad 3.5.18$$

Lampton et al supply values of ΔS for different numbers of parameters, N_p, and for different significance levels, S_1, so that a boundary may be defined:

$$\chi^2_b = \chi^2_{min} + \chi^2_{Np}(S_1)$$

The parameters [σ, δ and γ] are then incremented until χ^2_b is reached. Values for χ^2_b are given below:

$$\chi^2_3(0.32) = 3.5 \qquad \chi^2_2(0.32) = 2.3$$

$$\chi^2_3(0.10) = 6.3 \qquad \chi^2_2(0.10) = 4.6$$

A preference is expressed in section 3.7 for a different method of calculating errors. It seems that ΔS is simply not distributed as a χ^2 quantity: the formal errors are always larger than the errors calculated by any other method.

3.6 THE FOURIER DIFFERENCE

3.6.1 The Difference

Motivated by a desire to avoid forming the Fourier Quotient, while at the same time retaining the formalism of section 3.5, a calculation of the weighting function appropriate to a Fourier Difference is presented. These results have been adopted for the analysis of the data presented in other chapters.

The Fourier Difference uses the statistic:

$$\chi^2 = \sum_{k_{low}}^{k_{high}} \left| \frac{O(k) - \gamma T(k) B^*(k)}{\Delta(k)} \right|^2 \qquad 3.6.1$$

The two functions in the numerator of 3.6.1 are combined additively [with B(k) having no error]. The error function $|\Delta(k)|^2$ is therefore given by the sum in quadrature of the errors on O(k) and T(k).B(k):

$$|\Delta(k)|^2 = |\Delta O(k)|^2 + |\Delta[\gamma . T(k) . B^*(k)]|^2$$

$$= |\Delta O(k)|^2 + \gamma^2 |B(k)|^2 |\Delta T(k)|^2 \qquad 3.6.2$$

and these functions may be found from 3.5.2 and 3.5.13. Using the "f-notation" for counts per channel:

$$|\Delta(k)|^2 = \frac{N(f_o + f_{sky})}{f_o^2} + \frac{N\gamma^2 |B(k)|^2}{f_t} \qquad 3.6.3$$

where the template is assumed to have no noise component due to sky [it is trivially included]. If the channel to channel correlations in the noise are to be included then 3.6.3 should be multiplied by the appropriate noise power distribution. An example of the weighting function [normalised to 1.0 at high wavenumber] is given in figure 3.6.1.

The signal-to-noise [S/N] for a channel with photon counts governed by Poisson statistics is:

$$[S/N]_o = \frac{f_o}{\sqrt{f_o + f_{sky}}} \qquad 3.6.4$$

and so 3.6.2 may be re-phrased in terms of S/N:

$$|\Delta(k)|^2 = \frac{1}{[S/N]_o^2} + \frac{\gamma^2 |B(k)|^2}{[S/N]_t^2} \qquad 3.6.5$$

Normalised by its minimum value, the error function is:

$$E(k) = 1 + \gamma^2 |B(k)|^2 . \frac{[S/N]_o^2}{[S/N]_t^2} \qquad 3.6.6$$

which can be seen to depend only on σ, γ and the ratio of $[S/N]_o$ to $[S/N]_t$.

Figure 3.6.1 illustrates that the form of the expected errors as a function of wavenumber for Poisson noise is such that low wavenumbers are weighted less than higher wavenumbers. If the template is of high quality then the weighting is practically a constant. All this is saying is that, while it is true that the Fourier Difference is all noise at high wavenumbers, it is also true that the average value of the Difference is more certainly zero at high wavenumbers than at low wavenumbers. In practice, the instrumental profile suppresses high wavenumber noise, so the weighting at high wavenumbers could be even higher. The observed insensitivity of derived parameter values to the high wavenumber cut-off, k_{high}, makes such sophistication unnecessary.

An example of the variation of the χ^2 per degree of freedom with wavenumber is given in table 3.6.1. The table was produced by calculating a best fit, as if making a normal estimation of the parameters - residuals from this fit were then determined for the wavenumber regions specified.

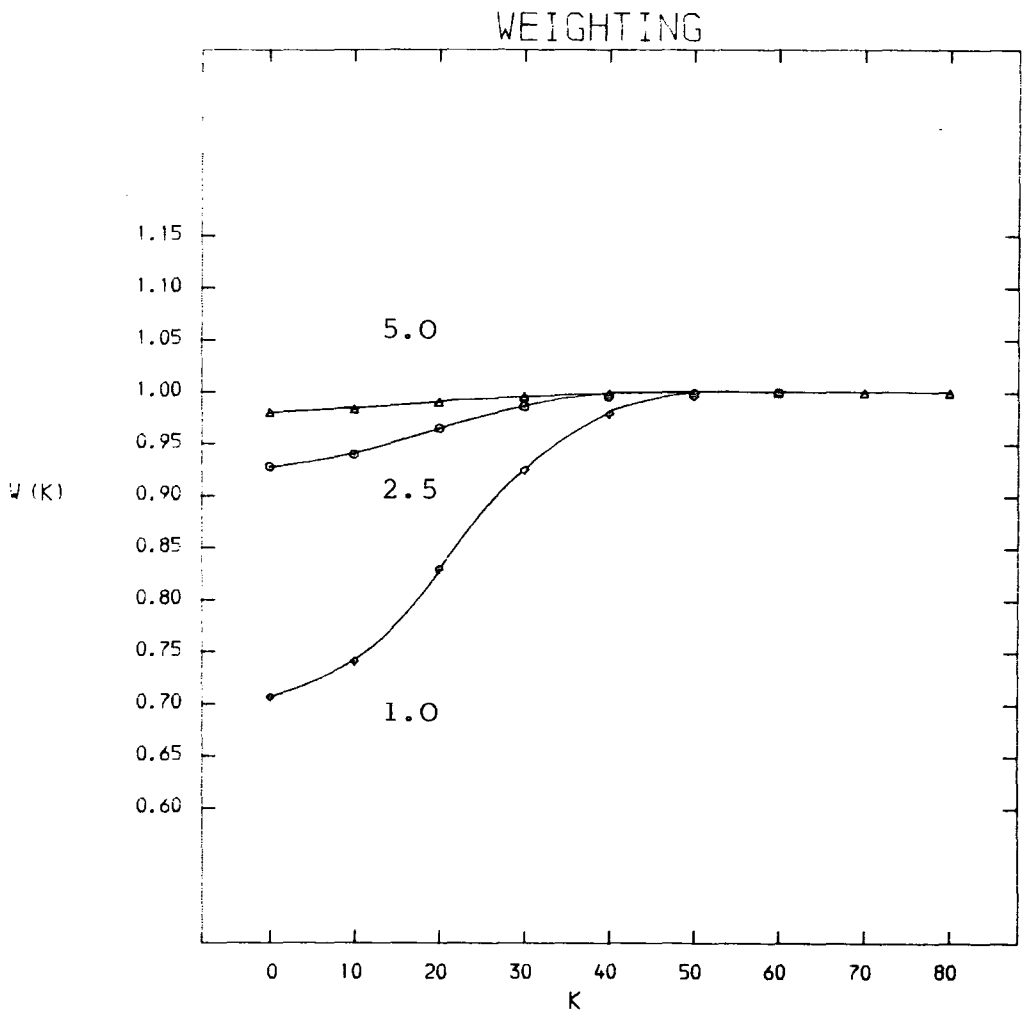

Figure 3.6.1

Fourier Difference Weighting Function

Three curves are shown, corresponding to weighting functions calculated for different ratios of template S/N to object S/N [indicated by each curve]. The weighting function, w(k), corresponds to $1/\sqrt{E(k)}$. The other parameters controlling the the shape of the curve are: γ=1.0 and σ/N=0.0071, where N is the number of data channels in the spectrum.

Table 3.6.1

Variation of χ^2 with Wavenumber

Fourier Difference comparison of A1631 with HD26262.
A nominal fit was obtained over the range (10,150).

γ : 1.25
σ : 249 kms^{-1}
v : 3987 kms^{-1}
χ^2 : 1.40

Range	χ^2
0-49	2.63
50-99	1.21
100-149	1.22
150-199	0.94
200-249	0.69
250-299	0.76
300-349	0.38
350-399	0.30
400-449	0.19
450-500	0.13

Range	χ^2
0-24	3.99
25-49	1.63
50-74	1.26
75-99	1.33
100-124	1.25
125-149	1.32
150-174	1.17
175-199	0.84

Table 3.6.2

Variation of Parameters with [S/N]

$[S/N]_o$	$[S/N]_t$	σ_D	σ_S	γ_D	γ_S	v_D	v_S
50.06	51.06	304	306	0.92	0.94	-51	-51
20	51.06	301	301	0.91	0.93	-54	-54
10	51.06	305	305	0.96	0.98	-48	-49
15	10	319	314	0.98	1.07	-47	-47

Subscript : D = Difference, S = SSBS Quotient.

While representing both a formal and an empirical improvement over the SSBS Fourier Quotient, the Fourier Difference still suffers from two of the three problems mentioned in the criticism of SSBS in section 3.5.2: the non-zero resolution width and the σ-γ correlation.

Since no quotient is formed in the Difference method, the explanation of the non-zero SSBS resolution width does not apply. However, there is an equivalent mechanism. The Fourier Quotient fits a smooth function, B(k), to a noisy function, Q(k); the Fourier Difference fits a noisy function B(k).T(k) to another noisy function, O(k). To minimise the χ^2, B(k) can be made highly peaked [ie larger σ] in order to suppress high wavenumber noise in B(k).T(k). Such a process will continue until deviations from O(k) at low wavenumbers balance the advantage gained by changing B(k) at high wavenumbers. If this is indeed the process, then a prediction can be made: addition of noise to objects should not systematically bias the derived parameters, whereas addition of noise to templates should make σ larger. The results of such a test are given in table 3.6.2. The object in this noise test is HD26262 broadened to 300 kms^{-1} and the template is HD106083. The object was degraded with forty different sets of noise, and the individual object results were then averaged to calculate the resultant change in parameter values. The degraded template result is a similar average of ten "noisy" templates, each compared with the original forty noise-degraded objects. The prediction is therefore shown to be consistent with the results. Real galaxies are found to be even more sensitive to the

S/N of template. After section 3.6.2, the similarity between the Fourier Difference method and the SSBS Fourier Quotient method will become more apparent.

Both the SSBS Fourier Quotient and the Fourier Difference exhibit a marked correlation between line-strength and velocity dispersion. Figure 3.6.2 illustrates the problem: a large number of sets of noise were added to an object spectrum; the resulting dispersions, line-strengths and velocities have been plotted against each other, such that the centre of each box is the mean value of the parameters obtained from the noise trials, and the scales range to three standard deviations either side of this mean. The dispersion and line-strength are correlated, as can be seen from the correlation coefficients:

$$r(\gamma,v) = 0.35 \times 10^{-4}$$

$$r(\gamma,\sigma) = 0.57$$

$$r(v,\sigma) = 0.66 \times 10^{-2}$$

The object was HD26262 broadened to 300 kms^{-1} and the template was HD106083. The S/N of the object was degraded to ten, and the results calculated using the Fourier Difference method. There is no significant difference between the Quotient and the Difference in the value of the correlation coefficients.

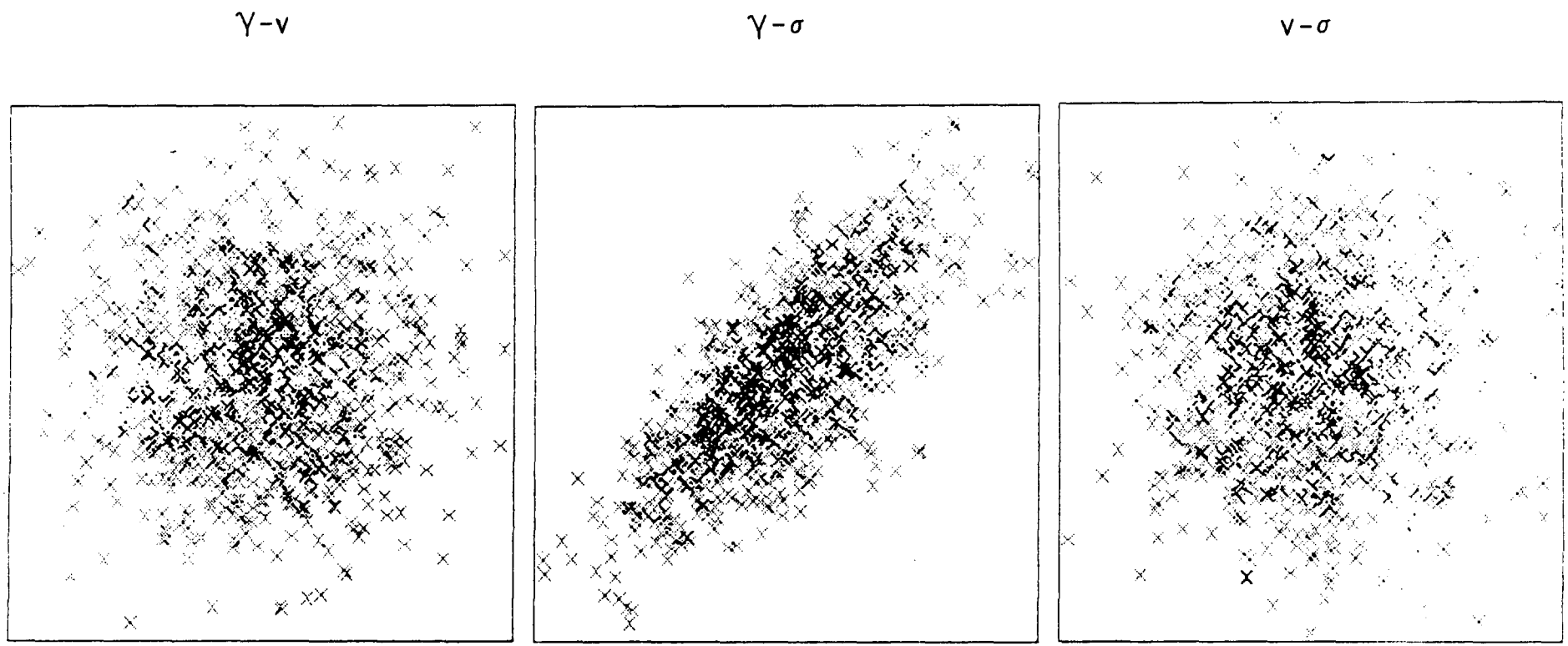

Figure 3.6.2 Distribution of derived parameters (scaled to ±3 s.d.)

These noise tests show an undeniable correlation between two of the derived parameters, but no evidence for bias, so long as the template is of very high [S/N]. The results of the astronomical analysis conducted in this work should therefore be acceptable as unbiassed estimates of velocity dispersion and radial velocity.

3.6.2 Symmetry

Cross-correlation, the Fourier Quotient and the Fourier Difference are closely related techniques. The Fourier Quotient method has been shown to defy a formal treatment and yet it is apparently successful. How closely is the Fourier Quotient related to the Fourier Difference?

Suppose the Fourier Quotient equations are written as Fourier Difference equations:

$$\chi^2 = \sum \left| \frac{O(k) - \gamma T(k) B^*(k)}{T(k) \Delta Q(k)} \right|^2$$

Then what is this error function T(k). Q(k)?

$$|\Delta^{SBS}(k)|^2 = |T(k) . \Delta Q(k)|^2$$

$$= |T(k)|^2 \left[\left| \frac{\Delta O(k)}{O(k)} \right|^2 + \left| \frac{\Delta T(k)}{T(k)} \right|^2 \right] \left| \frac{O(k)}{T(k)} \right|^2$$

$$= |\Delta O(k)|^2 + \left| \frac{O(k)}{T(k)} \right|^2 |\Delta T(k)|^2 \qquad 3.6.7$$

Clearly equation 3.6.7 is very similar to 3.6.2 and we may write:

$$\text{DIFFERENCE} : \quad |\Delta^{DIFF}(k)|^2 = |\Delta O(k)|^2 + \gamma^2 |B(k)|^2 |\Delta T(k)|^2$$

$$\text{QUOTIENT} : \quad |\Delta^{SSBS}(k)|^2 = |\Delta O(k)|^2 + |Q(k)|^2 |\Delta T(k)|^2$$

Because SSBS used the actual functions Q(k), O(k) and T(k) in estimating the expected error on Q(k), their method becomes [with the correction in 3.5.11] closely equivalent to the Fourier Difference method. The difference between the two methods is the replacement of a smooth function $\gamma.B(k)$ in the Difference by a noisy function Q(k) in the "SSBS Difference". This symmetry suggests that the treatment presented in this chapter is at least self-consistent. For good S/N spectra, when $Q(k)=\gamma B(k)$, the methods must produce the same results [and indeed they do]. For poorer S/N spectra, particularly if the template is poor, the Fourier Difference method might be expected to perform better, because the Q(k) term in the "SSBS Difference" method will be rather noisy.

The Fourier Difference method is adopted for the analysis of the data used in this study for two reasons: it performs better than the SSBS Fourier Quotient method and its derivation is free from some of the criticisms that can be levelled against both the Fourier Quotient and cross-correlation methods.

3.6.3 Dressler's Method

Dressler (1979) has already pointed out that there is an alternative to forming the Fourier Quotient from O(k) and T(k): that it is perfectly possible to minimise:

$$\chi^2 = \Sigma \left| \frac{O(k) - \gamma B^*(k) T(k)}{\Delta(k)} \right|^2 \qquad 3.6.8$$

where he used:

$$\Delta(k) = \langle T(k) \rangle \qquad 3.6.9$$

This weighting function is an empirically determined way of weighting the residuals from the fit "equally" and Dressler describes his method as "simply a heuristic way of deriving a quantity which behaves like a formal χ^2". This method differs from the Fourier Difference derived in this section only in the use of different weighting functions.

For good signal-to-noise data Dressler found that the values of σ, δ and γ were insensitive to changes in $\Delta(k)$, but that for poor data 3.6.9 worked best. In this work, Dressler's method was found to behave very similarly to the Fourier Quotient method as regards the critical k_{low}-σ test [see section 3.7], and was not therefore adopted.

3.7 COMPARISONS

3.7.1 Tests

A comparison of the three methods described in the preceding three sections is carried out in this section - to show whether the methods agree or not, and if one method is clearly preferable.

For high S/N spectra the Quotient and Difference must agree, because they are then closely equivalent. If the cross-correlation calibration is carried out correctly, then this method should also be in agreement. A comparison of parameter values derived from a high quality galaxy spectrum is presented in table 3.7.1. The agreement between methods for both velocities and velocity dispersions is excellent: to within 3 kms^{-1} for the velocities and 5 kms^{-1} for the dispersions.

The agreement between the cross-correlation and Fourier methods gets worse as the S/N is decreased but there are occasional discrepancies even for apparently good spectra. Inspection of the CCF for the discrepant cases usually reveals some asymmetry or obviously non-Gaussian shape for the peak. It is one of the great advantages of the cross-correlation method that gross errors can be spotted - the Fourier methods are generally too complex to sort out what is awry.

Table 3.7.1

Comparison of Methods

Galaxy : A978
Counts : 349 per pixel
Object/Sky : 3.8
Object S/N : 16.6
Template S/N : 50 (approx)
Time : 14,000 seconds

Diff./SSBS : 9-14 to 150
Correlation : 7,8,100,200

Template	σ_D	σ_S	σ_C	v_D	v_S	v_C	R	χ^2_D	χ^2_S	γ_D	γ_S
HD26262	251	251	251	16209	16210	16210	6.85	1.09	1.07	1.09	1.07
HD103423	248	249	254	16226	16227	16226	7.17	1.08	1.06	1.25	1.23
HD24291	249	250	251	16172	16174	16173	7.00	1.08	1.02	1.12	1.08
HD25537	246	245	245	16178	16180	16182	7.48	1.05	0.98	1.03	0.98
HD105784	245	244	248	16198	16202	16198	7.25	1.08	0.94	1.11	1.01
HD106083	258	258	252	16265	16266	16262	6.93	1.08	1.06	1.04	1.02
Average :	250	250	250	16208	16210	16209					

No heliocentric correction has been applied to the velocities.

WK1AAC

For reasonable S/N [>10] noise tests indicate that the methods behave very similarly. Table 3.7.2 shows that at S/N=10 the rms cross-correlation error in velocity dispersion is 35 kms^{-1}, almost exactly the same as the Fourier error of 33 kms^{-1}.

Broadening tests provide a useful consistency check for the methods. In this work, calibration of the cross-correlation method was acheived using broadening tests to fix the σ-w relation - so only the Fourier methods can be compared here.

Table 3.7.3 presents the results of a broadening test with two very high quality templates. In the first test HD106083 is broadened by σ_{in} and compared with HD26262 to produce σ_{out}, v_{out} and γ_{out}. In the second test HD26262 is used as the object and HD106083 as the template. The purpose of performing two tests is to check whether $\gamma(\text{test-1})=1/\gamma(\text{test-2})$. For the Difference method this is much more accurately true than for the Quotient method. If poor quality templates are used the difference in behaviour is considerable. Table 3.7.4 lists the results of a test involving a reasonably good template and a very poor template. Figure 3.7.1 gives a pictorial representation of "inverseness" for the data in tables 3.7.3 and 3.7.4 [and one other pair of templates from the AAT data]. This shows that the Difference is acting <u>consistently</u>. From the broadening tests it appears that the Fourier Difference is much more consistent for poor spectra and marginally more consistent for good spectra.

Table 3.7.2

Noise Tests

A spectrum of A978 was degraded to a S/N ratio of 10. Listed are the mean parameter values found for 40 noise trials, with the rms deviation about the mean. The template was HD26262. Nominal parameter values derived from an un-degraded spectrum are shown [taken from table 3.7.1].

	Difference	Quotient	CCF	Nominal
σ	249 ± 33	249 ± 33	246 ± 35	250
v	16213 ± 24	16215 ± 24	16207 ± 24	16209
γ	1.10 ± .13	1.07 ± .13		1.08
R			5.43 ± .63	6.85
χ^2	1.10 ± .08	0.97 ± .06		1.08

Table 3.7.3

Broadening Tests

Fourier Difference and Quotient tests performed for two SAAO templates (10,200) "both ways round".

Object : HD106083
Template : HD26262

σ_{in}	σ_D	σ_D/σ_{in}	σ_S	σ_S/σ_{in}	v_D	v_S	γ_D	γ_S	χ^2_D	χ^2_S
50	48.3	0.966	50.0	1.000	-52.3	-52.1	1.107	1.075	0.96	0.89
100	98.5	0.985	98.5	0.985	-51.6	-51.6	1.098	1.072	0.46	0.44
150	146.0	0.973	144.8	0.965	-50.5	-50.7	1.077	1.052	0.27	0.27
200	194.4	0.972	192.5	0.963	-49.5	-49.6	1.062	1.036	0.19	0.19
250	244.3	0.977	241.7	0.967	-49.4	-49.4	1.055	1.027	0.15	0.15
300	294.8	0.983	292.1	0.974	-50.7	-50.6	1.051	1.024	0.12	0.12
350	345.4	0.987	342.8	0.979	-53.3	-53.1	1.049	1.023	0.10	0.10
400	396.1	0.990	393.7	0.984	-56.5	-56.3	1.048	1.024	0.08	0.08

Object : HD26262
Template : HD106083

σ_{in}	σ_D	σ_D/σ_{in}	σ_S	σ_S/σ_{in}	v_D	v_S	γ_D	γ_S	χ^2_D	χ^2_S
50	54.3	1.086	55.2	1.104	+52.3	+52.4	0.907	0.886	0.88	0.84
100	105.2	1.052	104.9	1.049	+51.5	+51.4	0.918	0.901	0.42	0.41
150	157.2	1.048	155.8	1.039	+50.3	+50.2	0.934	0.915	0.25	0.25
200	207.6	1.038	205.6	1.028	+49.4	+49.3	0.942	0.921	0.18	0.18
250	256.9	1.028	254.6	1.018	+49.6	+49.4	0.944	0.922	0.14	0.14
300	306.2	1.021	303.7	1.012	+51.2	+51.0	0.944	0.922	0.12	0.11
350	356.0	1.017	353.7	1.011	+54.0	+53.7	0.945	0.924	0.09	0.09
400	406.0	1.015	403.9	1.010	+57.1	+56.8	0.945	0.927	0.08	0.08

WK1AAC

Table 3.7.4

Broadening Tests

Fourier Difference and Quotient tests performed for two AAT templates (15,300) "both ways round".

Object : SAO233152
Template : SAO249009

σ_{in}	σ_D	σ_D/σ_{in}	σ_S	σ_S/σ_{in}	v_D	v_S	γ_D	γ_S	χ^2_D	χ^2_S
200	208.3	1.042	198.9	0.995	+37.6	+38.1	1.125	0.899	0.81	0.66
225	232.6	1.034	222.2	0.988	+36.4	+37.4	1.117	0.900	0.73	0.59
250	257.0	1.028	246.2	0.985	+35.3	+36.7	1.110	0.901	0.65	0.53
275	281.7	1.024	270.8	0.985	+34.5	+36.3	1.104	0.908	0.59	0.48
300	306.5	1.021	295.7	0.986	+34.0	+36.2	1.099	0.906	0.53	0.43
325	331.6	1.020	320.8	0.987	+33.8	+36.4	1.095	0.909	0.48	0.40
350	356.8	1.019	346.0	0.989	+33.8	+37.0	1.091	0.912	0.44	0.36

Object : SAO249009
Template : SAO233152

σ_{in}	σ_D	σ_D/σ_{in}	σ_S	σ_S/σ_{in}	v_D	v_S	γ_D	γ_S	χ^2_D	χ^2_S
200	228.8	1.144	215.3	1.077	-37.2	-37.7	0.893	0.708	0.80	0.62
225	254.0	1.129	239.0	1.062	-35.9	-36.2	0.893	0.711	0.72	0.56
250	279.8	1.119	263.9	1.056	-34.9	-34.7	0.894	0.716	0.64	0.50
275	306.2	1.113	289.8	1.054	-34.2	-33.5	0.896	0.721	0.58	0.46
300	333.2	1.111	316.6	1.055	-33.8	-32.4	0.899	0.728	0.53	0.42
325	360.7	1.110	344.1	1.059	-33.7	-31.6	0.902	0.735	0.48	0.38
350	388.7	1.111	372.2	1.063	-33.8	-31.0	0.906	0.743	0.44	0.35

WK1AAC

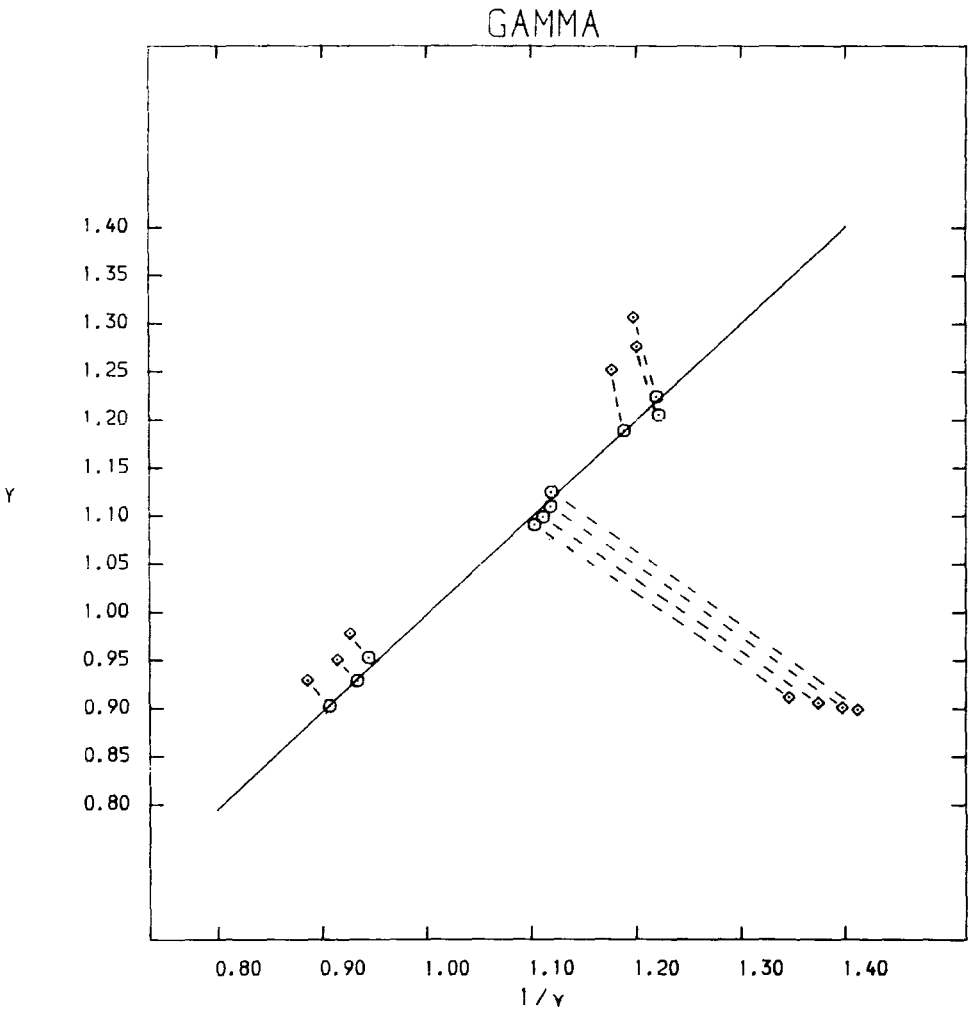

Figure 3.7.1 Line-strength Inverseness

Fourier Difference : ⊙

Fourier Quotient : ◈

There is a second situation in which the Fourier Difference performed better than the Fourier Quotient: in common with other authors, no dependence was found in this work between the derived parameter values and reasonable choices of the upper wavenumber limit for the fit. There was, however, a noticeable dependence on the lower wavenumber limit for some spectra. It would, of course, be very surprising if the derived dispersions were completely independent of k_{low}: low wavenumbers are contaminated by continuum residuals; the S/N of the Fourier functions compared in the fit decreases as the wavenumber increases, and there will be random fluctuations between parameter sets derived using different k_{low} values simply caused by noise. A wavenumber region must be found where σ does not depend systematically and significantly on k_{low}.

Table 3.7.5 shows two k_{low} tests: one for good data and one for poorer data. A general trend is found for low values of k_{low} to give high dispersions and high values of k_{low} to give low dispersions, which is plausible. Many such tests show that the poorer the S/N of the object the more the fluctuations in the plot of k_{low} against σ. In this work, therefore, all velocity dispersions are calculated as an average over a number of k_{low} values [usually five or six] in the flattest region of the k_{low}-σ plot [always the same for a given intrumental set-up]. For high S/N spectra the procedure has little effect, but for poorer spectra significant improvements are possible, since the sometimes considerable fluctuations with k_{low} tend to be smoothed out.

Table 3.7.5

The k_{low}-σ Relation

	Pks 2354-35 (AAT)					A1631 (SAAO)				
k_{low}	γ	v	σ			k_{low}	γ	v	σ	
10	1.107	14708	284	D		6	1.454	4080	274	D
	0.683	14723	285	S			1.380	4080	270	S
12	1.096	14709	283	D		7	1.326	4076	258	D
	0.661	14722	273	S			1.267	4076	255	S
14	1.116	14709	286	D		8	1.346	4074	260	D
	0.654	14722	276	S			1.295	4074	259	S
16	1.132	14712	289	D		9	1.285	4075	253	D
	0.610	14722	263	S	<-- adopted region -->		1.248	4075	253	S
18	1.065	14710	277	D		10	1.250	4077	249	D
	0.592	14721	257	S			1.210	4077	248	S
20	1.118	14713	286	D		11	1.159	4073	238	D
	0.638	14726	271	S			1.128	4073	237	S
22	1.058	14713	276	D		12	1.233	4079	246	D
	0.630	14725	269	S			1.203	4079	247	S
24	1.063	14713	277	D		13	1.242	4080	247	D
	0.623	14724	267	S			1.209	4080	247	S
26	1.038	14711	273	D		14	1.268	4079	250	D
	0.629	14723	268	S			1.237	4080	250	S
28	1.034	14713	273	D		15	1.218	4082	245	D
	0.598	14722	259	S			1.174	4083	243	S
30	1.005	14707	267	D	<--- Difference --->	16	1.192	4084	242	D
	0.581	14718	254	S	<--- Quotient --->		1.151	4085	241	S

Galaxy nucleus with SAO233152 (template 1) : k_{high}=300
Galaxy nucleus with HD26262 (template 1) : k_{high}=150

WK1AAC

For poorer data there may also be a significant and systematic difference betweeen the Difference and Quotient estimates of velocity dispersion. From the inspection of the k_{low} dependence of σ for many galaxy spectra, it is clear that the Difference produces a smoother and flatter k_{low}-σ relation. Figure 3.7.2 illustrates graphically the results contained in table 3.7.5. As an example of the sort of wavenumber limits chosen, the 1024 channel SAAO data was analysed using an average over k_{low}=9-14 and k_{high}=150, while the 2048 channel AAT data had k_{low}=14-18 and k_{high}=300. Fourier transforms of continua suggest that these values of k_{low} are adequate to eliminate residuals from continuum trends.

An internal test which shows clearly the nature of the errors involved in estimating velocities, is to compare the differences in estimates of velocities for different objects, using different templates. The aim is to find the relative velocities of the templates. The scatter about these inferred relative velocities then shows how well different templates agree, though no estimate of absolute accuracy is possible. Eleven galaxies and six templates observed at SAAO were analysed in this fashion and the scatter in velocity differences between a pair of templates was 4 kms^{-1} for the Fourier Difference method. This demonstrates that different templates tend to agree very well, but on a velocity which is presumably absolutely in error by some amount determined by the Tonry & Davis error distribution.

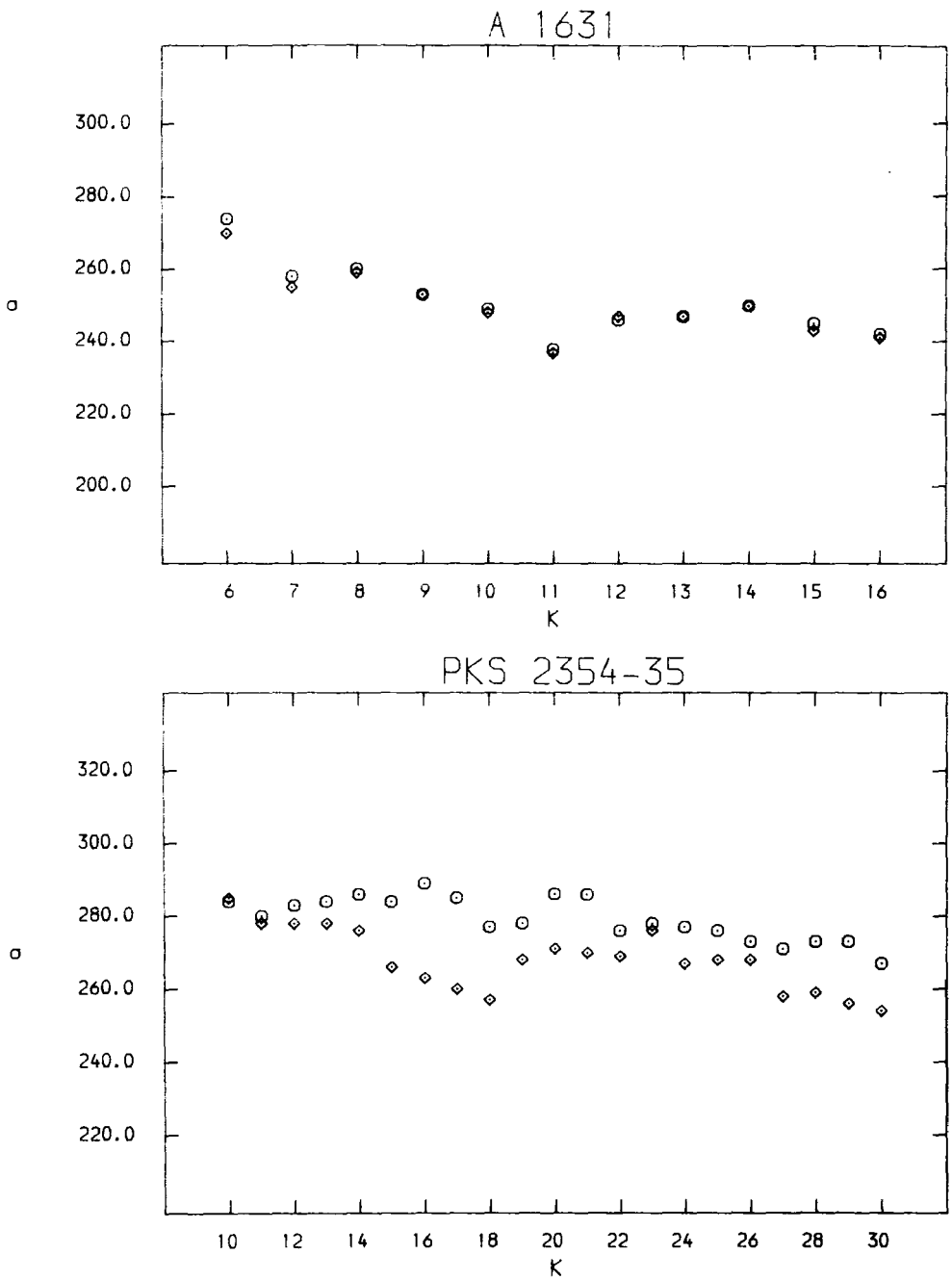

Figure 3.7.2 k_{low}-σ Relation

Fourier Difference : ⊙

Fourier Quotient : ◈

3.7.2 Adopted Procedure

No attempt has been made in this study to include possible systematic errors in the estimates of derived parameters caused by detector or telescope behaviour [arc lines drifting etc]. Such errors are small for the instrumental arrangements used, and no evidence has been found to warrant such a sophisticated treatment. However, in the errors quoted with the final results an estimate of the likely error from incorrect sky subtraction has been included. Each spectrum was analysed three times: once with the "correct" sky subtracted; once with 5% too little subtracted and once with 5% too much. Only in the outer regions of the long-slit data was any difference in the radial velocity or velocity dispersion noticed, and for such spectra the sky subtraction error has been included in quadrature with the formal estimate of the error.

From the results of this chapter the following analysis procedure is adopted: the spectra are first logged and cross-correlated to find an initial estimate of the radial velocity; a second logarithmic transformation is then performed on the original data so that the relative shift between object and template is small; the Fourier Difference method is then used to find the velocity dispersion, radial velocity and line-strength. Errors may then be calculated from a combination of the Tonry & Davis formal scheme and any sky-subtraction errors.

4 CHAPTER FOUR : SAAO OBSERVATIONS

4.1 INTRODUCTION

A considerable effort has been made in the preceding chapter to find a suitable method for determining velocity dispersions. The methods which have been discussed will be applied in subsequent chapters to a set of four galaxies - to form the principal astronomical analysis of this work. However, since no independent observations of the programme galaxies have been published in the literature, a set of observations is reported in this chapter to allow the data reduction procedures used in this work to be verified.

The observations were made as part of a continuing programme of investigations into the properties of rich clusters of galaxies, being carried out by the Durham Cosmology Group and the Oxford Galaxy Group. It is not appropriate to describe that programme here - the results are quoted solely to provide a set of data for comparison with published work.

4.2 SPECTROSCOPIC DATA

The observations were made over seven dark nights in January 1982 at the South African Astronomical Observatory, Sutherland. Table 4.2.1 gives details of the observations.

A number of catalogues of galaxy clusters with Bautz-Morgan classifications were examined to search for BM I clusters which might have candidate cD galaxies [principally Leir & van den Bergh (1977)]. Two extra candidate galaxies were kindly suggested by Harold Corwin, and a number of giant elliptical galaxies were also observed [including the Fornax A galaxy NGC1316].

Galaxy positions were determined from Schmidt plates kept at the Royal Observatory, Edinburgh. Residuals for stars with well known positions indicate an overall accuracy of a few seconds of arc. Galactic objects are more diffuse than stars and will therefore have somewhat greater errors, but the accuracy is quite adequate for the pointing capabilities of the 1.9m SAAO telescope. Table 4.2.2 lists the positions of the objects observed. Preliminary data reduction has been described in chapter 2.

Table 4.2.1

Observational Set-up

Nights	: 7
Dates	: 19/26-Jan-82
Telescope	: 1.9m
Spectrograph	: ITS
Detector	: RPCS
Grating	: 4
Dispersion	: 50 Å/mm
Data Window	: 1872 x 2
Spectrum Separation	: 25.3 arcsec
Slit Width	: 4 arcsec
Dekker Slot Width	: 6 arcsec
PA of Slit	: 90°
Wavelength Range	: 4800 Å - 5925 Å
Observatory	: 20°48'42' E
	: -32°22'42' N

Table 4.2.2

Observations

Object	RA (1950)	DEC	l^{II} (deg)	b^{II} (deg)
A1631[1]	12.8374	-15.1419	303.44	47.46
A496	4.5219	-13.3656	209.59	-36.49
A754	9.1018	-9.4269	239.20	24.70
A957	10.1847	-0.6769	242.91	42.83
A978	10.2989	-6.2744	249.99	40.34
Corwin #1	3.7337	-41.3586	246.00	-51.76
Corwin #2	9.5950	-20.1178	253.20	23.33
NGC1316	3.3463	-37.3850	240.16	-56.69
NGC1600	4.4867	-5.1917	200.42	-33.24
NGC5419	14.0118	-33.7394	319.62	26.54
NGC4696	12.7676	-41.3861	302.40	21.56

1. A1631 is a foreground object.

Template		RA (1950)	DEC
1	HD26262	4.1133	-42.9667
2	HD103423	11.8900	-46.3833
3	HD24291	3.8233	-45.4500
4	HD25537	4.0100	-46.2000
5	HD105784	12.1647	-46.4167
6	HD106083	12.1900	-43.9000

4.3 SPECTROSCOPIC RESULTS

The procedures of chapter 3 have been followed to produce the spectroscopic results presented in table 4.3.1. Comparison of results from the Fourier Difference, Fourier Quotient and cross-correlation methods shows:

$$\Delta v_{D-Q} = -0.5 \pm 0.4 \text{ kms}^{-1}$$
$$\Delta v_{D-C} = +0.5 \pm 2.5 \text{ kms}^{-1}$$

$$\Delta \sigma_{D-Q} = +2 \pm 1 \text{ kms}^{-1}$$
$$\Delta \sigma_{D-C} = -4 \pm 6 \text{ kms}^{-1}$$

It is clear from this comparison that the methods agree very well when the data is of high quality and is reduced consistently. In particular there is no evidence of bias in any of the methods - it is at poor S/N that differences between the methods may become significant.

Details of the spectra analysed are included in table 4.3.2. A comparison with published data is made in table 4.3.3. Zero point corrections for the data were determined by comparing the velocities of NGC1316, NGC1600, NGC4696 and NGC4472 with the Reference Catalogue, to provide a mean zero point correction for the set of six templates. Table 4.3.3 shows a mean velocity difference of 6 ± 39 kms^{-1} between the SAAO sample [excluding those galaxies used for the zero point correction] and the published velocities. The velocity dispersion differences are -2 ± 10 kms^{-1}. Again, no bias is evident - but there is certainly an unsatisfactorily large scatter.

Table 4.3.1

SAAO Results

Object	$v_\odot$ (kms^{-1})	v_{lg} (kms^{-1})	z_{lg}	σ (kms^{-1})
A1631	4024±14	3855	0.01285	251±17
A496	9946±28	9827	0.03276	279±35
A754	16430±19	16196	0.05399	305±24
A957	13366±24	13170	0.04390	333±30
A978	16168±17	15953	0.05318	250±21
Corwin #1	18191±25	18021	0.06007	304±31
Corwin #2	9966±13	9702	0.03234	240±16
NGC1316	1793±11	1650	0.00550	241±14
NGC1600	4776±22	4688	0.01563	340±27
NGC5419	4071±15	3897	0.01299	315±19
NGC4696	2933±22	2697	0.00899	286±27

Errors have been calculated with σ^{rep} = 205 kms^{-1}.

Unlogged channel size : 0.75 Å
Logged channel size : 38.6 kms^{-1}
Total channel number : 1024

Low wavenumber cut-off : 9-14 (k_{low})
High wavenumber cut-off : 200 (k_{high})

Correlation filter : 7,8,100,200
Cosine-bell : 51
Peak fit : ± 15 points

Table 4.3.2

Description of Objects

Object	Dwell (seconds)	S/N	Obj./Sky	Counts/Pixel (photons)
A1631[1]	6000	17.1	4.8	352
A496	11400	15.1	3.5	293
A754	15000	14.5	2.8	283
A957	9000	13.7	3.4	245
A978	14000	16.6	3.8	349
Corwin #1	15451	16.2	3.8	352
Corwin #2	9000	19.1	6.3	423
NGC1316	1200	29.3	-	860
NGC1600	3000	16.2	15.6	280
NGC5419	5700	18.4	10.3	370
NGC4696	4400	22.8	-	522

Description of Templates

Template	Dwell (seconds)	S/N	Type	Counts/Pixel (photons)
1	1500	50.1	K0 III	2506
2	1000	59.4	K0 III	3530
3	1500	40.5	K0 III	1642
4	3500	35.8	K0 III	1281
5	1500	31.9	G8 III	1018
6	1500	51.1	K0 III	2607

Table 4.3.3

Comparison with published results

	SAAO		MK[1]		Other	
Object	v_{lg}	σ	v_{lg}	σ	v_{lg}	σ
A1631	3855	251	3840	249±26		
A496	9827	279	9750	254±27	9780[2]	
A754	16196	305	16170	353±32		
A957	13170	333	13290	311±29	13110[2]	
A978	15953	250			15810[2]	
Corwin #1	18021	304				
Corwin #2	9702	240				
NGC1316	1650	241			1632[3]	240±20[4]
NGC1600	4688	340	4620	363±28	4743[3]	332±12[5]
NGC5419	3897	315			4095[3]	
NGC4696	2697	286			2690[3]	

1. Malumuth & Kirshner (1985)
2. Hoessel, Gunn & Thuan (1980)
3. Reference Catalogue
4. Bosma, Smith & Wellington (1985)
5. Davies et al (1983)

5 CHAPTER FIVE : THE DUMB-BELL GALAXY IC2082

5.1 INTRODUCTION

5.1.1 Previous Investigations

Faber, Burstein & Dressler (1977) were the first to look for velocity dispersion variations in a cD galaxy. However, the conclusions of their study of A401 were limited by large uncertainties in the observations. The only detailed study of a cD galaxy is that of Dressler (1979, 1981), where an attempt is made to compare the internal dynamics of a cD galaxy with the associated cluster environment. The need for more observations of supergiant galaxies is therefore acute.

Dressler studied the archetypal cD galaxy in the cluster A2029. The velocity dispersion was found to rise markedly with distance from the nucleus. This result contradicted expectations based on plausible single component dynamical models of the system [with constant M/L and isotropic velocity dispersions]. A three component dynamical model was produced to account for this behaviour: a bright elliptical galaxy was placed in a luminous halo of stellar debris from cannibalised galaxies, surrounded by a dark component of cluster binding material. Such a model represents a compromise between tidal stripping [Richstone (1976)] and galactic cannibalism [Ostriker & Hausman (1977)].

There are two pieces of evidence, in particular, which suggest that cD galaxies are very different from normal ellipticals: the frequent occurrence of multiple nuclei and the tendency of cD galaxies to be specially located within clusters. Is there some common link between these characteristic features?

On the assumption that multiple nuclei galaxies were bound systems, Jenner (1974) obtained estimates of cD galaxy masses. However, the physical association of multiple nuclei has recently been questioned by Tonry (1984, 1985) and Merritt (1984b), since the velocity differences between multiple nuclei are consistent with typical cluster velocity dispersions [Smith et al (1985)], but the M/L ratios of the parent galaxies are typical of normal ellipticals [Tonry (1984)]. The systems are, therefore, unlikely to be bound - but current explanations of this association are nevertheless made in terms of dynamical processes [Merritt (1984b), Tonry (1985)]. A number of authors have noted that cD galaxies are: centrally located [Carter & Metcalfe (1980)]; at the kinematical cluster centre [Quintana & Lawrie (1982), Beers et al (1984)]; associated with density enhancements in the cluster [White(1978), Dressler (1978a), Beers & Geller (1983)]. If a cD galaxy is at both the kinematical and physical centre, then it is probably at the bottom of the cluster potential well. Both the frequent occurence of multiple nuclei and the special location of cD galaxies therefore suggest that the properties of cD galaxies are intimately linked with the dynamical processes in a cluster of galaxies [Richstone (1976), Hausman & Ostriker (1978), Merritt (1984a)].

To examine these characteristics, this study includes observations of two multiple nuclei galaxies and one D galaxy located away from the cluster centre. The first of the multiple nuclei galaxies is the subject of this chapter: IC2082.

5.1.2 IC2082

The giant dumb-bell galaxy IC2082 lies towards the centre of a Bautz-Morgan type I-II cluster in Doradus [Sersic (1961)]. A photograph of the central region of the cluster is reproduced as figure 5.1.1 and the dumb-bell galaxy as figure 5.1.2. The cluster as a whole is included as figure 5.5.1 and a further print may be found in Westerlund & Smith (1966). The IC2082 cluster has a well developed core and is very regular [Dressler, Thompson & Schectman (1985)].

Dressler (1980b) reports the IC2082 cluster as DC 0428-53 and types the central galaxy [#45] as "D". The term BN [for brighter nucleus] is used throughout this text to describe the D galaxy part of the IC2082 dumb-bell system - even in situations where the whole galaxy is under discussion, rather than just the nucleus. The secondary nucleus is typed "E" and is referred to as the FN [for fainter nucleus]. The separation of the nuclei is approximately 12 arcsec on the sky.

IC2082 has an extended diffuse envelope which can be traced out to over 3 arcmin [190kpc]. The envelope is elongated [E3-E4] with a major axis position angle of 140°, which quite closely matches the line

Figure 5.1.1 Central Region of the IC2082 Cluster

WK3ABS

Figure 5.1.2

IC2082 Dumb-bell Galaxy

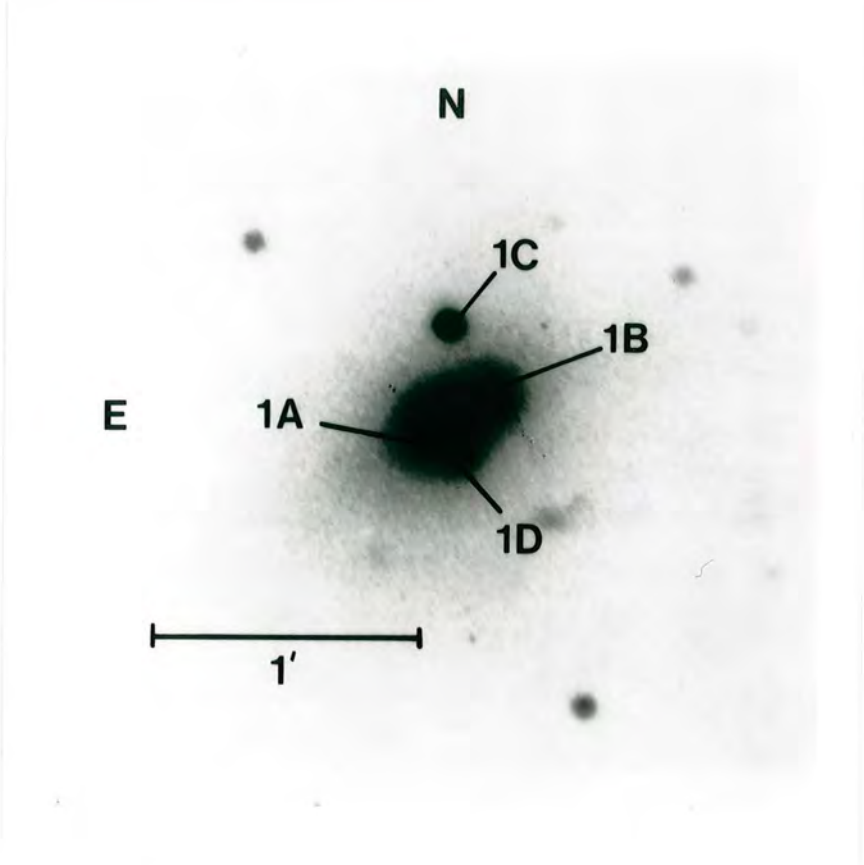

The print is taken from a prime focus IV-N plate.

1A	:	FN	1C	:	star
1B	:	BN	1D	:	star

SARAAC

defined by the two nuclei. Some of the elliptical appearance of the IC2082 envelope is due to the superposition of the secondary E galaxy on the primary D galaxy. Photometry carried out for this work suggests the separated images are rather less elliptical in the central regions [E1-E2].

Inspection of figure 5.1.2 shows several objects superimposed on the central D galaxy. The two nuclei are labelled 1A [BN] and 1B [FN]. The two other bright images, 1C and 1D, are foreground stars. The galaxy has been identified with the extended radio source Pks 0427-53.9 [Christiansen et al (1977)] and the cluster has an unusually high number of galaxies with active galactic nuclei [Dressler, Thompson & Schectman (1985)].

Velocities presented in section 5.8.5 [from Ellis et al (1984)] show that IC2082 is quite precisely at the kinematical centre of its cluster. In their analysis of the Dressler (1980b) catalogue, Beers & Geller (1983) note the IC2082 cluster as having two D galaxies, both at local density maxima. The second D galaxy corresponds to a sub-condensation of galaxies about 13 arcmin to the north of IC2082, centred on galaxy #4 in figure 5.5.1 [Dressler: #81]. The cluster galaxies within 8 arcmin of IC2082 form a flattened distribution approximately aligned with the major axis of IC2082.

IC2082 therefore provides a very interesting candidate for observation: it is a centrally located D type galaxy with an extended envelope and dumb-bell structure. Investigation therefore promises to provide insight into not only the

rotational and kinematical behaviour of D galaxies, but may also help to understand the properties of multiple nuclei systems. Subsequent sections describe the observations, the results, the cluster parameters and a dynamical model used for interpretation.

5.2 SPECTROSCOPIC DATA

The spectroscopic observations were made during January 1980 at the Anglo-Australian Telescope. Table 5.2.1 gives details of the observations.

The slit was oriented to lie along the line joining the two nuclei, which also corresponds to the major axis of the D galaxy envelope. During the nights of the observations the seeing was 3.5 arcsec FWHM, which is less than the data increment size of 5 arcsec. Because of the relatively large slit width, stars were trailed when template observations were made.

The redshift of IC2082 is 0.04, which produces a wavelength offset of 200 Å at 5000 Å. The grating was therefore tilted for template observations, so that the overlap between the rest frame spectra of the template and object was maximised. The spectra cover the region from the Ca H and K lines to the Mgb triplet.

Data reduction techniques have been dealt with in previous chapters. Table 5.2.2 lists the positions of the objects observed.

Table 5.2.1

Observational Set-up

Nights	: 3	
Dates	: 13,15,16-Jan-80	
Telescope	: 3.9m AAT	
Spectrograph	: RGO	
Detector	: IPCS	
Grating	: 1200B	
Dispersion	: 33 Å/mm	
Data Window	: 1020 x 40	
Spatial Resolution	: 5.0 arcsec/increment	
Spectral Resolution	: 2.4 Å FWHM	
Slit Width	: 6.7 arcsec	
PA of Slit	: 128°	
Wavelength Range	: 4320 Å - 5550 Å	[IC2082]
	: 4200 Å - 5430 Å	[templates]
Observatory	: 149°03'58" E	
	: -31°16'37" N	

Table 5.2.2

Observations

Object	RA (1950)	DEC	l^{II} (deg)	b^{II} (deg)
IC2082	$04^h28^m00^s$	-53°56'11"	262.42	-42.35

	Template		RA (1950)	DEC
1	SAO233152	(HD22231)	$03^h31^m05^s$	-50°32'51"
2	SAO249009	(HD28093)	$04^h21^m21^s$	-63°30'17"
3	SAO256145	(HD32440)	$04^h56^m37^s$	-75°00'53"

5.3 SPECTROSCOPIC RESULTS

Forty spatially resolved spectra were obtained. The signal in the outer data increments was judged too poor to analyse and results are therefore presented covering only increments 4-29. The outer increments of this range were combined to improve the accuracy of the results: photon counts in the outer increments of the object spectra then corresponded to 15-20% of sky. Velocity dispersions were calculated only for spectra with photon counts totalling $\geq$ 30-40% of sky.

Results are presented in table 5.3.1. Details of the spectra analysed are included as table 5.3.2 and the results are presented graphically in figure 5.3.1. Interpretation of the spectroscopic results is postponed until a later section. However, some general comments on the form of the results are appropriate.

There is no evidence of any systematic error in the reduction of velocities. Indeed, the velocities at the extremes of the rotation curve are almost identical, indicating that the increments 21-29 are free of significant contamination by light from the FN.

The velocity dispersion profile shows considerable variation. This is primarily accounted for by the presence of a differentially rotating secondary component. Where the rotation curve is rapidly changing [increments 17-18, 20] the measured velocity dispersion is high, because of the superposition of two populations of stars with a

Table 5.3.1

IC2082 Spectroscopic Results

Increment	r (arcsec)	v (kms^{-1})	σ (kms^{-1})	γ	R	χ^2
4 - 8	-48.1	11912 $\pm$ 70	-	-	1.7	-
9 - 11	-29.1	11922 $\pm$ 39	293 $\pm$ 49	0.67	3.8	1.5
12 - 13	-17.1	11986 $\pm$ 23	254 $\pm$ 29	0.85	7.1	1.4
14	-10.0	11955 $\pm$ 23	297 $\pm$ 29	0.97	7.2	1.3
15	-5.0	11982 $\pm$ 13	269 $\pm$ 16	0.97	13.3	1.6
16	0.0	12019 $\pm$ 12	277 $\pm$ 15	1.00	14.0	2.3
17	+5.0	11967 $\pm$ 16	308 $\pm$ 20	0.96	10.9	1.8
18	+10.0	11797 $\pm$ 14	271 $\pm$ 18	0.99	12.1	1.7
19	+15.0	11802 $\pm$ 13	237 $\pm$ 16	0.98	13.6	1.6
20	+20.0	11861 $\pm$ 23	310 $\pm$ 29	0.99	7.3	1.2
21 - 22	+27.2	11978 $\pm$ 31	306 $\pm$ 39	0.85	5.1	1.4
23 - 25	+39.5	11922 $\pm$ 30	226 $\pm$ 38	0.68	5.2	1.4
26 - 29	+56.4	11972 $\pm$ 44	-	-	3.2	-

Velocities for 4-8 and 26-29 are from cross-correlation.

Table 5.3.2

IC2082 Data Statistics

Increment	Dwell (seconds)	S/N	Object/Sky	Counts/Pixel (photons)
4 - 8	11400	4.7	0.16	157
9 - 11	11400	7.9	0.38	224
12 - 13	11400	11.7	0.79	309
14	11400	13.7	1.56	307
15	11400	26.0	4.25	838
16	11400	42.1	9.93	1956
17	11400	26.5	4.38	862
18	11400	26.7	4.42	871
19	11400	22.5	3.33	657
20	11400	11.1	1.16	229
21 - 22	11400	9.9	0.64	250
23 - 25	11400	7.8	0.38	217
26 - 29	11400	5.0	0.19	152

Scale at cluster : 0.944 arcsec/kpc [local group].

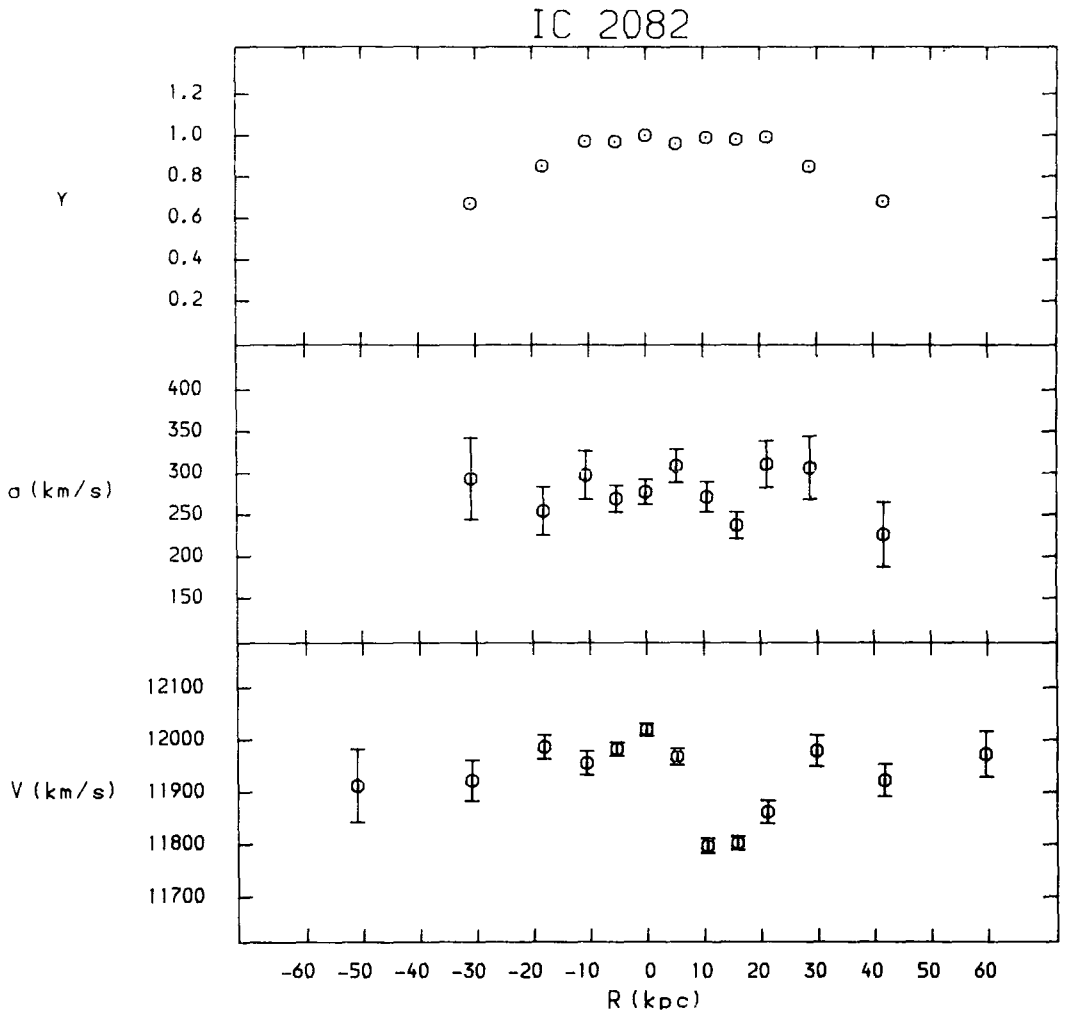

Figure 5.3.1 Spectroscopic Results for IC2082

Table 5.3.3

Description of Templates

Template	Dwell (seconds)	S/N	Type	Counts/Pixel (photons)
1	2029	43.7	K3 III[1]	1912
2	2200		G7 III[1]	
3	1000		K0[2]	

1. Bright Star Catalog.
2. IPCS log

Unlogged channel size	:	0.6 Å
Logged channel size	:	32.5086 kms^{-1}
Total channel number	:	2048
Low Wavenumber Cut-off	:	12-18 (k_{low})
High Wavenumber Cut-off	:	300 (k_{high})

significant relative velocity. For data increments in flat portions of the rotation curve, there is no evidence of systematic errors in the estimation of velocity dispersions. Comparison of velocity dispersions calculated by different reduction methods showed an average difference of less than 3 kms^{-1} between the Fourier Difference, Fourier Quotient and cross-correlation methods.

The data obtained from this study were not spectrophotometric, so no analysis will be presented for the line-strength, γ. Except for the outer increments, where sky-subtraction may be in error, the γ parameter is remarkably constant. This shows that the reduction is consistent [and the velocity dispersions are therefore good estimates] and indicates that there is certainly no large change in line-strength across the face of the galaxy, even when the light is dominated by the FN. Note that, had the γ parameter been constrained to be constant, as in Dressler (1979), the resulting velocity dispersions would have been quite artificially increased in the outer increments.

The mean heliocentric velocity of IC2082 (BN) is calculated as:

$$cz_{\odot} = 12018 \pm 25 \text{ kms}^{-1}$$

This is to be compared with the Reference Catalogue estimate of 12088 ± 270 kms^{-1}. The nuclear velocity corrected to the local group is 11799 kms^{-1}, which provides a scale at IC2082 of 0.944 arcsec kpc^{-1}. Heliocentric and local group corrections were made using a program written by the author with template

radial velocities taken from the "General Catalogue of Stellar Radial Velocities", R E Wilson (1963).

5.4 GALAXY CLUSTER CORE RADII

Later in this chapter, models are used to test whether the kinematics of the stars in IC2082 might be affected by their cluster environment. A mathematical form must be chosen to represent the distribution of the mass associated with this cluster background, and should reproduce the observed distribution of galaxies. In addition, the distribution should be simple to incorporate into a dynamical model. Various alternative forms are used in the literature [from Zwicky (1957) onward], but an analytical core radius parameterisation is well suited to the analysis here. Semeniuk (1982) provides a recent discussion of the techniques available for galaxy core radius estimation.

Examination of published estimates of cluster core radii shows some disagreement between authors. An attempt is therefore made in this section to reconcile some of these differences, so that it will be possible to obtain an idea of the confidence that may be placed on the value determined in this work for the core radius of the IC2082 cluster - which is a crucial element in the dynamical modelling of the galaxy velocity dispersion profile.

5.4.1 The Core Radius

The definition used here of the core radius, r_{core}, of a surface density distribution $\Sigma(r)$ is as that value of r for which $\Sigma(r_{core}) = 0.5\,\Sigma(0)$.

Many galaxy clusters may be represented [Dressler (1978b)] by an approximation to the King set of numerical surface density distributions [King (1972)].

$$\Sigma(r) = \frac{\Sigma(0)}{\left[1 + \left(\frac{r}{r_{core}}\right)^2\right]} \qquad 5.4.1$$

Ring counts may then be fitted to the integrated form of 5.4.1:

$$\Sigma'(r_u, r_l) = \frac{\Sigma(0)\, r_{core}^2}{r_u^2 - r_l^2} \ln\left[\frac{\{1 + (r_u/r_{core})^2\}}{\{1 + (r_l/r_{core})^2\}}\right] \qquad 5.4.2$$

where,

r_u = radius of upper ring boundary
r_l = radius of lower ring boundary

Note that the forms 5.4.1 and 5.4.2 may be made closely equivalent by the use of an effective radius:

$$r_{eff} = \sqrt{\tfrac{1}{2}\,(r_u^2 + r_l^2)}$$

5.4.2 Cluster Core Radii Data

A survey of the literature concerning cluster core radii for rich clusters shows considerable lack of agreement between authors [Dressler (1984b)]. In order to assess whether these discrepancies are real, or are the result of differing data reduction procedures, data from three studies was analysed. The studies were Austin & Peach (1974), Bahcall (1975) and Dressler (1978b) [AP74, B75 & D78]. Some additional results are also included in this discussion, derived from data in Green (1977) [G77] and Semeniuk (1982) [S82].

Surface densities were fit to the function defined in equation 5.4.2. Each residual in the fit was weighted according to the Poisson error expected for the absolute number of galaxies used to calculate the residual.

Study	r_{core} (Mpc) (this work)	r_{core} (Mpc) (original)	number of clusters
B75	0.36±.08	0.25±.04	11
AP74	0.31±.07	0.38±.11	9
D78	0.41±.15	0.45±.09	11
B75+AP74+D78[1]	0.36±.04	0.36±.08	-
G77	0.36	-	4
S82	-	0.35±.22	9

1. The error quoted on the mean core radius is the error on the mean of the three samples.

The core radius derived from Green (1977) was calculated by the author from the composite surface density distribution of Klemola 44, Pks 2354-35, Sersic 40/6 and A1146.

The re-analysis produces a significant improvement in the agreement of the sample means of the three studies analysed in detail. This shows that some of the scatter between authors is certainly due to different reduction procedures. Rich clusters have an average core radius of approximately 360 kpc, with a real scatter of at least 100 kpc.

5.4.3 The IC2082 Cluster Core Radius

Sersic (1961) gives radial number counts for the IC2082 cluster. These counts were analysed in the same way as the data in the preceding section, giving: r_{core} = 5.2 arcmin = 0.33 Mpc. The IC2082 photometry described in section 5.6 consists of photographic isophotal B magnitudes. Star-galaxy separation was performed automatically using the profile slope parameter defined by Godwin (1976). The critical profile slope was taken as -0.35. Ring counts were then calculated from 0.2 Mpc annuli centred on IC2082. All galaxies with absolute luminosities greater than $M_B = -19^m.0$ were included in the count [cf Green (1977)]. A background correction was computed from deep number counts supplied by the Durham Cosmology Group [Shanks et al (1984)]. Fitting the resulting surface density distribution gave: r_{core} = 6.3 arcmin = 0.40 Mpc.

Figure 5.4.1

Galaxy Cluster Surface Density Distributions

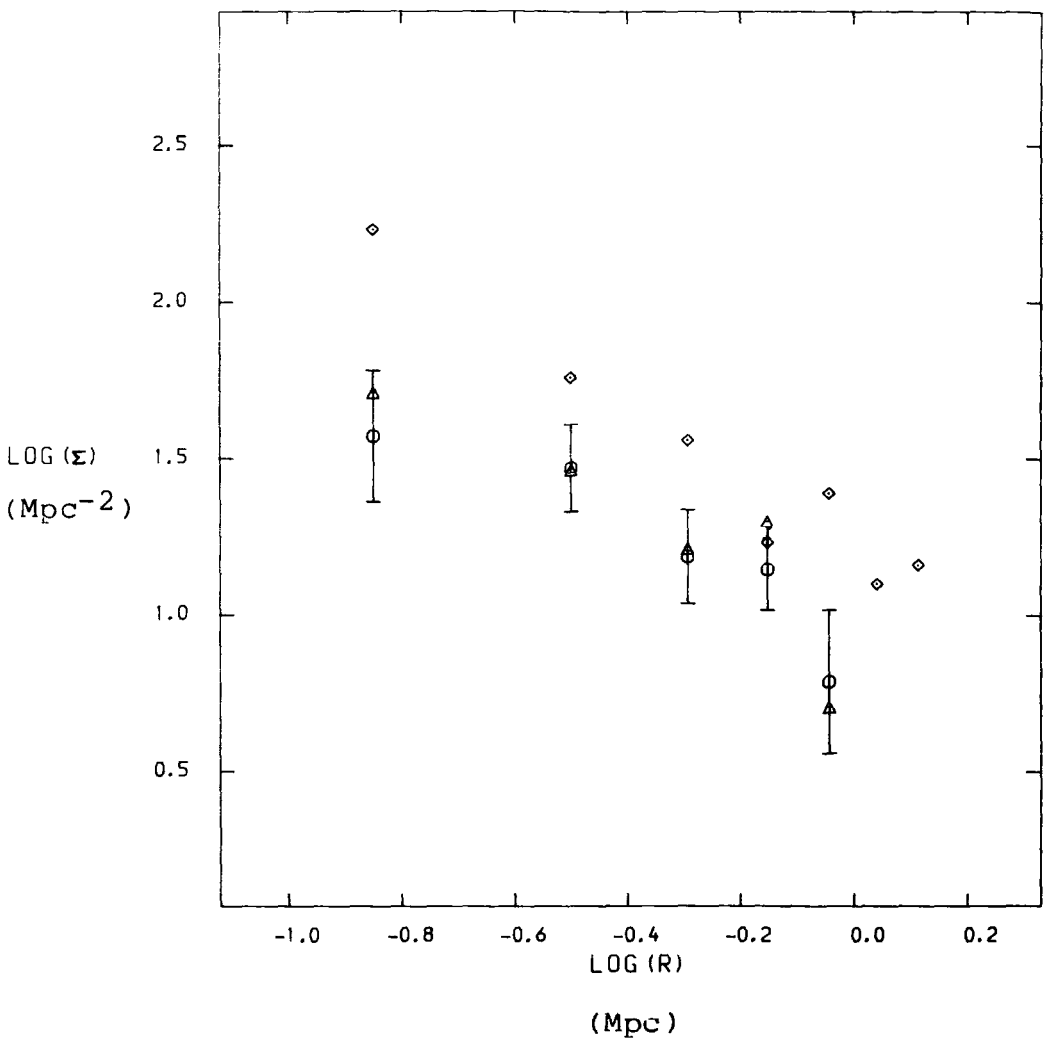

IC2082 : o
Sersic 40/6 : ◇
Pks 2354-35 : △

All galaxies brighter than $M_B = -19^m.0$ are included. The counts are binned into 0.2 Mpc annuli and are plotted against r_{eff}.

The core radius of the IC2082 cluster used in the dynamical model calculations was taken to be the average of the two estimates obtained in this section:

$$r_{core}\ (IC2082) = 365 \pm 50\ kpc$$

Figure 5.4.1 shows the IC2082 surface density distribution, compared with those of Green (1977). The Green surface density distributions include all galaxies brighter than $M_{B27} = -19^{m}.0$.

5.5 IC2082 CLUSTER VELOCITY DISPERSION

The velocity dispersion of the IC2082 cluster was calculated from data supplied by Ellis [priv.comm.] and since published in greater detail in Ellis et al (1984).

Table 5.5.1 lists the velocity information available. For calculation of cluster velocity dispersions the relativistic velocity should be used:

$$v_{rel} = c \cdot \left[\frac{(1 + z)^2 - 1}{(1 + z)^2 + 1} \right] \qquad 5.5.1$$

so, a relativistic velocity increment is:

$$\Delta v_{rel} = \Delta v_{cz} / (1 + z) \qquad 5.5.2$$

Table 5.5.1

Velocities in the IC2082 Cluster

Object		AAT[1]	AAT[2]	SAAO[3]	$cz_{\odot}$
E84	D80	(kms^{-1}/R)	(kms^{-1}/R)	(kms^{-1}/R)	(kms^{-1})
3	43	12108/6.0	12165/2.9	12106/4.0	12107
1B(FN)	46	11869/4.1	11800/13[4]	-	11817
32	25	12968/4.1	-	-	12968
34	29	11137/4.9	-	-	11137
38	28	10523/5.2	-	-	10523
1A(BN)	45	-	12019/14[4]	-	12019
4	81	-	12844/5.3	-	12844
14	64	-	-	12501/4.8	12501
5	101	-	-	12867/4.5	12867
19	68	-	-	12481/4.0	12481
23	57	11676/3.1	-	-	11676
39	27	12008/3.1	-	-	12008
18	30	11126/3.7	-	-	11126
11	40	13011/3.9	-	13028/2.6	13018
8	60	-	11759/3.5	-	11759
7	61	-	12607/3.0	12532/3.6	12566
6	62	-	-	10838/3.4	10838
59	56	12799/2.6	-	-	12799
10	26	11811/2.1	-	-	11811
9	16	12994/2.7	-	-	12994

E84 : Ellis et al (1984)
D80 : Dressler (1980b)

1. Ellis (priv.comm.) : E84
2. Carter (priv.comm.) : E84
3. Green (priv.comm.) : E84
4. this work

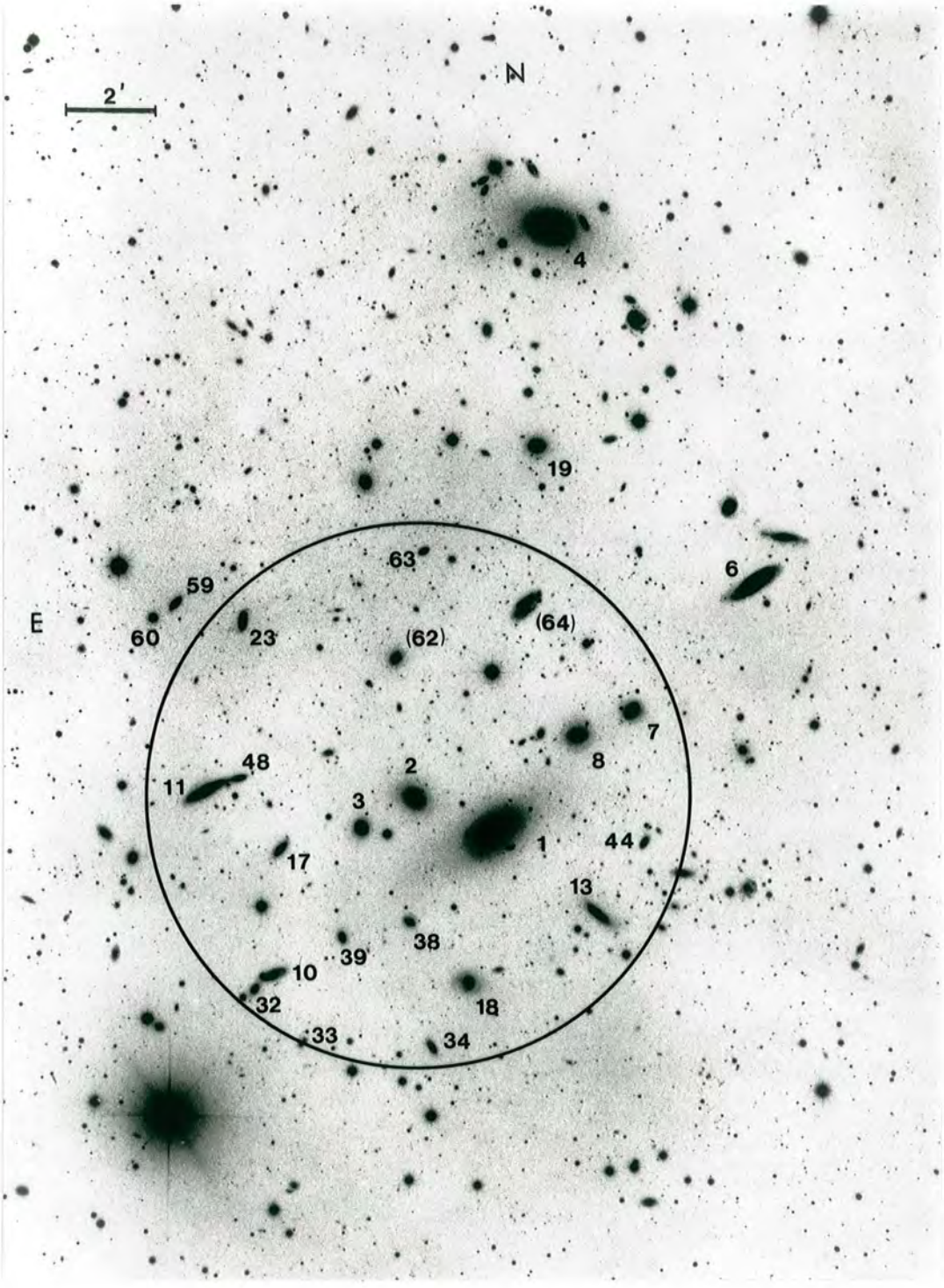

Figure 5.5.1 IC2082 Cluster

This figure is taken from a high contrast print, derived from a sky-limited IIIa-J plate [reproduced in Ellis et al (1984)]. Galaxies with measured velocities are indicated.

Various sub-samples of the data in table 5.5.1 were examined to ensure that poor, or spurious, data was not biassing the calculation. Sub-samples were defined by eliminating results from spectra whose cross-correlation function had less than a threshold R value. The galaxies observed are noted in figure 5.5.1.

R_{min}	$v_\odot$	σ_{cz}	σ_{rel}	n
4.0	12126 $\pm$ 251	795	765 $\pm$ 175	10
3.0	12015 $\pm$ 187	770	741 $\pm$ 126	17
2.0	12093 $\pm$ 170	760	731 $\pm$ 115	20

For further use, the value adopted for σ_{cl} is 741 $\pm$ 126 kms^{-1}.

A more complete study of the velocity dispersion of the IC2082 cluster is described in Ellis et al (1984). Their results do not differ significantly from this analysis: they quote σ_{cz} = 844 kms^{-1} for a sample including galaxies of all R values.

Note that the value adopted for the radial velocity of the BN is 12018 kms^{-1}, very close to the mean cluster velocity just derived. A study of seven poor clusters of galaxies [MKW & AWM] by Beers et al (1984) also found the D or cD galaxies to be at the kinematic centre of their clusters.

5.6 IC2082 PHOTOMETRY

Photometry of IC2082 is of interest to this study for two reasons: the scale length of the BN must be determined for use in the dynamical model and the total luminosities of BN and FN are required to calculate M/L ratios.

Photometry of the IC2082 cluster has been kindly supplied by Godwin [priv.comm.]. Photographic photometry was available from two AAT plates centred on IC2082. A IIIa-J [J1990] and a IIIa-F [F1991] plate were each reduced using the PDS micro-densitometer at the Royal Greenwich Observatory. The Oxford Galaxy Group photometric reduction package was used for data reduction. The IIIa-J reduction was found to be more satisfactory than the IIIa-F and is used here. The results for IC2082 [BN & FN] are presented in table 5.6.1 and graphically in figure 5.6.1. The photometry has a magnitude zero-point obtained from photometry of the nucleus of IC2082 provided by Green & Dixon [priv.comm.]. These observations consisted of B photoelectric measurements in concentric circular annuli centred on the IC2082 BN. The sky brightness relative to the galaxy images was then calculated to be 22.95 $\pm$ 0.06 B mag arcsec^{-2}. The scan area was centred on IC2082 and covered a square of side 27' 43".

An external check of the accuracy of the photometry is possible, by comparison with observations by Westerlund & Wall (1969), who found V = $13^{m}.69$ within a circular 36 arcsec diameter aperture centred on the BN. From the current photometry, the magnitude of the BN and FN within this aperture is B

Table 5.6.1 IC2082 Luminosity Profile

μ_B (mag arcsec^{-2})	$\sqrt{ab_{BN}}$ (arcsec)	$\sqrt{ab_{FN}}$ (arcsec)
19.75	0.92	-
20.00	1.45	-
20.25	1.89	0.65
20.50	2.15	1.30
20.75	2.55	1.59
21.00	3.11	2.00
21.25	3.58	2.38
21.50	4.37	3.00
21.75	5.36	3.69
22.00	6.08	4.18
22.25	6.84	4.70
22.50	7.64	5.25
22.75	8.58	5.90
23.00	9.53	6.55
23.25	10.74	7.39
23.50	12.16	8.36
23.75	14.06	9.67
24.00	16.14	11.09
24.25	18.30	12.58
24.50	20.61	14.17
24.75	22.93	15.76
25.00	25.36	17.43
25.25	27.47	18.88
25.50	29.39	20.20
25.75	30.96	21.28
26.00	32.67	22.46
26.25	34.42	23.66
26.50	36.05	24.78
26.75	37.80	25.98

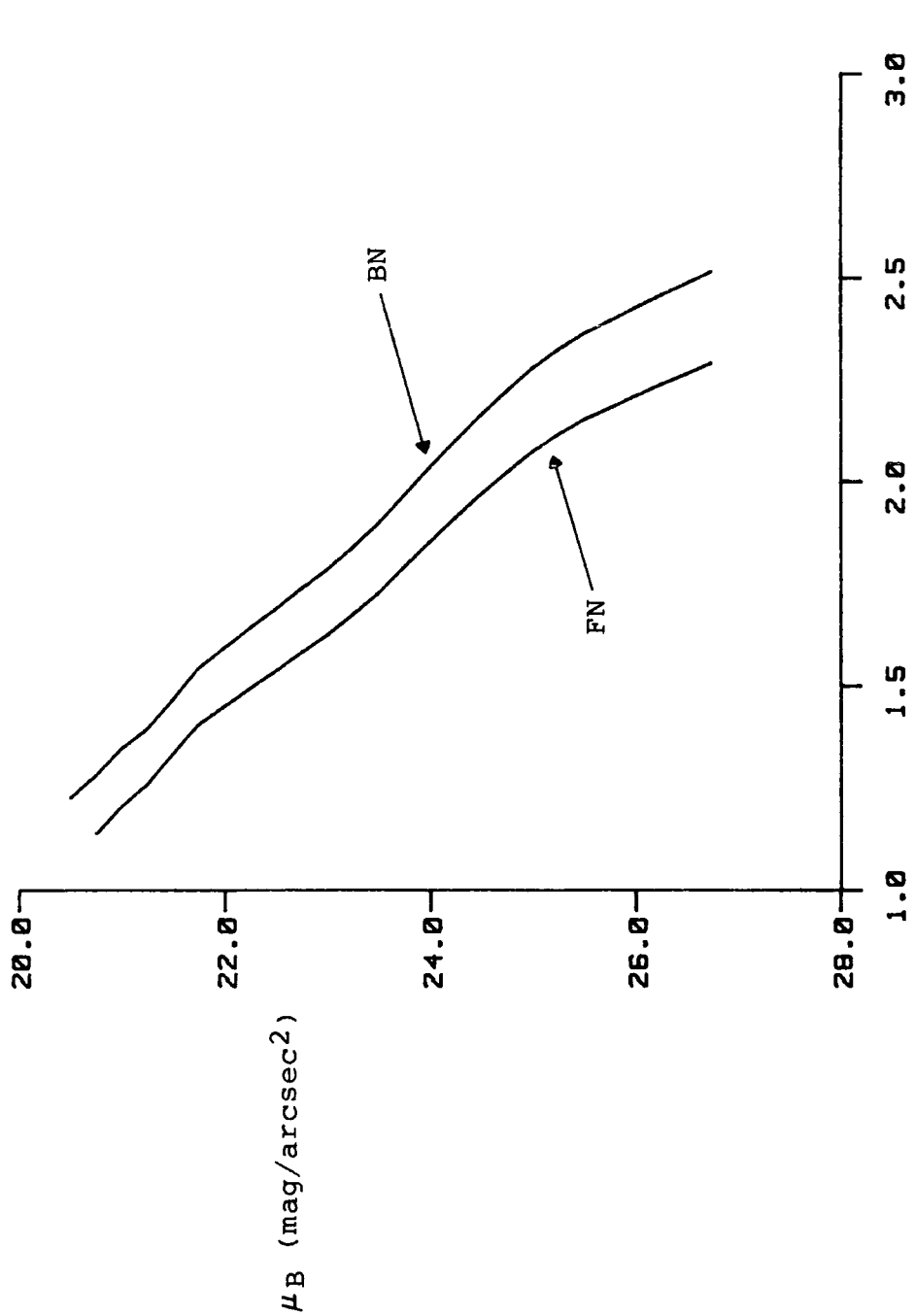

Figure 5.6.1 IC2082 Luminosity Profile

= $14^m.85$. This estimate was calculated correcting for those FN isophotes which lie partially outside the aperture, but neglecting eccentricity. Including extinction and K-corrections, we therefore find: B-V = $1^m.00$. This value agrees excellently with the standard B-V colour for elliptical galaxies of $0^m.98$ [Sandage (1973a)]. Agreement is also excellent with colours of cD galaxies in poor clusters: B-V = $1^m.01 \pm 0.05$ [Schild & Davis (1979)].

Many elliptical galaxies are well fit by an $r^{1/4}$ law luminosity profile [de Vaucouleurs (1948, 1953), Kormendy (1977) and de Vaucouleurs & Capaccioli (1979)]. In addition some D and cD galaxies can be well reproduced by this profile [Schneider, Gunn & Hoessel (1983b), Morbey & Morris (1983), Lugger (1984)]. IC2082 is tolerably well fit by a de Vaucouleurs profile, as can be seen from figure 5.6.1, and an effective radius may be derived using:

$$r_e = \left[\frac{-8.327}{d\mu / d\psi} \right]^4 \qquad 5.6.1$$

where μ is the surface-brightness and $\psi = r^{1/4}$.

	μ_B (mag arcsec^{-2})	r_e (arcsec)
BN	20.50 - 25.25	12.8 ± 0.5
FN	20.75 - 25.25	9.4 ± 0.5

The errors quoted are from a least squares fit over the surface-brightness range specified.

A number of independent estimates have been made of the effective radius of IC2082. The Reference Catalogue gives r_e = 19±4 arcsec and Carter et al (1985) calculate r_e = 29.6 arcsec from R band CCD frames taken at the AAT.

Davies et al (1983) give a relationship between blue magnitude [$-M_B$] and r_e. It is therefore possible to check whether the values determined for the effective radii of the components of the IC2082 dumb-bell system are typical or not. Shown below are the predicted values of r_e for IC2082.

Object	$m_{26.75}$	m_T	M_{BT}	predicted r_e (arcsec)	actual r_e (arcsec)
BN	14.91	14.57	-22.57	8.8	12.8
FN	15.92	15.52	-21.62	5.5	9.4
BN+FN	14.55	14.19	-22.94	-	-

Extrapolation to total magnitude has been estimated as the average of $m_T = m(<r_e) - 0.7526$ and $m_T = \mu(r_e) - 5\log r_e - 3.3885$ [all in arcsec units]. The two estimates agree for the BN, but differ by $0^m.2$ for the FN, indicating that the extrapolation to total magnitude may be invalid for the FN. The distance modulus was corrected to the local group. Note that the Reference Catalogue quotes $B_T = 13^m.9$, which would indicate $-M_{BT} = 23^m.23$.

The value of 12.8 arcsec for the effective radius of IC2082 is adopted as standard. Where conclusions may be significantly affected by an error in this estimate, results are also quoted for 30 arcsec.

Estimates of the effective radius of the components of the IC2082 system, based on current photometry, suggest that the galaxies are rather more extended than expected from the sequence of normal elliptical galaxies studied by Davies et al. Supergiant elliptical galaxies have the flattest luminosity profiles of all elliptical galaxies [Bahcall (1977)] and the larger value of r_e found for IC2082 is confirmation that IC2082 is indeed an extended galaxy.

Estimates of the ellipticity and major-axis position angle for the two components of the dumb-bell were calculated.

Object	ε		PA (deg)		radius (arcsec)	
	J	F	J	F	J	F
BN	0.14	0.18	142	130	4.37	4.49
FN	0.17	0.17	147	127	3.00	2.93

The mean radius of the 26.75 B isophote is 37.80 arcsec for the BN, and 25.98 arcsec for the FN. CCD photometry of IC2082 reported in Carter et al indicates an overall ellipticity of 0.35-0.36, showing the strongly elliptical nature of the outer envelope.

5.7 DYNAMICAL MODELS

The principal result of the observations of IC2082 is that the velocity dispersion profile does not fall off as quickly as an isotropic velocity dispersion, constant M/L, dynamical model would suggest.

A number of mechanisms have been discussed in the literature to account for flat or rising velocity dispersion profiles in elliptical galaxies. The two commonly quoted mechanisms involve relaxing either the assumption of constant M/L, or the assumption of isotropic velocity dispersions.

Allowing M/L to vary is well motivated physically by noting the evidence for dark matter associated with galaxies and galaxy clusters [Rubin, Ford & Thonnard (1978), Rood et al (1972)]. In his study of the cD galaxy in A2029, Dressler (1979) used a multiple component model with varying M/L to explain the rising velocity dispersion profile.

Anisotropy in the space velocity dispersion affects the observed velocity dispersion because a Doppler method only samples the line of sight velocity distribution. Stellar motions along a line of sight through the nucleus will be primarily radial, whereas in the outer regions of a galaxy the observed motions will be primarily tangential. Enhanced tangential motions might therefore be able to explain a flat, or rising, velocity dispersion profile [Tonry (1983)]. Negative anisotropy is required to enhance tangential motion, where anisotropy is defined by $\beta = 1 - \sigma_{tang}/\sigma_{radial}$.

Goodman & Binney (1984) give an example of an accretion mechanism which could do this.

Computer programs were developed by the author to produce two component models with varying M/L. Models of isotropic and anisotropic systems have been developed by collaborators for an independent analysis reported in Carter et al (1985).

A simple model is proposed to predict the velocity dispersion profile. The model has two components with independent mass distributions. The first component represents a normal elliptical galaxy with isotropic velocity dispersions. The density distribution for this component is derived from a de Vaucouleurs luminosity profile [Young (1976)]. A second, non-luminous, component is then introduced with a pseudo-King model density distribution [King (1972)]. This second component represents matter stripped from other cluster galaxies, debris from cannibalised galaxies, or perhaps the material required to bind the cluster.

The purpose of the modelling is to determine the general characteristics of a second component and then to identify this second component with a physical structure [for example, the cluster]. The models attempt to reproduce the observed velocity dispersion profile using the composite nature of the galaxy-cluster mass distribution, but without any reference to the composite nature of the cD luminosity profile [Oemler (1976), Dressler (1979)]. No account is taken of the dynamical effect of the dumb-bell FN component, nor of the elliptical nature of the galaxy outer envelope.

5.7.1 The De Vaucouleurs Component

Firstly, a model of the velocity dispersion for a galaxy having a de Vaucouleurs luminosity profile must be generated and, to do this, the equation of hydrostatic equilibrium was integrated numerically. The scaling in the model is provided by:

r_e : de Vaucouleurs effective radius
M_T : total mass of de Vaucouleurs galaxy
G : gravitational constant

Defining dimensionless quantities:

$s = r/r_e$: radius
$\rho^*_c(s) = \rho_c(s).r_e^3/M_T$: component density
$\rho^*_t(s) = \rho_t(s).r_e^3/M_T$: total density
$v^{*2}_c(s) = v_c^2(s).r_e/(G.M_T)$: space velocity dispersion

The integral form of the equation of hydrostatic equilibrium may then be written:

$$\overline{v^{*2}_c}(s) = \frac{3}{\rho^*_c(s)} \int_s^\infty \frac{m^*_T(s')\ \rho^*_c(s')}{(s')^2}\, ds' \qquad 5.7.1$$

The mass within a radius s is then:

$$m^*_T(s) = 4\pi \int_0^s \rho^*_T(s')\ (s')^2\ ds' \qquad 5.7.2$$

$$= \frac{M_T(s)}{M_T}$$

A finite difference technique was used to integrate the equations, for which functions should be defined at roughly equal intervals in the integrated variable. A logarithmic transformation is appropriate for the Young tabulations: z = ln(s).

$$\overline{v_c^{*2}} = \frac{3}{\rho_c^*(s)} \int_z^\infty m_T^*(z') \rho_c^*(z') e^{-z'} dz' \qquad 5.7.3$$

Both m*(s) and ρ*(s) were taken from Young (1976). The integration techniques were tested by using ρ*(s) to generate m*(s) by a suitably transformed version of 5.7.2. In addition, ρ*(s) was projected to produce a luminosity profile for comparison with a de Vaucouleurs $r^{1/4}$ law. Such numerical tests proved completely satisfactory. Note that, in the first instance, a single component de Vaucouleurs model was generated, for which $\rho_c(s) = \rho_t(s)$.

The space velocity dispersion is $\overline{v_c^{*2}}$. The observed velocity dispersion is a luminosity weighted combination of the space velocity dispersions for all points along the line of sight. Two projected velocity dispersion quantities were therefore calculated to enable a comparison between observation and theory.

Following the nomenclature of Bailey & MacDonald (1981), the quantities calculated were σ^*_{proj} and σ^*_{ap}. $\sigma^*_{proj}(s)$ is the projected line of sight velocity dispersion at a radius s - and $\sigma^{*2}_{ap}(s)$ is the mean of $\sigma^{*2}_{proj}(s)$ over a centred circular aperture of radius s. The quantity σ^*_{ap} is required

only to establish a common velocity dispersion scale between the observations and the dimensionless theory. The increment of data centred on the nucleus has a velocity dispersion determined by $\sigma^*_{ap}(<s)$, whereas the other observations are assumed to be given by $\sigma^*_{proj}(s)$.

In general, the projected stellar velocity distribution resulting from the luminosity weighted combination of a series of gaussian velocity distributions will not be itself gaussian. The quantity of interest to us, however, is not the precise form of the distribution, but its second moment:

$$\sigma^{*2}_{proj}(s) = \frac{\int_0^\infty 1/3\ \overline{v_c^{*2}}(y)\ \rho_c^*(y)\ dt}{\int_0^\infty \rho_c^*(y)\ dt} \qquad 5.7.4$$

where, $y = \sqrt{s^2 + t^2}$

The aperture averaged projected dispersion is defined:

$$\sigma^{*2}_{ap}(s) = \frac{\int_0^s \sigma^{*2}_{proj}(t)\ 2\pi t\ \mu^*(t)\ dt}{\int_0^s 2\pi t\ \mu^*(t)\ dt} \qquad 5.7.5$$

where,

$$\mu^*(s) = -3.33071\ (s^{1/4} - 1) \qquad 5.7.6$$

The quantities $\sqrt{v^{*2}}$ and σ^{*}_{proj} are plotted in figure 5.7.1 and tabulated in table 5.7.1. To show that some elliptical galaxies may be adequately fit by a de Vaucouleurs dynamical model, observations of the giant elliptical galaxy NGC5813 [Efstathiou et al (1982)] have been superimposed on the σ^{*}_{proj} curve. The model calculations agree with Bailey & MacDonald (1981).

The D galaxy in the IC2082 dumb-bell system has a de Vaucouleurs effective radius of 13 arcsec. The data increment size is 5 arcsec and therefore the maximum extent of the nuclear increment is 2.5 arcsec. Model predictions may then be converted to physical units according to:

$$s = 2.5/13.0 = 0.2$$
$$\sigma^{*}_{ap}(\text{central}) = 0.46$$
$$\sigma_{\text{central}} = 277 \text{ kms}^{-1}$$

$$\sigma(s) = \sigma^{*}_{proj}(s) \cdot \frac{\sigma_{\text{central}}}{\sigma^{*}_{ap}(\text{central})} \qquad 5.7.7$$

In the modelling procedure, σ_{central} is simply a scaling factor which may be adjusted as required.

Figure 5.7.1

De Vaucouleurs Velocity Dispersion Profile

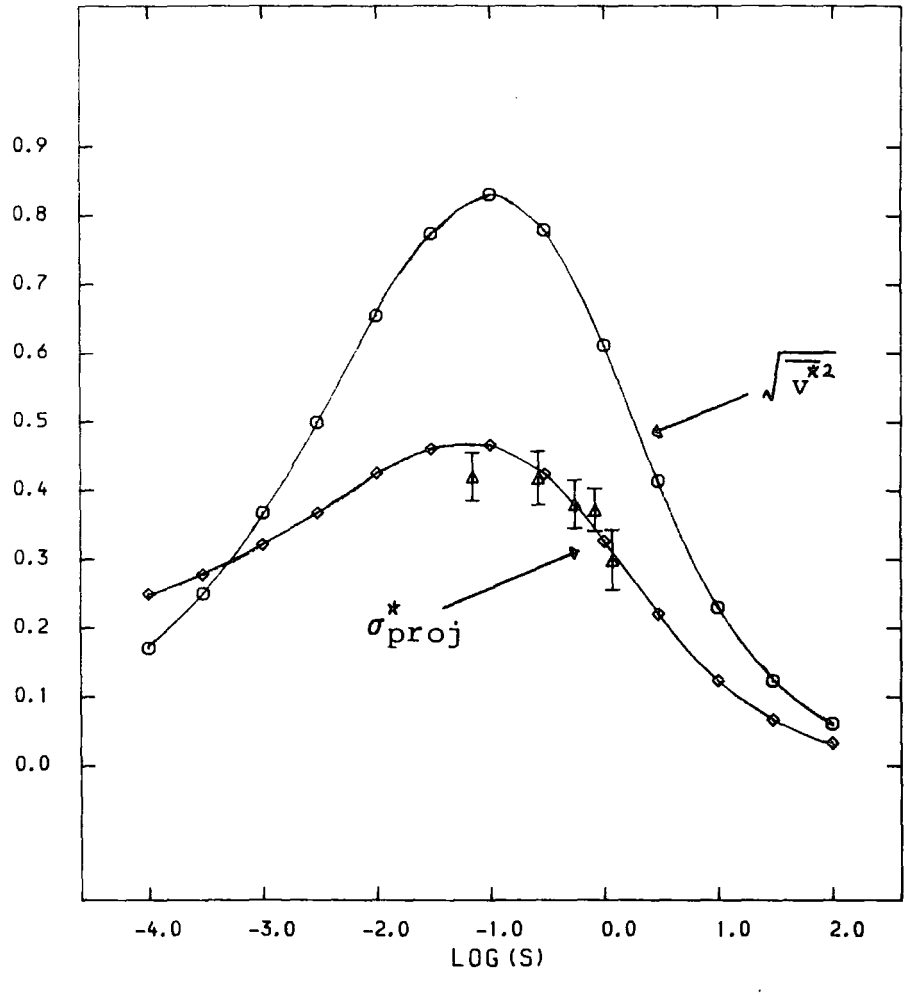

The two dimensionless quantities shown are :

- unprojected space velocity dispersion ($\sqrt{\overline{v^{*2}}}$).
- line of sight projected velocity dispersion (σ^*_{proj}).

Table 5.7.1

De Vaucouleurs Model

s	$\sqrt{\overline{v^{*2}}}$	σ^*_{proj}	σ^*_{ap}
1×10^{-4}	.1709	.2498	.2393
3×10^{-4}	.2503	.2782	.2640
1×10^{-3}	.3674	.3215	.3007
3×10^{-3}	.4993	.3677	.3431
1×10^{-2}	.6546	.4251	.3948
3×10^{-2}	.7745	.4605	.4380
0.1	.8317	.4663	.4615
0.3	.7793	.4238	.4514
1	.6116	.3267	.4100
3	.4141	.2203	.3670
10	.2300	.1237	.3409
30	.1237	.0670	.3353
100	.0611	.0332	.3348

$s = r/r_e$

Equation 5.7.4 defines σ^*_{proj}.
Equation 5.7.5 defines σ^*_{ap}.

A mass may be calculated for a de Vaucouleurs galaxy by the following formula:

$$M_T = 2.075 \times 10^{11} . r_e . \sigma_{central}{}^2 . \frac{\sigma^*_{ap}{}^2(\varpi)}{\sigma^*_{ap}{}^2(central)} \qquad 5.7.8$$

where:

M_T	has units	$M_\odot$
r_e	has units	10 kpc
$\sigma_{central}$	has units	100 kms^{-1}

Note that $3.\sigma^*_{ap}{}^2(\varpi) = 0.3361$ [Bailey & MacDonald (1981) or Young (1976)].

For the case of IC2082, the following equation results:

$$M_T(M_\odot) = 1.099 \times 10^{11} . r_e(10kpc) . [\sigma_{central}(100kms^{-1})]^2$$

With r_e = 13 arcsec [13.77 kpc] and $\sigma_{central}$ = 277 kms^{-1} the mass of the BN is therefore 1.2×10^{12} $M_\odot$. The mass of the FN is 5.9×10^{11} $M_\odot$ with r_e = 9 arcsec [9.53 kpc] and $\sigma_{central}$ = 237 kms^{-1}. σ^*_{ap}(central) is a function of r_e, but a weak one for s in the range 0.1 to 0.3.

5.7.2 The King Component

The second component in the model has a density distribution similar to that of a galaxy cluster. The King form has been chosen as being both appropriate and mathematically simple. An approximation is used to represent the radial density distribution of a King model [King (1972)].

$$\rho_K(r) = \frac{9\,\sigma_K^2}{4\pi G\, r_{core}^2}\left[\,1 + \left(r / r_{core}\right)^2\,\right]^{-3/2} \qquad 5.7.9$$

where, r_{core} is the core radius of the King component and σ_K is its central velocity dispersion. This approximation reproduces a King model quite closely in the region of the velocity dispersion data to be modelled [$r/r_{core} \leq 0.1$] and is adequate considerably beyond that region.

The King component may be combined with the de Vaucouleurs component after a common density scale has been established. This is done by eliminating the gravitational constant, G, between the de Vaucouleurs and King expressions for density.

Thus:

$$\rho_k(s) = \frac{9\,\sigma_K^2\, r_e^2\, \sigma_{ap}^{*2}(central)}{4\pi\, \sigma_{central}^2\, r_{core}^2}\left[\,1 + \left(r_e s / r_{core}\right)^2\,\right]^{-3/2} \qquad 5.7.10$$

A central density may therefore be defined:

$$\rho_o^* = \frac{q\,\sigma_K^2\,r_e^2\,\sigma_{ap}^{*2}(central)}{4\pi\,\sigma_{central}^2\,r_{core}^2} \qquad 5.7.11$$

The density may then be integrated to obtain:

$$m^*(s) = 4\pi\rho_o^*.\,(s')^3\,ln\left[\left(\frac{s+t}{s'}\right) - \left(\frac{s}{t}\right)\right] \qquad 5.7.12$$

where,

$$s' = r_{core}/r_e$$

$$t = \sqrt{s^2 + (s')^2}$$

This mass component may then be included in equation 5.7.3. Models may now be generated for combinations of the following parameters:

de Vaucouleurs effective radius	:	r_e
de Vaucouleurs central dispersion	:	$\sigma_{central}$
King core radius	:	r_{core}
King central dispersion	:	σ_K

If the King component is identified with the galaxy cluster itself then <u>all these parameters are directly observable</u>.

Applications of this modelling technique to the IC2082 system are presented in section 5.8.3.

5.8 DISCUSSION

The conclusions of the IC2082 study are described in three sections and summarised in a fourth. Firstly, the relative rotation of the two nuclei of the dumb-bell system is described, then the search for envelope rotation and finally the velocity dispersion profile [which includes the dynamical modelling].

5.8.1 Relative Rotation

Inspection of figure 5.3.1 shows that the D galaxy nucleus of IC2082 has a somewhat higher velocity than its envelope. Defining the envelope velocity as the mean of the outermost three radial velocity measurements on either side of the nucleus we find:

$$\begin{aligned} v_{BN}\ (BN - \text{envelope}) &= +67\ \text{kms}^{-1} \\ \underline{v_{FN}\ (FN - \text{envelope}) &= -156\ \text{kms}^{-1}} \\ v\quad (BN - FN\ ) &= +223\ \text{kms}^{-1} \end{aligned} \qquad 5.8.1$$

The mean heliocentric velocity of the envelope is calculated to be 11949 $\pm$ 42 kms^{-1}. The velocity dispersion of the IC2082 cluster is 741 kms^{-1} [σ_{Cl}] which gives $v_C/\sigma_{Cl} = 0.2$. This is to be contrasted with the sample of multiple nuclei presented by Smith et al (1985) which were found to have higher relative velocities [comparable with the cluster velocity dispersion].

If cD galaxies grow by the accretion of cluster members it is possible that, as the cD core becomes extended [Hausman & Ostriker (1978)], a compact galaxy may survive disruption until it eventually slows down by dynamical friction [Tremaine (1976)]. Such a system would be a multiple nucleus or dumb-bell system, depending on the relative sizes of cannibal and victim.

For a circular orbit, viewed edge-on:

$$\tau = 2\pi . (r_p/v_p) \qquad 5.8.2$$

$$v_c = [G.M(<r_c).(v_p/r_p)]^{1/3} \qquad 5.8.3$$

$$r_c = r_p.(v_c/v_p) \qquad 5.8.4$$

where, τ is the orbital period, r_p the [observed] projected radius and v_p the [observed] projected velocity. The FN is assumed to have a speed, v_c, in a circle of radius r_c about the BN. Assuming circularity, it can be seen from equation 5.8.2 that the period is directly calculable, and for IC2082 is 5.0×10^8 years [r_p = 12.7 kpc and v_p = 156 kms^{-1}].

Equations 5.8.3 and 5.8.4 are coupled through the mass $M(<r_c)$, but may be solved given a model of the mass distribution. Both r_e and $\sigma_{central}$ have been determined for IC2082, so a model is available of the distribution of mass: r_c and v_c can therefore be calculated.

The procedure for solution is: calculate r_c as that value of radius [s] for which M(<s) from a de Vaucouleurs model produces a projected velocity of v_p, at a projected radius of r_p. This amounts to the solution of:

$$M^*(<s) = \frac{r_e^3}{G \cdot M_T} \cdot \left[\frac{v_p}{r_p}\right]^2 \cdot s^3 \qquad 5.8.5$$

For IC2082, r_c is calculated to be 27 kpc, compared to the projected separation of only 12.7 kpc. The circular velocity of the FN is then 330 kms^{-1}. Having obtained some idea of the geometry and kinematics of the IC2082 dumb-bell system, we may now estimate how long the merging process is likely to take.

A condition for the survival of the FN in the BN at any given time is that the central density of the FN exceeds that of the ambient BN material. In a King model, where r_{BN} and r_{FN} are the core radii and σ_{BN} and σ_{FN} are the central velocity dispersions, the condition may be written:

$$\frac{\sigma_{FN}^2}{r_{FN}^2} > \frac{\sigma_{BN}^2}{r_{BN}^2} \left[1 + \left(\frac{r_c}{r_{BN}}\right)^2\right]^{-3/2} \qquad 5.8.6$$

It is not clear, however, that this expression will be very meaningful as a guide to when the FN may be considered to have been disrupted. Mergers of galaxies considered by Hausman & Ostriker (1978) and Malumuth & Kirshner (1985) suggested that the merger process is likely to cause an expansion of the dominant galaxy, though the balance between core and

envelope expansion is uncertain. In such a situation, all the elements present in 5.8.6 may be unknown functions of time. However, it is possible to estimate the time taken for the FN to slow down, by consideration of the action of dynamical friction.

Carter et al (1981) present an estimate of the timescale of dynamical friction based on arguments used by Tremaine (1976):

$$\tau_{df} = \frac{M_{BN}(r<r_c)}{M_{FN}} \cdot \tau_{orb} \qquad 5.8.7$$

where τ_{orb} is the orbital period of the FN in its assumed circular orbit about the BN. Tonry (1985) suggests that perhaps 30% of observed multiple nuclei galaxies are actually in bound circular orbits. The masses in 5.8.7 may be approximated by calculating the mass of each galaxy within the separation distance r_c = 27 kpc. Using the effective radii calculated in section 5.6 and central velocity dispersions from table 5.3.1 we find $M_{BN}(<r_c) = 6.8 \times 10^{11} M_\odot$ and $M_{FN}(<r_c) = 4.3 \times 10^{11} M_\odot$. The condition 5.8.7 therefore reduces to $\tau_{df} \geq 1.4\ \tau_{orb}$ [cf Rood & Leir (1979)]. The inequality is introduced into the condition to represent the probable overestimation of the mass of the FN. The timescale for the effect of dynamical friction is therefore $<10^9$ years, rather less than the likely age of the cluster [4.5×10^9 years, Gunn & Gott (1972)].

It has already been noted that the IC2082 nuclear velocity is rather higher than that of the envelope of the galaxy. It is tempting to suggest that this velocity difference may represent a reaction by the core of the D galaxy to the approach of the FN. Hoessel et al (1985) observed four dumb-bell systems and found two to have large relative velocities, whereas the other two did not. The two galaxies with small relative motions showed evidence of tidal distortion of their luminosity profiles. It seems possible therefore, that a combined study of luminosity profiles and rotation curves might be used to establish real physical association for dumb-bell systems.

For two masses conserving angular momentum:

$$\frac{v_{BN}}{v_{FN}} = \sqrt{\frac{M_{FN}}{M_{BN}}} \qquad 5.8.8$$

Using the masses just calculated, the theoretical prediction for the ratio of velocities relative to the centre of mass is 0.8. In fact, the observations give 0.4, showing that the BN has not taken up all the angular momentum contained in the present FN orbital motion. The argument is aspect independent, but neglects completely the effect of the finite extent of the two galaxies and the precise mechanism of energy transfer. A detailed numerical simulation would be required to deal adequately with this problem.

5.8.2 Envelope Rotation

The rotation curve of the IC2082 dumb-bell system is distorted by the presence of a secondary nucleus moving at about 200 kms^{-1} with respect to the D galaxy nucleus. However, it is of considerable importance for this work to examine the rotation curve for evidence of envelope rotation, since this bears on the problem of whether the shapes of apparently elliptical galaxies are supported by rotation or by some other mechanism [Binney (1982) and references therein].

Averaging the two outermost radial velocities and differencing the resulting mean envelope velocities from either side of the nucleus, gives a velocity difference of 43 $\pm$ 68 kms^{-1} over some 92 kpc. Within the limits of the errors, IC2082 does not rotate.

In studies of rotation in elliptical galaxies and elliptical-like spiral bulges [Davies et al (1983)] it is now customary to scale the observed maximum rotation velocity, v_{max}, by the central velocity dispersion, σ_c. This provides a quantity which may be predicted by dynamical models of rotationally supported spheroids with isotropic velocity dispersions [Binney (1978)]. IC2082 therefore has $v_{max}/\sigma_c = 0.08$, with a large uncertainty [0.2].

Figure 5.8.1 is reproduced from data to be found in Davies et al (1983). With an E3.3 envelope IC2082 has a v/σ value which suggests that the ellipticity of the envelope cannot be supported by rotation. Davies et al present a study of a number of faint

Figure 5.8.1

Rotation in cD Galaxies vs Shape

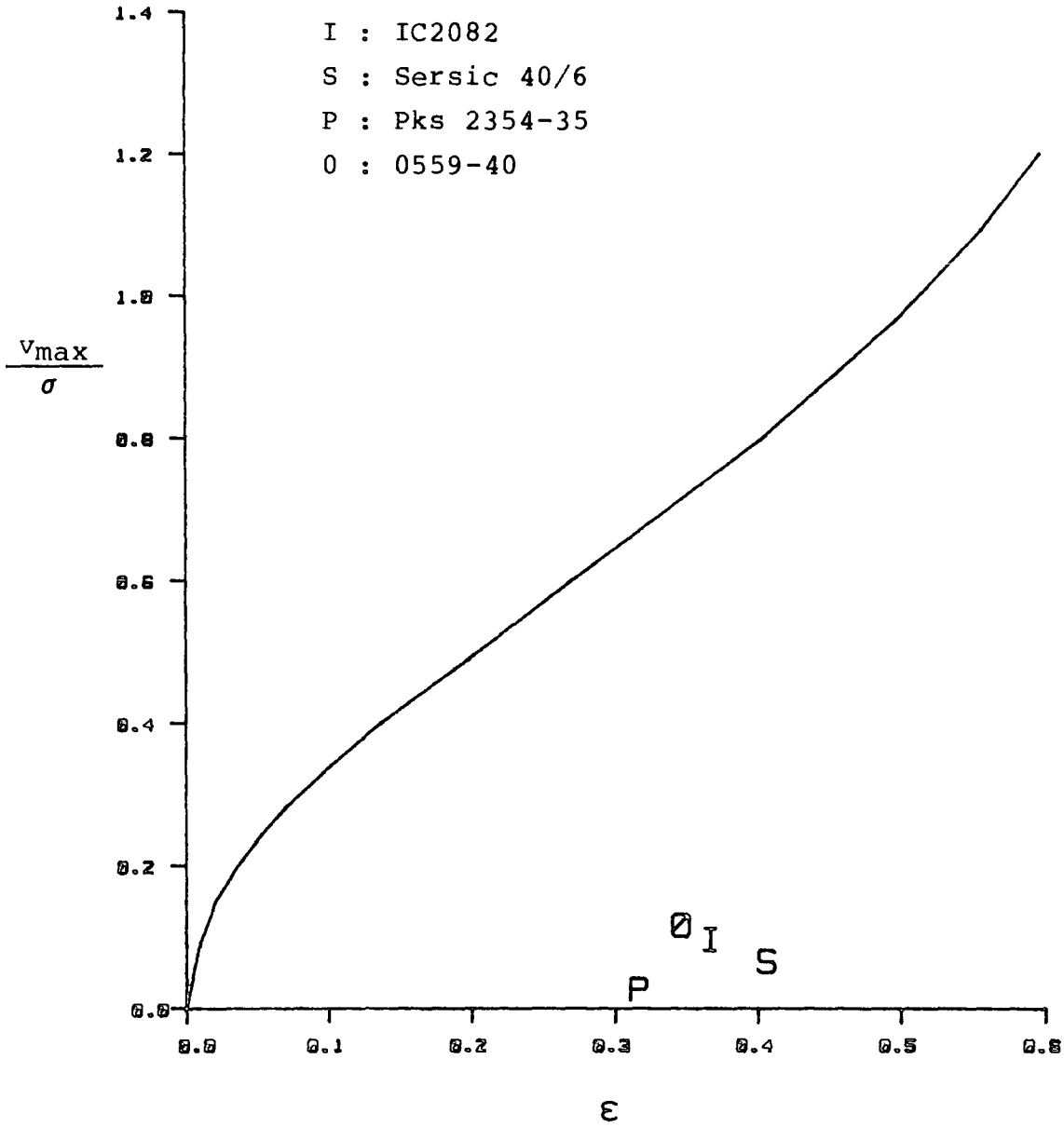

WK3ABR

elliptical galaxies which they include in a compilation of estimates of v/σ , ε and $-M_B$. They examine whether there is any correlation of the dynamical significance of rotation [v/σ] with the absolute magnitude of the galaxy [$-M_B$]. The results show that the brighter the galaxy the less important rotation becomes.

The lack of rotation in IC2082 helps confirm, for D galaxies, a result which has been found for the whole range of normal elliptical galaxies. cD galaxies tend to be more elliptical than first ranked cluster galaxies in non-cD clusters [Leir & van den Bergh (1977)], so the null result found for the rotation of IC2082 is even more striking.

5.8.3 Velocity Dispersions

5.8.3.1 Luminosity - Velocity Dispersion Relationship

Considerable interest has been shown in the form of the relationship between the luminosity of elliptical galaxies and their central velocity dispersions [Faber & Jackson (1976), Terlevich et al (1981), Malumuth & Kirshner (1985)]. How does IC2082 fit into the framework set up by these studies?

The luminosity excesses found for the BN and FN, from the L-σ relations reported in Terlevich et al (1981) and Malumuth & Kirshner (1985) are:

Object	σ_c	$-M_B$	ΔM_T	ΔM_{MK}	$\overline{\Delta M}$
BN	277	22.57[1]	+0.59	+0.96	+0.78
FN	237	21.22[2]	-0.12	+0.22	+0.05

1. B_T : de Vaucouleurs total magnitude.
2. $B_{26.75}$: the FN is a poor fit to an $r^{1/4}$ law.

The two studies do not produce consistent L-σ relationships, but allow a summary of the results for IC2082. The BN has a luminosity which exceeds that expected for its velocity dispersion by $0^m.78$, whereas the FN has almost precisely the luminosity appropriate for its velocity dispersion. This result very much supports the idea that the FN is a normal elliptical galaxy, being consumed by a D galaxy which already has considerable excess luminosity. Malumuth & Kirshner (1985) find their sample of brightest cluster member galaxies to have an average excess of $1^m.22$ in V.

5.8.3.2 Velocity Dispersion Profile

Because of the dumb-bell nature of the IC2082 system it is necessary to exclude from consideration some velocity dispersion measurements. Table 5.8.1 is calculated by excluding data increments 17-20 in table 5.3.1, corresponding to the portion of the velocity dispersion profile contaminated by the FN. The final values in table 5.8.1 were then calculated as a weighted mean of the remaining increment pairs. Note that there is no evidence for a <u>rise</u> in the velocity dispersion with radius.

Table 5.8.1

Velocity Dispersion Profile of IC2082

r (kpc)	σ (kms^{-1})
2.69	277 ± 15
7.35	279 ± 25
23.22	268 ± 26
35.95	266 ± 21

The velocity dispersion profile of IC2082 is plotted in figure 5.8.2. Two model curves [A and B] are also plotted. These models are not attempts to fit the data, but represent interesting special cases.

Model A shows the best estimate de Vaucouleurs velocity dispersion profile [r_e = 13 arcsec]. The IC2082 profile remains very flat and does not show the rapid fall off exhibited by the model. If the effective radius of IC2082 were considerably in error, as suggested by a recent estimate from Carter et al (1985), then the discrepancy between model and observation will be reduced if the new estimate of r_e is larger than the old estimate. Carter et al estimate r_e = 29.6 arcsec, for which the velocity dispersion discrepancy is reduced by about 40%, to 75 kms^{-1} at the outermost 36 kpc measurement. The discrepancy is still significant at more than 3σ.

Model B shows that the profile cannot be accounted for by inclusion of a second component, which has a central density and density distribution scale length the same as the cluster itself. Model B has been generated with the parameter set : r_e = 13 arcsec, $\sigma_{central}$ = 277 kms^{-1}, r_{core} = 378 kpc, σ_{cl} = 720 kms^{-1} and evidently fails to reproduce the profile. More mass is required from the second component in the central regions to keep the dispersion profile from falling. Either the measured cluster velocity dispersion has been greatly underestimated [by a factor of about 2], or the mass in the second component is distributed with a scale length considerably less than that of the cluster. A similar result was obtained by Dressler (1979) for the cD in A2029. He found a good fit to

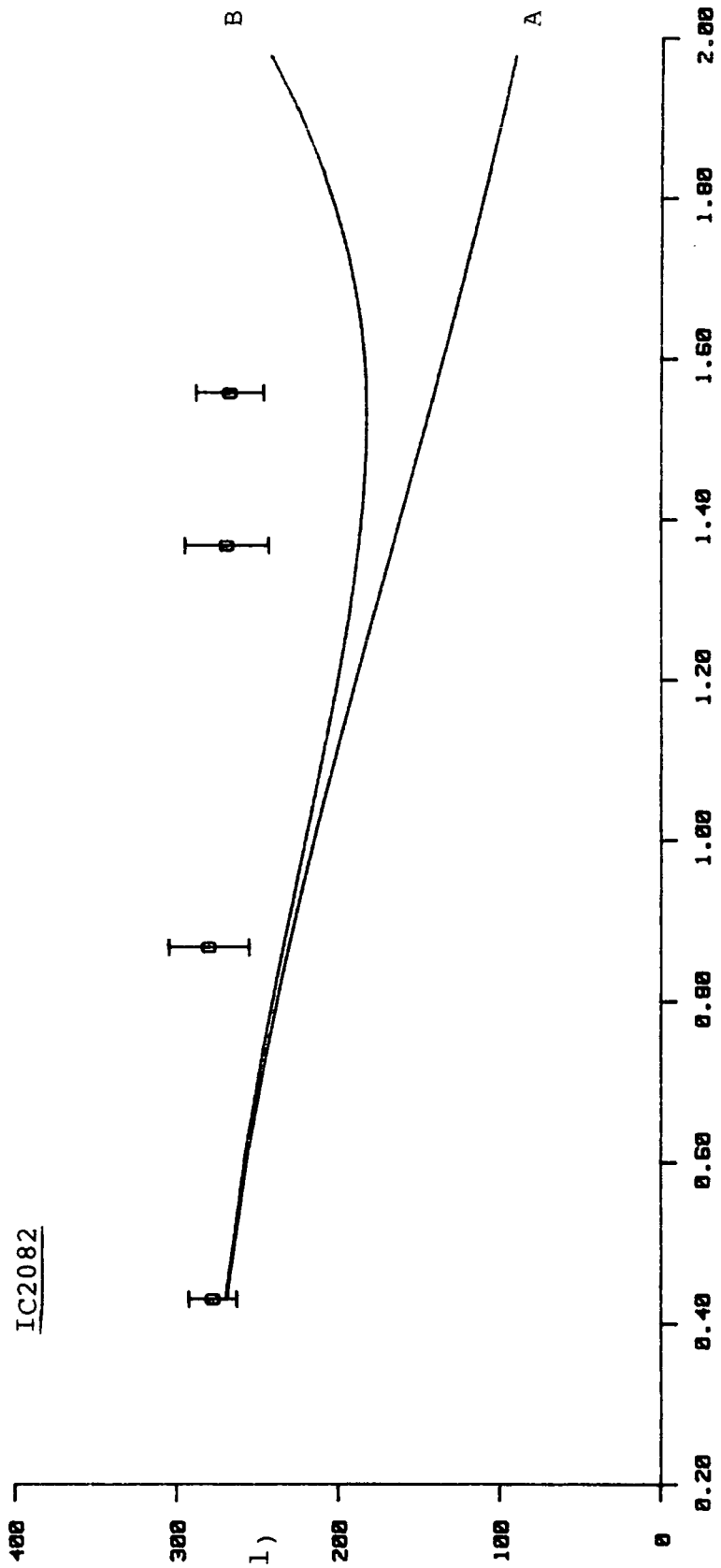

Figure 5.8.2 Velocity Dispersion Profile

both the luminosity and velocity dispersion profiles by introducing a component with a scale length and velocity dispersion intermediate between the central galaxy and the galaxy cluster. Such a component could plausibly arise from tidally stripped material [Richstone (1975)]. The rate of stripping is approximately proportional to the local galaxy density [Carter et al (1985)] and stripped material should therefore be considerably more concentrated than the distribution of cluster galaxies. These results are particularly interesting in the light of recent results from Beers & Geller (1983) on the local nature of the D galaxy phenomenon.

The two-component models assume that IC2082 is at the centre of the second component mass distribution. If the second component were to be identified with the cluster, then IC2082 would have to be centrally located in the cluster. Sersic (1961) comments that the dumb-bell galaxy is indeed centrally located and IC2082 is quite accurately at the kinematical centre of its associated cluster [Ellis et al (1984)]. Placing IC2082 away from the centre would tend to exaggerate the failure of the best estimate cluster model [B] to reproduce the velocity dispersion profile.

5.8.3.3 Models Which Fit

It has been shown in the previous section that no two-component model with isotropic velocity dispersions could be constructed which reproduced the IC2082 velocity dispersion profile using cluster and galaxy parameter values determined from observation. We now consider those sets of parameter values which do reproduce the velocity dispersion profile.

The modelling procedure used in this work defines a "fitting model" as a model whose velocity dispersion at a chosen radius [r_{edge}] is equal to a specified value [σ_{edge}]. There is no significant structure in the velocity dispersion profile of IC2082 and therefore a modelling procedure has been adopted which does not attempt to find the single best fitting model, but rather a set of models which adequately reproduce the profile. Presented graphically, this procedure rapidly conveys an idea of the range of "fitting parameters" which reproduce the profile. This allows a direct comparison of the models with observation, including the effects of errors.

The two component models studied in this work have four parameters [$\sigma_{central}$, r_e, σ_K, r_{core}]. The "sets" of models mentioned above are generated by keeping constant the two parameters which are least interesting [$\sigma_{central}$, r_e] whilst varying the remaining parameters [σ_K, r_{core}]. The resulting plot of the two free parameters for fitting models defines a curve against which observed parameter values may be directly compared.

Figure 5.8.3 includes five model sets which show the effect on the models of any errors in the effective radius [r_e], or the velocity dispersion fitting criterion [σ_{edge}].

Model Set	r_e (arcsec)	σ_{edge} (kms^{-1})	
A	13	265	r_e varies
B	30	265	
C	19	245	
D	19	265	σ_{edge} varies
E	19	285	

r_{edge} = 28.6 arcsec
$\sigma_{central}$ = 277 kms^{-1}

The curves for model sets A and B show the effect of allowing r_e to change, using the two estimates of r_e quoted in section 5.6.2. The model curves with larger r_e evidently lie closer to the observed values of r_{core} and σ_K. Increasing r_e simply re-scales the de Vaucouleurs velocity dispersion profile to larger radii, thus improving the agreement. The curves for model sets C, D and E show the effect of varying σ_{edge}.

The data point plotted in figure 5.8.3 corresponds to estimates made in this work of the cluster parameters. In other words, the data point represents the identification of the King component of the two-component model with the cluster. The set of parameter values represented by model curve A

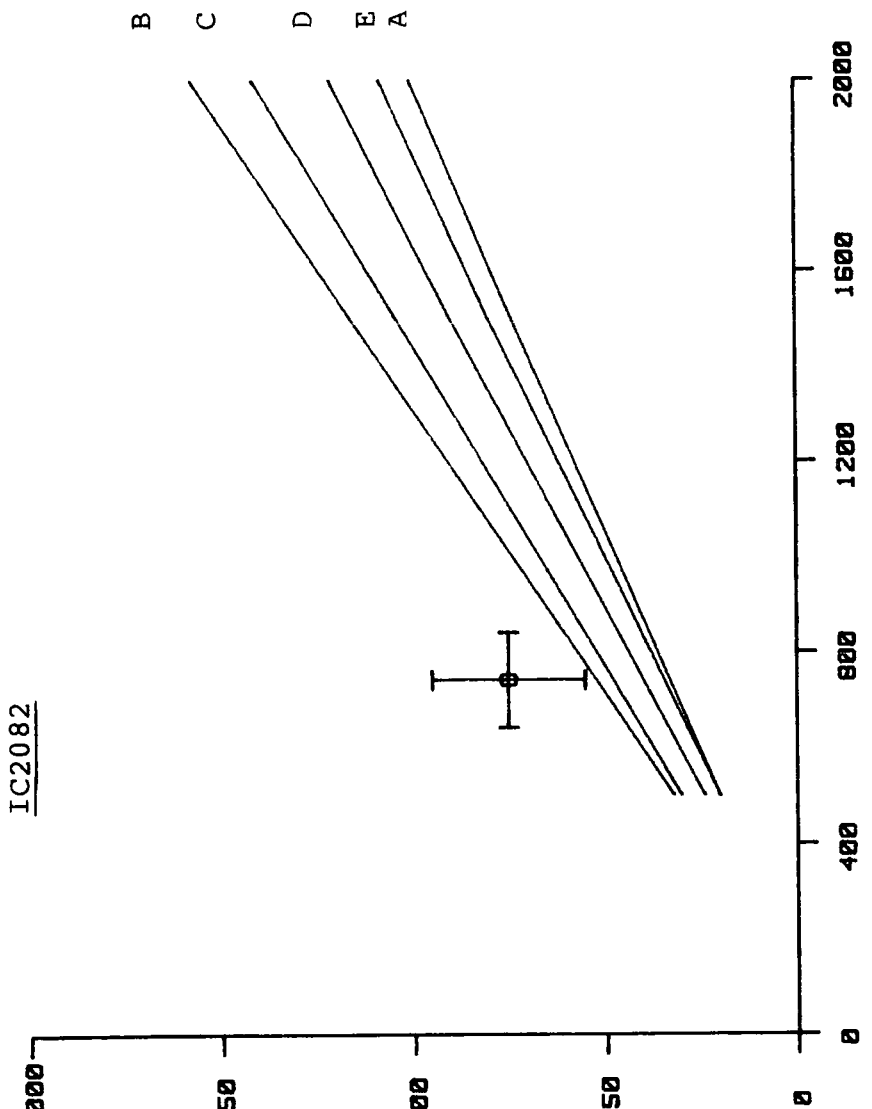

Figure 5.8.3 IC2082 Dynamical Models

rejects the identification of the second component with the cluster at a level of 2σ. Model curve B rejects the identification at a level of only 1σ.

The conclusions of the two-component modelling are that it is possible to reproduce the IC2082 velocity dispersion profile with physically reasonable models. If the velocity dispersion of the material in the dark component is of the order of the cluster velocity dispersion [720 kms^{-1}] then we require that the dark material is more concentrated than the galaxies in the cluster. Such a model is well motivated if we identify the dark material as resulting from tidal stripping of nearby galaxies [Richstone (1975)], which we would expect to be most important where the galaxy density is greatest - at the centre of the cluster. Beers & Geller (1983) find, from a study of the distribution of galaxies in clusters, that the processes which govern the formation of the luminous haloes in D and cD galaxies are apparently determined by local rather than global galaxy densities. Two very different methods of investigation therefore support the same conclusion: the cD phenomenon is a local phenomenon.

Carter et al (1985) calculated models based on the Blandford-Smarr (1982) mass distribution and came to the same conclusion. They also found that the velocity dispersion profile of IC2082 was not well reproduced by models which used anisotropic velocity dispersions. The IC2082 velocity dispersions reported in Carter et al (1981, 1985) show a small rise not found in this work, but differences between the two data reductions are marginal for IC2082, and do not affect the conclusions of this study.

Any conclusion we might draw from modelling IC2082 as a two-component system will be somewhat weaker than the principal result of these observations: that the velocity dispersion profile is not that of a constant M/L, isotropic velocity dispersion, de Vaucouleurs galaxy. The need for observations of more galaxies is therefore acute: if extra galaxies studied show the same second component behaviour as IC2082, these conclusions would be very much stronger. A program of observation to obtain this extra evidence is described in chapter 6.

5.8.3.4 Mass/Light Ratios

A two-component mass model has been used to reproduce the IC2082 velocity dispersion profile. Only one of the two components is luminous. In terms of the mass in the de Vaucouleurs component, M_{deV}, and the mass in the King component, M_{King}, the M/L ratio may be written:

$$M/L = [\ 1 + (M_{King}/M_{deV})\ ]\ (M/L)_{deV} \qquad 5.8.9$$

The mass/light ratio of the de Vaucouleurs component may be estimated by calculating the total mass and total luminosity indicated by the observations reported in this chapter. Using equation 5.7.8 with r_e = 13.6 kpc, $\sigma_{central}$ = 273 kms^{-1} and σ^*_{ap} = 0.46, a total mass of 1.12 x $10^{12} M_\odot$ is obtained for the BN. The absolute luminosity of the BN is 1.66 x $10^{11} L_\odot$ [$M_{BT} = -22^m.57$].

The M/L ratio of the IC2082 BN is therefore:

$$(M/L)_B = 6.7$$

The central value of the velocity dispersion is unaffected by the existence of a second component, which contributes only 3-4% to the mass within 10 arcsec of the nucleus. This allows the separation of the calculation of the de Vaucouleurs component (M/L) from the two-component (M/L). The FN has a M/L ratio of 8.4. This value may include an excessive FN mass, caused by overestimation of the FN effective radius or central velocity dispersion.

Table 5.8.2 shows M/L calculations for four illustrative models. Models 1 and 3 show the insensitivity of the M/L ratio, for two fitting models with the same r_e, but very different σ_{cl} and r_{core} [ie models in the same "set"]. Models 21 and 23 show the effect of increasing r_e to 30 arcsec. The absolute scale of the M/L ratios for the 30 arcsec models is rather uncertain. This is because the luminosity was calculated from the photometry of section 5.6 [for which the best estimate of r_e is 13 not 30 arcsec] and may therefore be a significant underestimate.

The mass contributed by the dark component, in order to reproduce the velocity dispersion profile, is significant: 35% for r_e = 13 arcsec, but only 12% if r_e is increased to 30 arcsec.

Table 5.8.2

M/L Ratios for Models of IC2082

Model #	r_e (arcsec)	σ_{cl} (kms^{-1})	r_{core} (kpc)	M/L_B core	M/L_B $\leq$30kpc	M/L_B 30kpc
1	13	500	100	6.7	10.9	31
3	13	1500	370	6.7	9.8	25
21	30	500	160	11.9	13.9	21
23	30	1500	580	11.9	13.3	18

$\sigma_{central}$ = 277 kms^{-1}
σ_{edge} = 265 kms^{-1}
r_{edge} = 28.6 arcsec

5.8.4 Summary

The observational results have been discussed in three parts: dumb-bell rotation, envelope rotation and velocity dispersion. In general, the conclusions of this study are consistent with the predictions of the theory of galactic cannibalism, as described by Hausman & Ostriker (1978) and the process of tidal stripping proposed by Richstone (1975).

IC2082 is a giant dumb-bell galaxy with two prominent nuclei. One component is a D galaxy [$M_B = -22^m.6$] approximately a magnitude brighter than the second component, which is an elliptical galaxy. The fainter nucleus in this dumb-bell system has a velocity relative to the brighter nucleus of a approximately 200 kms^{-1} and is expected to come to rest at the centre of the system in a few orbital periods - through the action of dynamical friction.

Comparison of the central velocity dispersions and luminosities of the two components shows that the D galaxy is overluminous for its velocity dispersion, whereas the fainter galaxy is apparently a normal elliptical. This result supports the idea that the luminosities of D and cD galaxies are the result of some special formation mechanism.

The velocity dispersion profile of IC2082 does not fall off as fast as plausible single component models suggest. However, the profile can be accounted for by a two-component model in which a normal elliptical galaxy is placed in a background of dark material, which is considerably more

concentrated than the galaxies in the cluster. This indicates that the processes which determine the special features of D galaxies may be of a relatively local nature. The rise in M/L suggested by models of the velocity dispersion profile of IC2082 is from $M/L_B = 6.7$, in the core, to $M/L_B = 26$ at 30 kpc.

More galaxies require investigation to confirm whether the results found for IC2082 are common properties of D galaxies. The programme started in this chapter is continued in the next.

6 CHAPTER SIX : THREE SOUTHERN SUPERGIANT GALAXIES

6.1 INTRODUCTION

Continuing the study begun with IC2082, three additional southern galaxies have been observed and results are presented in this chapter. The data reduction, analysis and dynamical modelling are conducted in the same manner as for IC2082.

6.1.1 Sersic 40/6 [S40/6]

Sersic 40/6 [Sersic (1974)] is a BM I cluster containing a bright, centrally located, cD galaxy [$M_{B27} = -23^{m}.70$, Green (1977)]. The central galaxy has a dumb-bell structure embedded in an extended envelope with a luminosity profile slightly flatter than r^{-2} [Green (1977)], making it a typical cD galaxy.

S40/6 has Abell richness class 1 [Melnick & Quintana (1981a)] and is centrally condensed. The cluster is both a radio source [Pks 0429-61] and has been identified as a luminous X-ray source [2A0430-615 = 4U0427-61, see references in Quintana & Melnick (1982) and Materne et al (1982), for the X-ray observations]. Because of its X-ray properties, S40/6 has attracted considerable interest and has a well determined cluster velocity dispersion. Melnick and Quintana (1981b) find $\sigma_{cl} = 1517$ kms^{-1} from 29 velocity measurements, and this large value is confirmed by Carter, Teague & Gray (1984), who find 1583 kms^{-1} for this cluster. Prints of the

cluster appear in Melnick & Quintana (1981a,b) and isophotal maps of the central dumb-bell are presented in Green (1977). Melnick & Quintana also note that the mean velocity of the dumb-bell galaxy in S40/6 is within 250 kms^{-1} of the mean cluster velocity.

The two nuclei of the central dumb-bell cD galaxy are separated by approximately 8 arcsec and, as with the IC2082 system, the line joining the brighter nucleus [BN] and fainter nucleus [FN] matches the major axis of the cD envelope [E4], as well as the distribution of galaxies in the cluster [Green (1977)]. In B, the BN is $0^m.58$ brighter than the FN and the S40/6 dumb-bell system is some $0^m.8$ brighter than IC2082.

6.1.2 Pks 2354-35

Though even less rich than S40/6, the cluster associated with the radio source Pks 2354-35 is nevertheless dominated by a very bright cD galaxy [$M_{B27} = -23^m.75$]. Photographic photometry is described in Bucknell (1977) and Green (1977). The galaxy is evidently a radio source [Bolton & Ekers (1966)] and shows 3727 Å emission.

A cluster velocity dispersion is available from Green (1977), though the result is rather sensitive to the rejection of non-members. A value of 894 kms^{-1} is found for 11 velocity measurements, compared with only 425 kms^{-1} after exclusion of two possible non-members.

Photometry by Green of Pks 2354-35 and S40/6 shows increasing ellipticity with radius for the central galaxies and mild reverse luminosity segregation of cluster galaxies.

Pks 2354-35 is of special interest because, of the four galaxies studied in this work, it is the most classically "cD". In particular, the absence of dumb-bell structure should make the interpretation of the kinematical results rather more direct than for IC2082 or Sersic 40/6.

6.1.3 0559-40

The cluster 0559-40 is included in the Dressler (1980b) survey of 55 rich clusters. Dressler classified the brightest cluster galaxy as D (#48) at $05^h\ 59^m\ 03.1^s$ and -40° 02' 41". Rather unusually for clusters in the Dressler sample, 0559-40 has the primary D galaxy located along a low density spur to the south-east of the cluster [some 775 kpc from the cluster centre, Beers & Geller (1983)]. In addition, a galaxy classified D/E by Dressler (#100) is associated with a low density clump to the north-west. The cluster as a whole is rather irregular.

The failure of the IC2082 velocity dispersion profile to fall with radius may be explained by the presence of darker material distributed on a scale roughly comparable to the optical extent of the cD halo. Such a scheme is physically well motivated only if the cD galaxy is at some special position in the cluster: a position where tidal debris,

infalling gas or galaxies are preferentially to be found. A D galaxy in a low density environment, such as 0559-40, would not be expected to show the effects of any background material [cf Davies & Illingworth (1983)].

A weighted mean of values from Dressler [priv.comm.] and Green et al (1984) gives a moderate value of 837 kms^{-1} for the cluster velocity dispersion.

6.2 SPECTROSCOPIC DATA

The observational set-up for the data reported here was very similar to that used for the observations of IC2082 reported in the previous chapter. Because of the low surface-brightness of the cD galaxy haloes, the observations require long exposures and must be very carefully reduced. To improve the signal-to-noise of the spectra, while not degrading the velocity information obtainable, the spectral resolution was chosen to be somewhat lower than for IC2082 [5 Å as against 2.4 Å for IC2082]. In other respects the data reduction was identical.

Data reduction techniques have been dealt with in chapters 2 and 3. Table 6.2.1 lists the details of the observations and table 6.2.2 lists the positions of the objects observed.

Table 6.2.1

Observational Set-up

Nights	: 2
Dates	: 03-Nov-80, 08-Dec-80
Telescope	: 3.9m AAT
Spectrograph	: RGO
Detector	: IPCS
Grating	: 600 lines/mm blazed at 5000 Å
Dispersion	: 66 Å/mm
Data Window	: 2044 x 40
Spatial Resolution	: 4.7 arcsec/increment
Spectral Resolution	: 5.0 Å FWHM
Slit Width	: 3.35 arcsec
PA of Slit	: major axis
Wavelength Range	: 4000 Å - 6200 Å

Table 6.2.2

Observations

Object	RA (1950)	DEC	l^{II} (deg)	b^{II} (deg)	PA
Sersic 40/6	$04^h30^m33^s$	-61°33'37"	272.18	-40.09	75°
Pks 2354-35	$23^h54^m26^s$	-35°02'15"	356.69	-76.02	170°
0559-40	$05^h59^m03^s$	-40°02'40"	246.52	-26.30	75°

Template		RA (1950)	DEC
1	SAO233152 (HD22231)	$03^h31^m05^s$	-50°32'51"
2	SAO249009 (HD28093)	$04^h21^m21^s$	-63°30'12"
3	HD42505	$06^h06^m19^s$	-62°40'36"
4	SAO246853	$21^h01^m22^s$	-56°19'13"
5	HD199213	$20^h54^m24^s$	-56°02'51"
6	HD42505	as template 3	

Templates 1 & 2 are in common with IC2082.
Templates 3 & 6 are treated separately for reduction.

6.3 SPECTROSCOPIC RESULTS

Spectroscopic results and statistical information about the Sersic 40/6, Pks 2354-35 and 0559-40 data are presented in tables 6.3.1 - 6.3.8 and figures 6.3.1 - 6.3.3.

The spectra were reduced in the same way as IC2082. For velocity dispersion estimation, data was combined to form spectra with photon counts totalling at least 30-40% of sky. Errors introduced by imperfect sky subtraction are significant only for the outermost spectra in each of the three galaxies and these errors are even then small [20 kms^{-1}] compared to the statistical uncertainties at such low S/N [>40 kms^{-1}].

Suitable templates were chosen by comparison of their line-strengths relative to the nuclear spectra of the three program galaxies. The following table of line-strengths illustrates the procedure:

Object	Template					
	5	2	1	4	3	6
Sersic 40/6	1.451	1.152	1.028	0.730	0.639	0.596
Pks 2354-35	1.557	1.279	1.104	0.769	0.686	0.630
0559-40	1.371	1.178	1.048	0.744	0.658	0.591
Average γ	1.46	1.20	1.06	0.75	0.66	0.61

Recall that templates 3 and 6 are merely different observations of the same star. The table is reproduced in full to show the stability of the line-strength calculation between templates.

Templates 5, 3 and 6 were discarded as too discrepant in line-strength to be used individually as templates, but were included in a composite template containing all the stars observed. A second composite template was constructed consisting of templates 1, 2 and 4. Before combination into composite templates, spectra were shifted to produce zero velocity relative to template 2. The results presented in this section are the average of the results of templates 1, 2 and 4 and the highest R value composite template.

The rotation curve of Sersic 40/6 was calculated differently from the two other galaxies, because of the importance of obtaining an accurate estimate of the rotation curve of Sersic 40/6 beyond the region contaminated by the FN. To improve the match between object and template, the nuclear spectrum was used as template and the results then corrected to the heliocentric scale defined by measurements of the absolute radial velocity of the nuclear spectrum.

Different templates agreed very well in their estimates of the nuclear velocity dispersions of the three galaxies [to about 10 kms^{-1}], but did not always agree in the outer regions. No template produced systematically high or low dispersions, so the fluctuations must be accepted as being simply due to the poor S/N.

Two problems arose in the reduction of this low dispersion data which had not been encountered with either of the high dispersion studies described in the previous two chapters. Firstly, in the SSBS Fourier Quotient method, a dependence was found of velocity dispersion on the value chosen for the low wavenumber cut-off [k_{low}]. Secondly, inconsistencies in the radial velocity scale suggest a systematic error in velocity estimates of 40 kms^{-1}.

The procedures used to resolve these problems are described below, but the source of the inconsistencies has not been adequately explained and some caution must therefore be used in the interpretation of the results presented here.

The data was initially reduced using the SSBS Fourier Quotient method. An unacceptable dependence was found of σ on k_{low}. Indeed, the need to eliminate this dependence was the motivation for the development of the Fourier Difference method. The Fourier Difference method largely eliminates the trend in the k_{low}-σ relation seen in the Fourier Quotient results derived from this data. The k_{low}-σ problem is discussed in chapter 3 and is illustrated graphically for Pks 2354-35 in figure 3.7.2.

The second difficulty arose while reducing the radial velocity data to a heliocentric scale. Radial velocities are available for templates 1 and 2, which are in common with the IC2082 observations. Each set of data was reduced independently to estimate residual errors in the heliocentric reduction. After correction for heliocentric motion, internal consistency tests using relative

velocities between the three IC2082 templates and the nucleus of IC2082 showed residual velocity errors of only 15 kms^{-1}. Similar consistency tests with the low dispersion data revealed residual velocity errors of 60 kms^{-1}.

There is considerable spectral overlap [4200-5330 Å] between the high dispersion IC2082 templates and the low dispersion templates 1 and 2. Cross-correlation of the overlapping regions of these template spectra showed template 1 to be 43 kms^{-1} in error, after appropriate heliocentric correction. Template 2 [SA0249009] had a velocity relative to the IC2082 observation of SA0249009 of less than 1 kms^{-1}. The heliocentric scale for the observations reported in tables 6.3.1 - 6.3.8 was therefore defined by template 2. The mean nuclear radial velocities are listed below.

Object (nucleus)	$v_\odot$ (kms^{-1})	v_{lg} (kms^{-1})	z_{lg}
Sersic 40/6	18271 $\pm$ 40	18042	0.06014
Pks 2354-35	14802 $\pm$ 40	14798	0.04933
0559-40	13877 $\pm$ 40	13630	0.04543

An error of $\pm$40 kms^{-1} is assigned to each velocity to represent the possible error in the heliocentric scale.

Comparison of these results with other authors is possible for two of three galaxies and the results are listed below [all corrected to the local group]. Agreement is excellent for S40/6.

	v_{lg}(kms^{-1})	Source
Sersic 40/6	18042	this work
	18000	Melnick & Quintana (1981b)
	18025	Materne et al (1982)
	18030	Vidal (1975)
	18041	West & Fransden (1981)
	17852	Green (1977)
Pks 2354-35	14798	this work
	14606	Whiteoak (1972)
	14592	Green (1977)

Investigation of the photon counts along the spectrograph slit for Sersic 40/6 showed an object approximately 1 arcmin west along the slit from the BN. Inspection of the positions of objects in the Sersic 40/6 cluster enabled this object to be identified with Green object #15. This galaxy is 63 arcsec from the BN, defining a slit position angle of 77° [very close to the recorded value of 75°]. It has a magnitude of B_{27} = $16^{m}.80$ and a velocity relative to the BN of -1761$\pm$26 kms^{-1} [R = 6.3].

Table 6.3.1 — Sersic 40/6

Increment	r (arcsec)	v (kms^{-1})	σ (kms^{-1})	γ	R	χ^2
14 - 16	-27.23	18330 ± 47	416 ± 59	0.90	3.0	1.6
17 - 18	-16.21	18213 ± 36	518 ± 45	0.87	4.1	1.5
19	-9.40	18112 ± 38	326 ± 48	0.66	3.9	1.6
20	-4.70	18163 ± 20	301 ± 25	0.82	8.4	1.5
21	0.00	18243 ± 15	316 ± 19	0.95	11.6	2.9
22	+4.70	18149 ± 21	355 ± 26	0.82	7.8	2.0
23	+9.40	17831 ± 17	256 ± 21	0.88	9.8	3.4
24	+14.10	17899 ± 27	236 ± 34	0.61	6.0	1.6
25 - 27	+22.09	18048 ± 42	439 ± 53	0.89	3.5	1.6

Table 6.3.2

Increment	Dwell (seconds)	S/N	Object/Sky	Counts/Pixel (photons)
14 - 16	9000	6.2	0.28	177
17 - 18	9000	7.6	0.45	188
19	9000	8.1	0.73	153
20	9000	13.7	1.49	314
21	9000	38.8	8.01	1689
22	9000	23.5	3.40	717
23	9000	35.3	6.94	1423
24	9000	13.1	1.41	292
25 - 27	9000	6.6	0.30	188

Scale at cluster : 0.642 arcsec/kpc [local group].

Table 6.3.3

Rotation Curve of Sersic 40/6 with Nuclear Template

Increment	r (arcsec)	v (kms^{-1})	
15 - 17	-22.51	+118	
18	-14.10	-16	
19	-9.40	-1	
20	-4.70	0	(1)
21	0.00	+70	(2)
22	+4.70	-3	
23	+9.40	-283	
24	+14.10	-215	
25	+18.80	-50	
26 - 28	+27.43	+19	

1. Zero velocity is defined by increment 20.
2. The nuclear spectrum is increment 21.

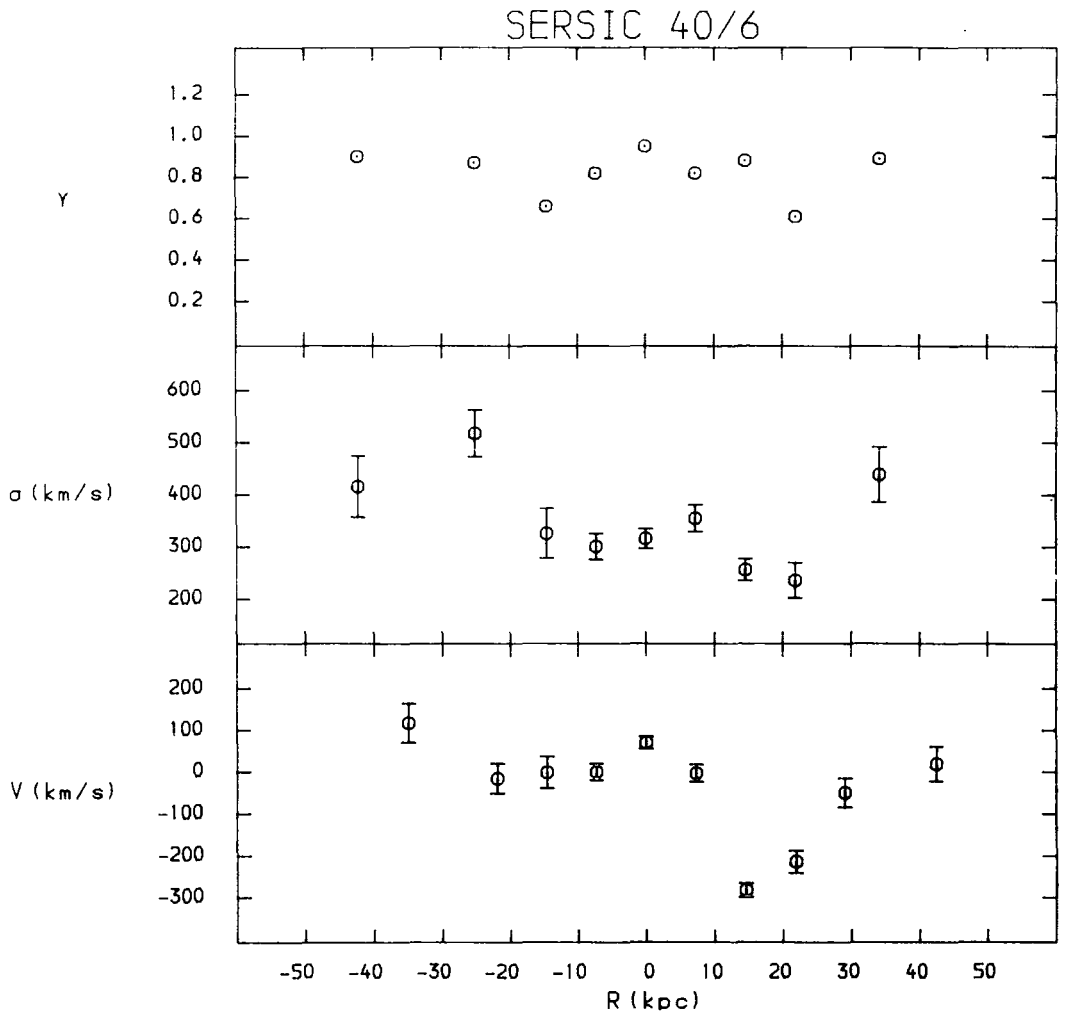

Figure 6.3.1 Spectroscopic Results for Sersic 40/6

WK3ABR

Table 6.3.4 Pks 2354-35

Increment	r (arcsec)	v (kms^{-1})	σ (kms^{-1})	γ	R	χ^2
15 - 17	-21.10	14709 ± 34	316 ± 43	0.69	4.4	1.9
18	-12.69	14687 ± 30	274 ± 38	0.74	5.3	1.8
19	-7.99	14717 ± 21	283 ± 26	0.89	7.9	1.7
20	-3.29	14723 ± 18	309 ± 23	1.02	9.2	2.8
21	+1.41	14758 ± 18	284 ± 23	1.02	9.2	3.2
22	+6.11	14710 ± 19	287 ± 24	0.90	9.6	2.3
23	+10.81	14710 ± 31	331 ± 39	0.74	5.1	1.9
24 - 26	+19.03	14719 ± 32	317 ± 40	0.78	4.8	1.9

Table 6.3.5

Increment	Dwell (seconds)	S/N	Object/Sky	Counts/Pixel (photons)
15 - 17	10000	9.0	0.40	286
18	10000	9.1	0.78	188
19	10000	13.7	1.34	326
20	10000	23.9	3.05	757
21	10000	28.2	3.98	994
22	10000	16.6	1.77	429
23	10000	10.3	0.92	221
24 - 26	10000	9.6	0.43	309

Scale at cluster : 0.767 arcsec/kpc [local group].

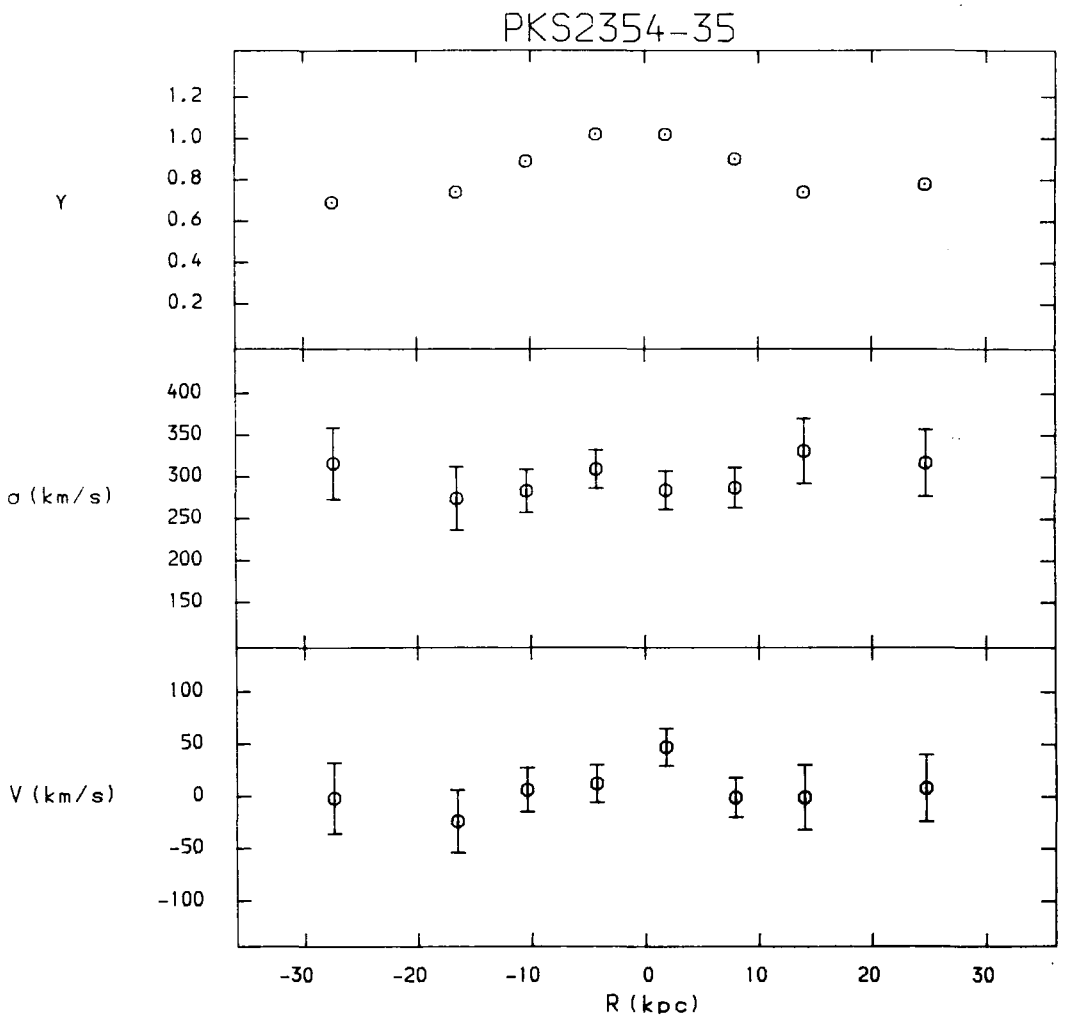

Figure 6.3.2 Spectroscopic Results for Pks2354-35

Table 6.3.6 0559-40

Increment	r (arcsec)	v (kms^{-1})	σ (kms^{-1})	γ	R	χ^2
16 - 18	-18.64	13809 ± 37	194 ± 46	0.58	4.1	1.7
19	-10.34	13903 ± 31	246 ± 39	0.72	5.1	1.5
20	-5.64	13897 ± 18	274 ± 23	0.79	9.3	1.8
21	-0.94	13861 ± 14	280 ± 18	0.97	12.4	2.6
22	+3.76	13839 ± 16	271 ± 20	0.86	10.9	2.2
23	+8.46	13859 ± 25	245 ± 31	0.65	6.4	1.5
24 - 26	+16.57	13963 ± 54	291 ± 54	0.51	3.4	1.7

Table 6.3.7

Increment	Dwell (seconds)	S/N	Object/Sky	Counts/Pixel (photons)
16 - 18	7400	6.8	0.35	180
19	7400	8.3	0.86	150
20	7400	16.9	2.37	407
21	7400	32.3	6.96	1197
22	7400	23.5	4.02	692
23	7400	10.8	1.24	212
24 - 26	7400	8.2	0.43	221

Scale at cluster : 0.827 arcsec/kpc [local group].

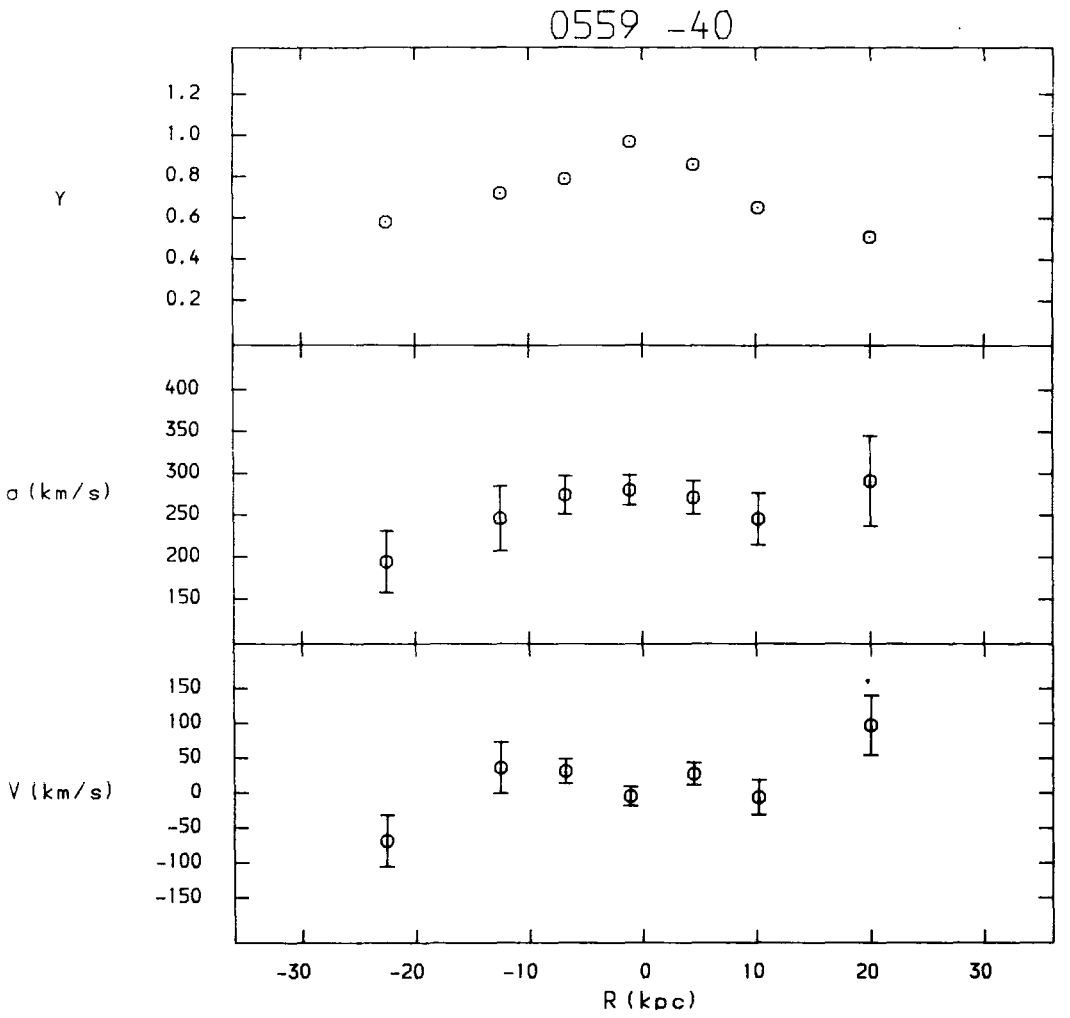

Figure 6.3.3 Spectroscopic Results for 0559-40

WK3ABR

Table 6.3.8

Description of Templates

Template	Dwell (seconds)	S/N	Type	Counts/Pixel (photons)
1	1000	22.1	K3 III[1]	487
2	1000	25.6	G7 III[1]	657
3	1000	20.4	K0[2]	418
4	1000	25.9	K0[3]	670
5	1000	21.5	G0[2]	464
6	1000	18.7	K0[2]	350

1. Bright Star Catalog.
2. Henry Draper Catalog.
3. SAO Catalog.

Unlogged channel size : 1.2 Å
Logged channel size : 59.8254 kms^{-1}
Total channel number : 2048
Low Wavenumber Cut-off : 14-18 (k_{low})
High Wavenumber Cut-off : 300 (k_{high})

6.4 MODEL PARAMETERS

The parameters used as input to the models are described in this section. As with IC2082 the important quantities are the galaxy velocity dispersion profile; the galaxy effective radius; the cluster velocity dispersion and the cluster core radius.

The velocity dispersion profiles of the three galaxies are listed in table 6.4.1. Dispersions and positions have been calculated as averages of values on either side of the nucleus, weighted inversely by the dispersion error. The profiles of Sersic 40/6 and Pks 2354-35 both rise, whereas 0559-40 has a falling velocity dispersion.

De Vaucouleurs effective radii are available for all three galaxies determined from B and R photometry. Table 6.4.2 summarises the B photometric results [including IC2082] and surface-brightness profiles are plotted in figure 6.4.1. The magnitudes and surface-brightnesses have not been corrected to the galaxy rest frame [10log(1+z), Stock & Schueking (1957)].

The CCD R photometry reported in Carter et al (1985) is reproduced in table 6.4.3. Direct comparison of R photometry is possible for 0559-40, from photographic surface brightness data supplied by Spencer [priv.comm.]. Agreement is excellent: an effective radius of 24.4 arcsec is found from the photographic photometry as compared with 25.4 arcsec determined from the CCD R photometry. However, comparison of tables 6.4.2 and 6.4.3 show large

Table 6.4.1

Velocity Dispersion Profile of Sersic 40/6

r (kpc)	σ (kms^{-1})
3.66	316 ± 19
7.21	310 ± 26
33.24	463 ± 30

Velocity Dispersion Profile of Pks 2354-35

r (kpc)	σ (kms^{-1})
6.13	297 ± 16
9.14	285 ± 18
15.33	302 ± 27
26.11	317 ± 30

Velocity Dispersion Profile of 0559-40

r (kpc)	σ (kms^{-1})
2.84	280 ± 18
5.60	272 ± 15
11.23	245 ± 25
21.39	239 ± 35

Table 6.4.2 B Photometry

Object	r_e (arcsec)	μ_e (mag/arcsec^2)	m_T	m-M	ext	K	M_T	L_T ($10^{11} L_\odot$)
Sersic 40/6 [1]	82.5	26.54	13.57	37.787	0.072	0.320	-24.61	10.86
Pks 2354-35 [1]	49.8	25.10	13.22	37.356	0	0.262	-24.40	8.95
0559-40 [2]	31.2	25.27	14.41	37.178	0.163	0.242	-23.17	2.88
IC2082 [3]	12.8	23.49	14.57	36.864	0.063	0.209	-22.57	1.66

1. Green (1977) 2. Spencer (priv.comm.) 3. this work

Table 6.4.3 R_C Photometry

Object	r_e (arcsec)	μ_e[1] (mag/arcsec^2)	m_T	M_T	B-R_C
Sersic 40/6 [2]	71.1	24.34	11.69	-26.10	1.49
Pks 2354-35 [2]	80.2	24.28	11.37	-25.99	1.59
0559-40 [2]	25.4	22.83	12.42	-24.76	1.59
IC2082 [2]	29.6	22.86	12.12	-24.74	2.17

1. Corrected for extinction with assumed zero K correction.
2. Carter et al (1985)

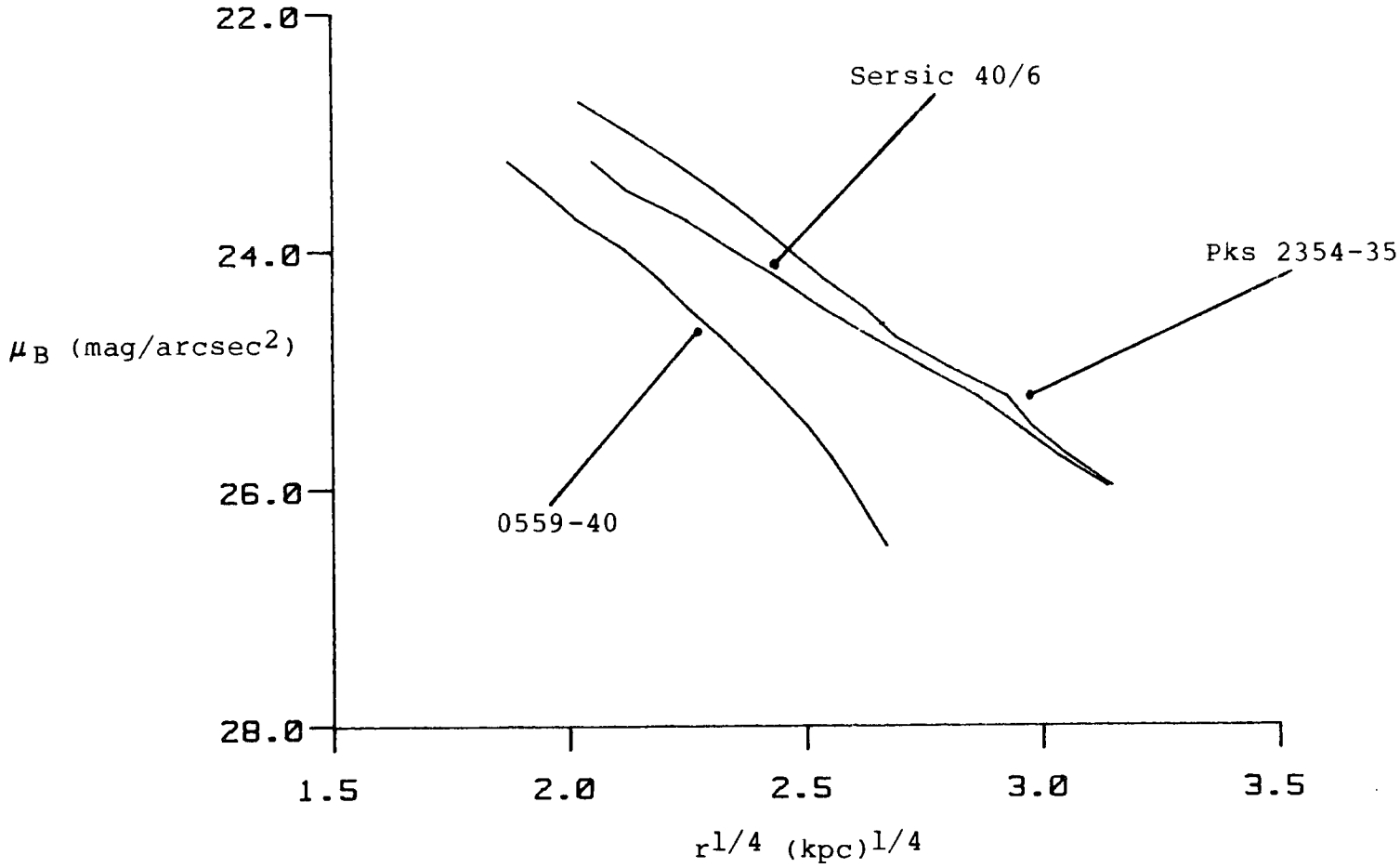

Figure 6.4.1 De Vaucouleurs Law Comparison

discrepancies in estimates of r_e for Pks 2354-35 and IC2082. Such discrepancies could be due to B-R colour gradients. However, the colour-aperture effect [Sandage & Visvanathan (1978)] is in the opposite sense and is present chiefly in U-B rather than B-R colours. In addition, the size of the colour-aperture effect is rather less dramatic. A more likely explanation is that some D and cD galaxies are not well reproduced by a de Vaucouleurs law, or some error is present in the photometry.

The de Vaucouleurs law has been found to be appropriate for many BCM galaxies, as evidenced by a number of recent studies [Schneider, Gunn & Hoessel (1983b), Morbey & Morris (1983) and Lugger (1984)]. Four galaxies are common to these three studies [A2147, A2162, A2199, A1413]. Including the four galaxies discussed in this work and Sersic 31/3 [Spencer, priv.comm.] provides a sample of 9 BCM or cD galaxies with B, V or R estimates of effective radii. The mean ratio of R to B or V effective radius for this small sample is 1.7 $\pm$ 1.1 (sd). This result confirms the impression that R photometry seems to generate larger effective radii, but probably reflects differences between authors rather than photometric bands. The differences evident in tables 6.4.2 and 6.4.3 are therefore not so unusual, and highlight the need for consistently reduced photometry.

$B-R_C$ colours have been calculated from the total magnitudes of tables 6.4.2 and 6.4.3 to reveal any gross discrepancies in effective radii. R_C is the Cousins R waveband, for which $V-R_C = 0^m.61 \pm 0.03$ [Carter, priv.comm.]. Using the canonical

elliptical galaxy value of B-V = $0^m.98$ [Sandage (1973a)], we find $B-R_C = 1^m.59$. Excepting IC2082, this value of $B-R_C$ is in good agreement with table 6.4.3. The difference in B and R effective radii for IC2082 seems, therefore, to be certainly the result of error. Though there is no particular evidence to suggest errors in the photometry reported in this work, the possibility is admitted and a general policy is adopted to calculate important results for both B and R effective radii where these differ significantly.

Cluster core radii have been calculated for Sersic 40/6 and Pks 2354-35, for which detailed cluster photometry is available from Green (1977). The estimation procedure was identical to that used in the analysis of section 5.4 and uses the surface density distributions reported there as figure 5.4.1. No core radius was calculated for 0559-40 as the cluster is neither centrally concentrated nor symmetric, and the D galaxy is not centrally located [Beers & Geller (1983)]. The purpose of the dynamical modelling is to attempt to reproduce the behaviour of the D galaxy velocity dispersion profile: the poor symmetry of 0559-40 as a cluster and the large distance of the D galaxy from the cluster centre suggest that a simple dynamical model of the cluster would be physically unrealistic - the cluster background density would anyway be small at such a large distance from the centre [approximately 20% of the central density]. Cluster velocity dispersions have already been discussed in the introduction to this chapter and are included with the core radii in table 6.4.4.

Table 6.4.4

Cluster Parameters

Object	r_{core} (kpc)	σ_{cl} (kms^{-1})
Sersic 40/6	330	1517
Pks 2354-35	320	425-894
0559-40	-	837
IC2082	365	741

.5 DISCUSSION

The same order of presentation of the discussion is adopted as for IC2082: the dumb-bell rotation of S40/6 is discussed briefly; the size of the envelope rotation in the three programme galaxies is then estimated and the velocity dispersion profiles are compared with dynamical models.

.5.1 Relative Rotation

Sersic 40/6 is a dumb-bell cD galaxy with a secondary component comparable in luminosity [$M_{B27} = -22^m.53$] with the primary component of the IC2082 dumb-bell system [$M_{BT} = 22^m.57$]. Sersic 40/6 also has a larger cluster velocity dispersion [1517 kms^{-1} compared with 741 kms^{-1} for IC2082] and a larger velocity difference between BN and FN:

$$v_{BN}\ (BN - envelope) = + 70\ kms^{-1}$$
$$\underline{v_{FN}\ (FN - envelope) = - 283\ kms^{-1}}$$
$$v\ \ (BN - FN) \qquad\quad = + 353\ kms^{-1}$$

The mean heliocentric velocity of the envelope [defined by data increments 18-20, 26-28] is 18200 $\pm$ 15 kms^{-1}. Scaled by the cluster velocity dispersion the relative rotation velocity is $v_{FN}/\sigma_{cl} = 0.2$, identical to IC2082.

To obtain an estimate of the lifetime of the dumb-bell system, the analysis of the motion of the FN carried out for IC2082 may be repeated [again, assuming physical association]. Indeed, the rather simplistic dynamical arguments used in this analysis

take some justification from the similar features of these two systems: each dumb-bell is aligned with both the D/cD envelope and the distribution of cluster galaxies [Carter & Metcalfe (1980)]. If the primary components of these systems are oblate [Ftaclas & Struble (1983)] then the major axis plane acquires a dynamical significance, particularly if the effects of dynamical friction are considered [Binney (1977)]. While these pieces of evidence do not prove the FN orbit is bound and circular, they do suggest that the orbit is more plausibly edge-on than face-on.

Assuming edge-on circular motion: the orbital period is 2.7×10^8 years; the derived circular radius is 22 kpc [cf r_p = 12.5 kpc] and the circular velocity is 490 kms^{-1}. The Sersic 40/6 and IC2082 FN's have similar velocities relative to the cluster velocity dispersion [S40/6: v_c/σ_{cl} = 0.32 and IC2082: v_c/σ_{cl} = 0.44] suggesting that the two systems are at roughly comparable stages of evolution.

The BN mass interior to r_c is $12.0 \times 10^{11} M_\odot$. No surface photometry is available for the FN to estimate the effective radius, but the half mass [assuming $M/L_B = 9$] is $7.0 \times 10^{11} M_\odot$. The time-scale for dynamical friction is then $\tau_{df} = 1.7\ \tau_{orb}$. Though the de Vaucouleurs total magnitude of the Sersic 40/6 cD is $2^m.04$ absolutely brighter than IC2082, the two dumb-bell systems have quite similar lifetimes because of the roughly equal magnitude difference [and therefore mass ratio] of BN and FN.

A study of two dumb-bell galaxies does not constitute a valid statistical sample. However, a consistent picture is emerging of systems with expected dynamical life-times of about 7×10^8 years. In the time since the collapse of the cluster [4.5×10^9 years, Gunn & Gott (1972)] a cD galaxy might be expected to have undergone several complete mergers, depending on the collision rate in the cluster core [perhaps 1 collision/10^9 years, Hoessel (1980)].

6.5.2 Envelope Rotation

There is no dynamically significant rotation in any of the programme galaxies. Table 6.5.1 summarises the results for all four galaxies in this study. The v/σ values are plotted in figure 5.8.1.

6.5.3 Velocity Dispersions

Magnitude excesses over the L-σ relation defined by Terlevich et al (1981) and Malumuth & Kirshner (1985) are listed in table 6.5.2. These results confirm the large excess luminosities of the brighter cD galaxies over that expected from observations of normal elliptical galaxies.

Comparisons of the observed velocity dispersion profiles with best-estimate single component de Vaucouleurs models are illustrated in figure 6.5.1. Both Sersic 40/6 and Pks 2354-35 show significant excess velocity dispersions over the model predictions, confirming the result found for IC2082.

Table 6.5.1

Envelope Rotation

Object	v_{max} (kms^{-1})	r_{max} (kpc)	v/σ	ϵ [1]
Sersic 40/6	16 ± 25	36	0.05	0.40
Pks 2354-35	4 ± 20	21	0.01	0.31
0559-40	27 ± 18	16	0.10	0.34
IC2082	22 ± 24	46	0.08	0.36

1. Carter et al (1985)

Table 6.5.2

Luminosity Excesses

Object	σ (kms^{-1})	M_{BT}	ΔM_T (1)	ΔM_T (2)	$\overline{\Delta M_T}$
Sersic 40/6	309	-24.61	+2.07	+2.46	+2.27
Pks 2354-35	293	-24.40	+2.10	+2.48	+2.29
0559-40	275	-23.17	+1.15	+1.53	+1.34
IC2082 BN	273	-22.57	+0.59	+0.96	+0.78
IC2082 FN[3]	237	-21.22	-0.12	+0.22	+0.05

1. Terlevich et al (1981)
2. Malumuth & Kirshner (1985)
3. $M_{B26.75}$

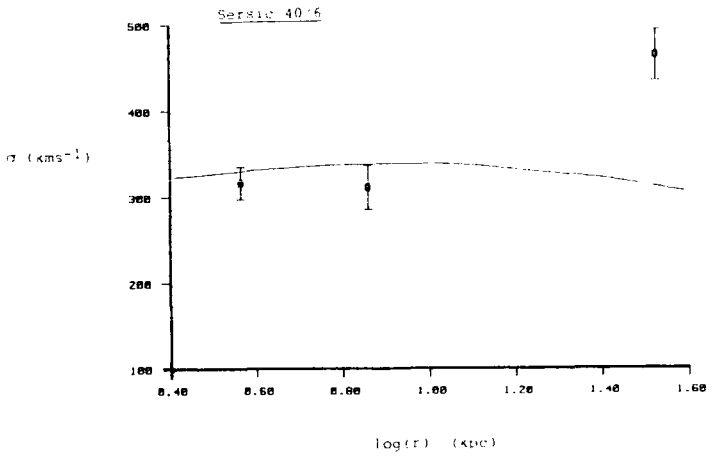

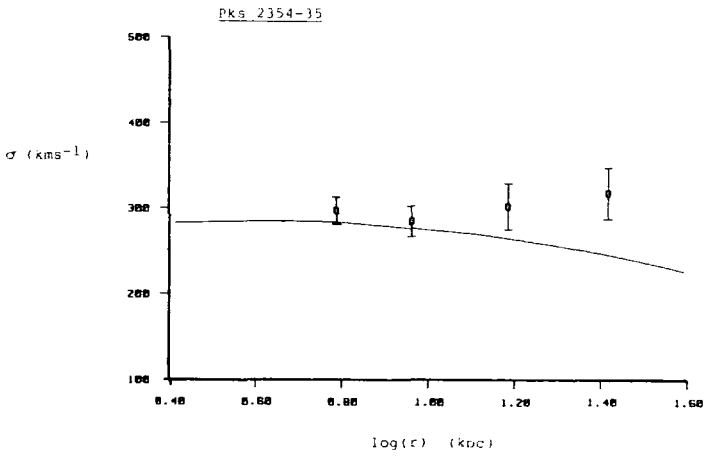

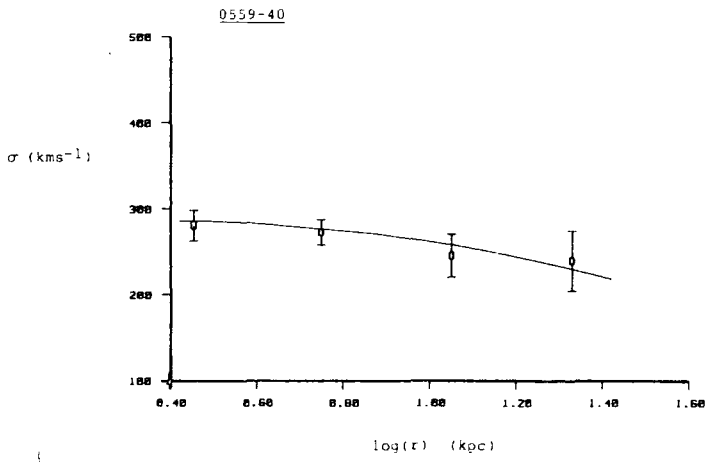

Figure 6.5.1

Velocity dispersion profiles with de Vaucouleurs models

Interestingly, the profile of the non-central D galaxy in 0559-40 is well reproduced by the best estimate de Vaucouleurs model. According to our model hypothesis, this may be interpreted as suggesting that there is no evidence for a background component and that the high luminosity and large size of the D galaxy results from mergers.

Two component dynamical model sets were generated for Sersic 40/6 and Pks 2354-35 to reproduce the observed velocity dispersion profile. No attempt was made to model 0559-40 because it is so well fitted by a de Vaucouleurs model and because the cluster parameters are poorly determined.

The models depicted in figures 6.5.2 and 6.5.3 are:

Object	Model	r_e (kpc)	σ_{cent} (kms^{-1})	σ_{edge} (kms^{-1})	r_{edge} (kpc)
Sersic 40/6	A	110	316	463	33
Pks 2354-35	B	58	280	317	26
	C	104	280	317	26

The modelling of Sersic 40/6 shows that the cD galaxy velocity dispersion profile is reproduced by a background mass distribution rather less concentrated than that expected from observations of the cluster. The Sersic 40/6 cluster has a high cluster velocity dispersion which, on conventional assumptions, suggests the presence of a large amount of unseen matter. The effect of this matter on the velocity dispersion of the stars of the central cD is dramatic, causing a sharp rise in the profile. Approximately 7% of the mass within 10 arcsec of the

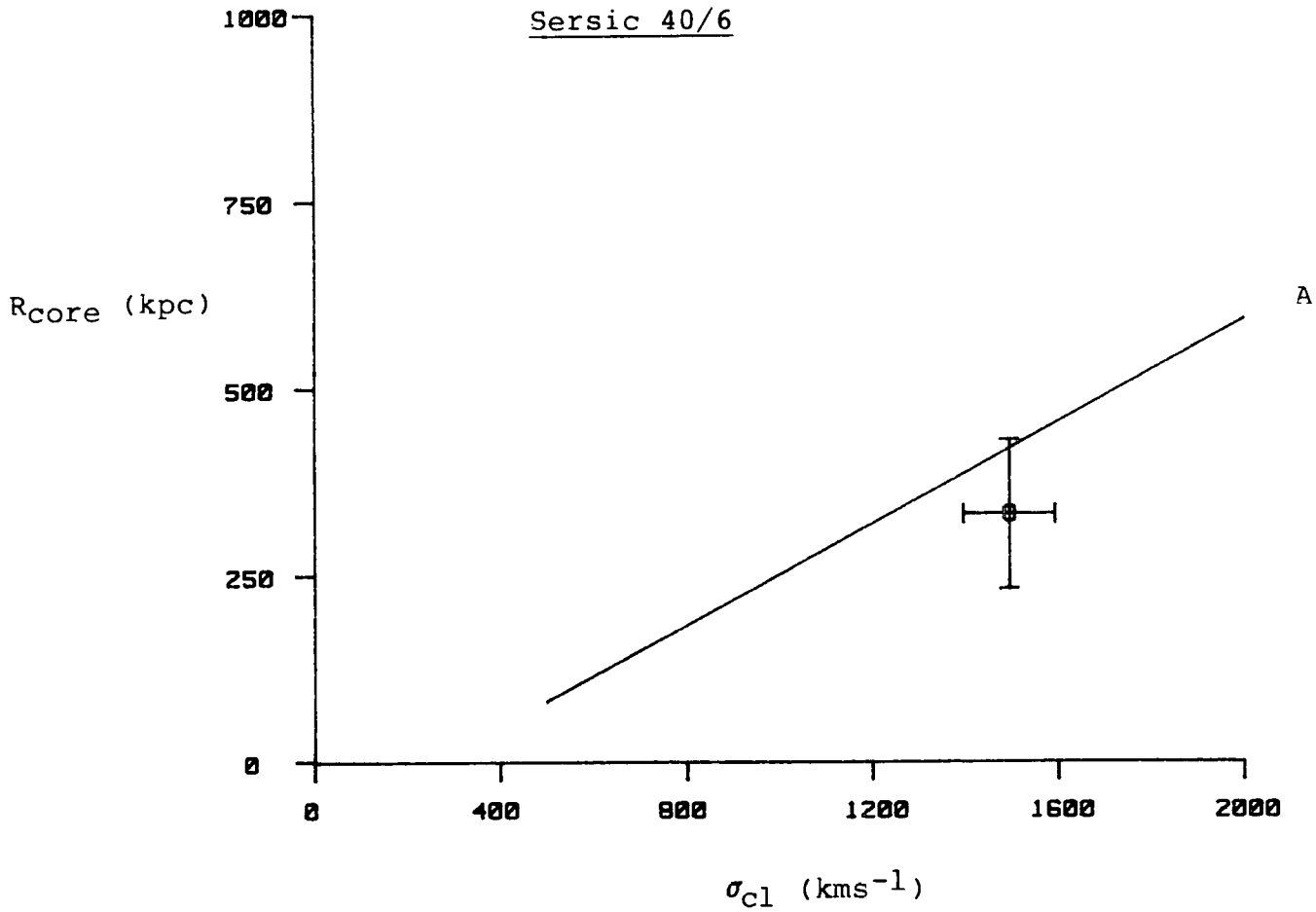

Figure 6.5.2 Sersic 40/6 Dynamical Models

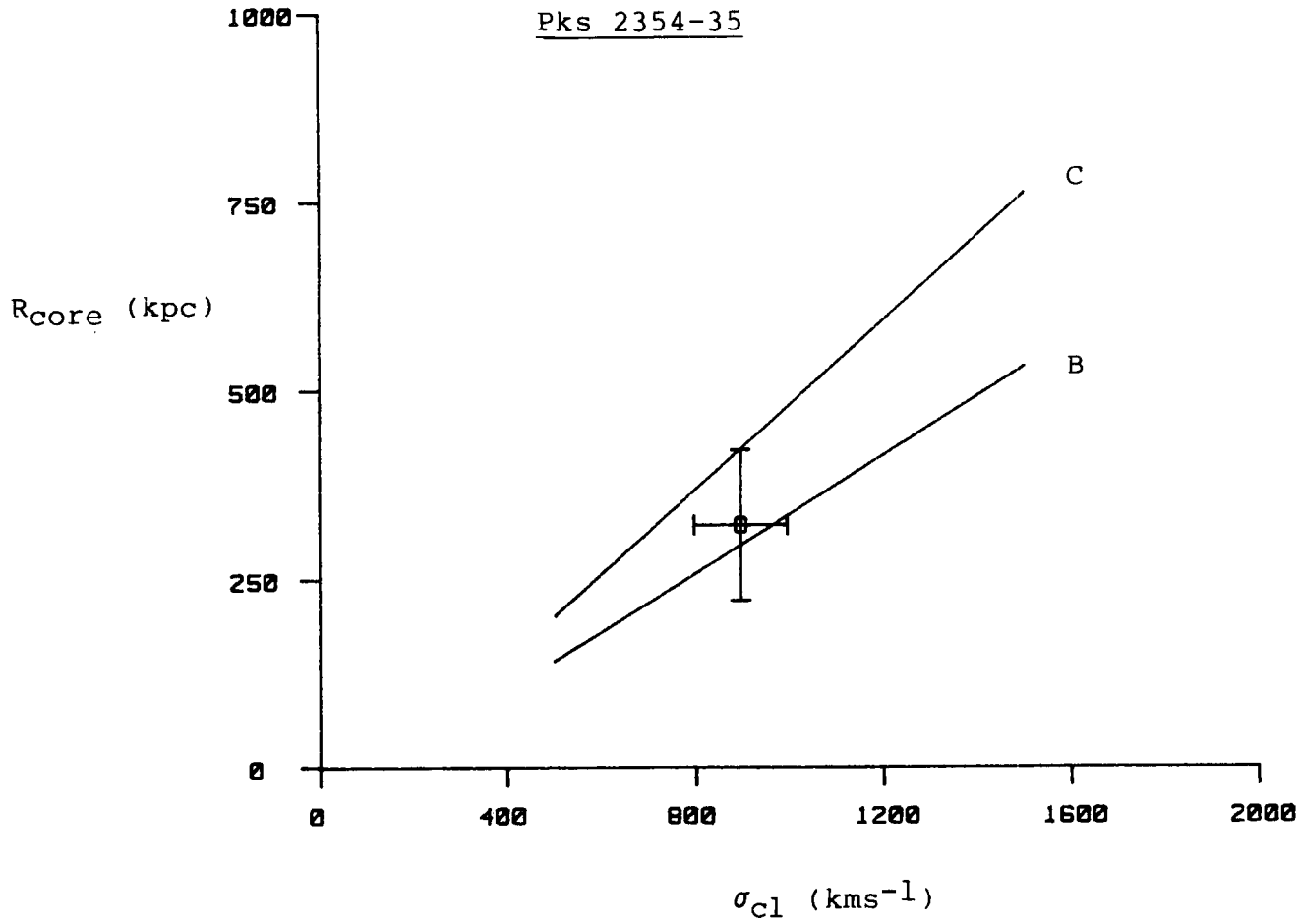

Figure 6.5.3 Pks 2354-35 Dynamical Models

cD core is from the cluster background. At the extreme of the velocity dispersion measurements [21 arcsec], the fraction of total mass contributed by the second component is about 22%. These results may be compared with IC2082, for which a second component more concentrated than the cluster was required to account for the velocity dispersion profile.

Two model sets were generated for Pks 2354-35: one for each of the estimates of de Vaucouleurs effective radius of the galaxy. The two curves in figure 6.5.3 bracket the observations of cluster core radius and velocity dispersion. No strong statement can therefore be made about the likely scale length of the second component required to reproduce the velocity dispersion profile, only that a model generated from the observed cluster and galaxy parameters would fit the galaxy velocity dispersion profile quite well. Only 2-3% of the mass interior to 10 arcsec is attributable to the background matter, rising to 6-11% at 20 arcsec. The range in mass fraction reflects the choice of a larger or smaller effective radius.

Total galactic masses and mass-to-light ratios are reported in table 6.5.3. A comparison with other estimates of M/L for elliptical and brightest cluster member galaxies is presented in table 6.5.4. This table includes the values reported in Carter et al (1985) which have been converted from the Cousins R band to B using: $(B_J-R_C) = 1^m.59$ for a typical elliptical or BCM galaxy [Carter, priv.comm.] and $(B_J-R_C)_\odot = 1^m.02$ [using $(V_J-R_C) = 0^m.71\ (V_J-R_J)$, Cousins (1976)].

Table 6.5.3

Masses, Luminosities and M/L Ratios

Object	σ (kms^{-1})	r_e (kpc)	σ^*_{ap}	M ($10^{12}M_\odot$)	L_B ($10^{11}L_\odot$)	M/L_B
Sersic 40/6	309	128.5	.436	15.01	10.86	13.8
Pks 2354-35	293	64.9	.451	6.37	8.95	7.1
0559-40	275	37.7	.459	3.15	2.88	10.9
IC2082	273	13.6	.459	1.12	1.66	6.7

Table 6.5.4

M/L Comparisons

Sample	M/L_V	M/L_{RC}	M/L_B	Source
25 BCM	9.0 ± 0.8	-	12.2 ± 1.1	MK
8 E	6.5 ± 0.7	-	8.8 ± 1.0	MK
A2029	12	-	16.3	D
13 E	-	-	7.0 ± 1.0	EEC
4 BCM	-	6.5 ± 0.6	10.9 ± 1.0	CIEEG
4 BCM	-	-	9.6 ± 1.7	I

MK : Malumuth & Kirshner (1985)
D : Dressler (1979)
EEC : Efstathiou, Ellis & Carter (1980)
CIEEG : Carter et al (1985)
I : this work

$M/L_B = 1.36(M/L_V)$ and $M/L_B = 1.69(M/L_{RC})$

The M/L ratios determined in this work have a considerable spread, ranging from a value typical of a normal elliptical galaxy [IC2082] to a value typical of brightest cluster member galaxies [Sersic 40/6]. The greatest uncertainty involved in calculating these M/L estimates is in the effective radii used, which accounts for the difference between this work and Carter et al.

The mean value of M/L found for the four objects studied here [9.6 $\pm$ 1.7] is consistent with that found for other elliptical and brightest cluster member galaxies [Malumuth & Kirshner (1985)]. This suggests that, over a wide range of mass, elliptical-like galaxies have much the same stellar content. These results also suggest that the observations reported in this work are consistent.

Determination of M/L ratios helps considerably in understanding the significant luminosity excesses found for the BCM galaxies studied in this work. We must first examine the $L-\sigma^4$ relation, which is intimately connected with galaxy M/L ratios.

For de Vaucouleurs galaxies, the $L-\sigma^4$ relation may be derived by noting two proportionalities:

$$M \alpha r_e.\sigma^2$$
$$L \alpha I_e.r_e^2$$

If I_e is constant for all galaxies, then

$$L \alpha r_e^2 \quad \text{or} \quad r_e \alpha L^{\frac{1}{2}}$$

and so $$M \alpha L^{\frac{1}{2}}.\sigma^2.$$

If, further, M/L is constant for all galaxies, then:

$$\frac{M}{L} \quad \alpha \quad \frac{\sigma^2}{L^{\frac{1}{2}}} \quad = \text{constant}$$

or $L \quad \alpha \quad \sigma^4$

Thus, if the power of the relationship between L and σ is really four, we might conclude:

I_e = constant
M/L = constant.

One mechanism which can explain the luminosity excesses of BCM galaxies and additional properties, is that of homologous mergers [as described in chapter 1, or Ostriker & Hausman (1977)].

The galaxies in this study are tolerably well fit by de Vaucouleurs luminosity profiles. If the present state of these galaxies is the result of a number of mergers, then the original galaxies probably also were de Vaucouleurs profile galaxies. Without specifying the merger process in detail, but considering the potential energy of merging systems, it is possible to show that the homologous merger product of N equal mergers will have:

$R = N \; R_o$
$I = {}^1/_N \; I_o$

where R_o and I_o were the original values of the effective radius [r_e] and the surface-brightness at r_e [I_e].

In such a situation:

$$I_e . r_e = \text{constant}$$

The M/L ratio is clearly conserved in the merger because it describes the material of the galaxies, which remains unchanged in the mergers considered here, so:

$$\frac{M}{L} \alpha \frac{\sigma^2}{I_e . r_e} = \text{constant}$$

or $\sigma^2 = \text{constant}$.

Homologous mergers therefore produce galaxies which have the features seen in the BCM galaxies studied in this work: large effective radii [cf Davies et al (1983)], velocity dispersions typical of normal elliptical galaxies and low surface-brightnesses [ie the M/L ratios are typical of normal elliptical galaxies]. The explanation of the luminosity excesses is now apparent: the luminosity increases as each merger takes place, but the central velocity dispersion remains unchanged. Homologous merger products do not follow the $L-\sigma^4$ relation because the surface-brightness, I_e, is reduced each time a merger occurs and the constant I_e condition for the relationship is violated.

The general form of the $L-\sigma$ relation has been predicted by more sophisticated merger models, such as those described by Farouki et al (1983) and Duncan et al (1983). These N body simulations include an initial hierarchical phase, [where $L \alpha \sigma^4$] followed by a cannibalism phase [during which

increases in the luminosity are not matched by correspondingly large increases in the central velocity dispersion].

It should be noted that the luminosity excesses of the four BCM galaxies studied in this work are not attributable to the extensive diffuse envelopes which characterise the brightest cD galaxies. The photometry used in this study shows no trace of any diffuse haloes.

6.5.4 Summary

The observation of three additional D or cD galaxies has extended and confirmed the results found from the investigation of IC2082 and its cluster.

There is no dynamically significant rotation in the envelopes of any of the programme galaxies. Their substantially elliptical appearance is either due to velocity anisotropy or is a consequence of the formation process.

All three galaxies studied show significant luminosity excesses relative to the normal galaxy luminosity - velocity dispersion relation. Such excesses would be a natural consequence of homologous mergers. The Sersic 40/6 dumb-bell system is quite plausibly in the process of merging, having a merger timescale of a few orbits.

Both Sersic 40/6 and Pks 2354-35 have flat or rising velocity dispersion profiles. These have been modelled as showing the influence of dark material distributed with the same scale length as the cluster galaxies themselves. The D galaxy in 0559-40 can be modelled without recourse to a second component - a result which directly links the internal stellar dynamics of D galaxies with the morphology of the surrounding cluster. The background material itself remains unexplained: any identification of this material with stripped tidal debris would, from the present work, be a purely circumstantial inference. Interpretation of X-ray emission from clusters could help this identification considerably.

M/L ratios calculated for this work are consistent with values measured by other authors for elliptical and brightest cluster member galaxies. D and cD galaxies are evidently composed of much the same stellar material as normal elliptical galaxies: it is their enormous scale which is so unusual.

7 CHAPTER SEVEN : SUMMARY & CONCLUSIONS

7.1 INTRODUCTION

This work is based on observation. There are two types of result which might be obtained from such an investigation and each has a different validity and importance.

Firstly, many of the results derived in this work are essentially independent of the general framework of astronomical interpretation. The velocity dispersion profiles derived in this work could, for example, be used directly by other investigators to aid their own researches, without accepting the interpretation made here. It is clear that an important outcome of any observational study is the data itself, independent of any interpretation which may subsequently be applied, and these "specific" results are described in section 7.2.

However, the purpose of this investigation is not only to gather evidence [ie specific results] but is also to interpret this evidence in the light of current theories [such as galactic cannibalism]. These more general conclusions are reported in section 7.3.

Some comments about the current work and suggestions for future work are made in section 7.4.

7.2 SPECIFIC RESULTS

The following results have been obtained from the investigation reported in the previous chapters of this work.

a) Rotation curves, velocity dispersion profiles and M/L ratios have been determined for four southern D/cD galaxies.

b) There is no significant envelope rotation in any of the four sample galaxies.

c) The relative velocities of the dumb-bell components of the two multiple nucleus systems studied are much less than the corresponding cluster velocity dispersions, but are typical of the internal stellar velocity dispersions of the galaxies themselves.

d) The velocity dispersion of one of the sample galaxies falls with distance from the nucleus, whereas it remains constant, or rises, in the other three galaxies.

e) The sample galaxies are significantly over-luminous for their central velocity dispersions [relative to the normal elliptical galaxy L-σ relation].

f) M/L ratios determined in this work span the range typical of normal elliptical and BCM galaxies.

g) A sample of 27 galaxy clusters has been analysed to provide an estimate of the mean galaxy cluster core radius.

h) Redshifts and central velocity dispersions have been determined for a sample of eleven southern elliptical and BCM galaxies.

i) A Fourier Difference method is recommended for the analysis of spectroscopic absorption-line data to obtain radial velocities, velocity dispersions and [particularly] line-strengths.

j) The theoretical dependence of velocity dispersion on radius has been calculated for a galaxy having a de Vaucouleurs luminosity profile, and is tabulated for direct use by other investigators.

7.3 GENERAL RESULTS

A theme running through this work has been the recognition that the explanation of cD galaxy formation lies in the dynamical properties of galaxies and clusters of galaxies, and that cD galaxies have therefore formed by a process which is primarily evolutionary.

We have seen that the stellar content of D/cD galaxies is much the same as that of normal elliptical galaxies [though there is a considerable spread in M/L] - and yet these galaxies do not form a natural continuation of the dynamical sequence of normal elliptical galaxies [as judged by the offset

and scatter about the L-σ relation]. Merger theory can account for the form of the L-σ relation over a wide range of elliptical galaxy luminosity, and other evidence also suggests that cD galaxies might consist of material once associated with other galaxies. Possible direct evidence for evolution by galactic cannibalism comes from the examples of dumb-bell galaxies studied in this work.

Models of the velocity dispersion profiles of the sample galaxies suggest that any dark component present in the clusters is distributed with a scale length less than or equal to that of the cluster galaxies themselves. This confirms a result found from studies of cD cluster morphology: that the occurence of a cD galaxy in a cluster is often linked with a possibly quite local enhancement of galaxy density. Theories of cluster formation should explain this apparent inhomogeneity in the structure of galaxy clusters.

Mergers cannot be a complete explanation of the cD galaxy phenomenon. Evidence has been found in this work to indicate that differences exist between the dynamical characteristics of centrally located and peripheral galaxies. There are known morphological differences between such galaxies and it is now clear that any convincing formation mechanism for cD galaxies must explain the dependence of their detailed properties on location [the tidal stripping mechanism, for example, quite naturally emphasises the importance of location].

7.4 FUTURE WORK

This work has been very much concerned with how to make observations. It is therefore appropriate to indicate what could be done in the future to continue the investigation begun here.

The importance of consistency in data reduction cannot be overstated for both spectroscopic and photometric data. It has long been accepted that consistency in photometric data reduction is painstakingly difficult to achieve - and it is clear from this work that similar care may be needed in the reduction of spectroscopic data. Future work might benefit from the use of fixed pixel detectors working at moderately high dispersion [33 Å/mm]. In addition, the availability of consistent photometry must be a compelling factor in the selection of the sample of galaxies to be observed.

When planning observations whose goal is to derive a set of parameters which are to be compared with some model, an assessment must be made of the errors in these parameters which can be tolerated before our ability to reject this model is significantly degraded. All the parameters of the two-component dynamical model used in this work were observable, and were observed. It is clear that the two parameters which require the most attention in the future are the galaxy effective radius and the cluster core radius. The likely errors in galaxy and cluster velocity dispersions are understood, whereas the errors in the parameters derived from photometry seem to be relatively larger and more difficult to assess.

Future work which might be contemplated as a result of this investigation includes the following.

a) New and more accurate observations as described in this work, looking at both centrally located and peripheral D/cD galaxies.

b) Galactic cannibalism requires the association of multiple nucleus components to be physical, and this might be established by detailed observations of rotation curves and luminosity profiles.

c) The kinematical approach followed in this work should be extended to include line-strength and colour variations across and between elliptical galaxies of all luminosities - as a direct test of an intrinsic galaxy property.

d) Theoretical work on mergers and anisotropic velocity dispersions should attempt to explain consistently: the ellipticities of cD galaxies; their velocity dispersions; their luminosity profiles and lack of rotation. In addition, a mechanism for producing velocity anisotropies must be firmly established.

This work has significantly extended the available kinematic data on supergiant elliptical galaxies. Future workers should attempt to build up a large sample of accurate data, so that any predictive theory of cD galaxy formation may be challenged unambiguously.

ABBREVIATIONS OF PUBLICATIONS

AJ
Astronomical Journal.

Ann Rev Astr Astrophys
Annual Review of Astronomy & Astrophysics.

ApJ
Astrophysical Journal.

ApJ (Suppl)
Astrophysical Journal, Supplement Series.

Astr Astrophys
Astronomy & Astrophysics.

Astr Astrophys (Suppl)
Astronomy & Astrophysics, Supplement Series.

Aust J Phys
Australian Journal of Physics.

Mem RAS
Royal Astronomical Society, Memoirs.

MNRAS
Royal Astronomical Society, Monthly Notices.

PASP
Astronomical Society of the Pacific, Publications.

BIBLIOGRAPHY

Aaronson M, Huchra J, Mould J - ApJ 229:1 (1979)

Abell GO - ApJ (Suppl) 3:211 (1958)

Abell GO - "Stars & Stellar Systems", 9, Galaxies & the Universe, ed Sandage A, [Chicago:University of Chicago Press] (1973)

Albert CE, White RA, Morgan WW - ApJ 211:309 (1977)

Allen CW - "Astrophysical Quantities", 3rd edition, [London:Athlone Press] (1973)

Austin TB, Peach JV - MNRAS 167:437 (1974)

Bahcall NA - ApJ 198:249 (1975)

Bahcall NA - Ann Rev Astr Astrophys 15:505 (1977)

Bailey ME, MacDonald J - MNRAS 194:195 (1981)

Bautz LP, Morgan WW - ApJ 162:L149 (1970)

Bautz LP, Abell GO - ApJ 184:709 (1973)

Beers TC, Geller MJ - ApJ 274:491 (1983)

Beers TC, Geller MJ, Huchra JP, Latham DW, Davis RJ - ApJ 283:33 (1984)

Bertola F, Capaccioli M - ApJ 200:439 (1975)

Binney JJ - MNRAS 181:735 (1977)

Binney JJ - MNRAS 183:501 (1978)

Binney JJ - Ann Rev Astr Astrophys 20:399 (1982)

Blandford RD, Smarr L - pre-print (1982)

Bolton JG, Ekers RD - Aust J Phys 19:559 (1966)

Bosma A, Smith RM, Wellington KJ - MNRAS 212:301 (1985)

Brault JW, White OR - Astr Astrophys 13:169 (1971)

Bucknell MJ - DPhil, Oxford (1977)

Burbidge EM, Burbidge GR, Fish RA - ApJ 133:393 (1961)

Burbidge EM, Burbidge GR, Fish RA - ApJ 133:1092 (1961)

Burbidge EM, Burbidge GR, Fish RA - ApJ 134:251 (1961)

Capaccioli M - "Photometry, Kinematics & Dynamics of Galaxies", ed Evans DS, [Austin:University of Texas at Austin], p165 (1979)

Carter D, Metcalfe N - MNRAS 191:325 (1980)
Carter D, Efstathiou G, Ellis RS, Inglis I,
Godwin JG - MNRAS 195:15P (1981)
Carter D, Teague PF, Gray PM - "Groups & Clusters
of Galaxies", ed Mardirossian F,
[Dordrecht:Reidel] (1984)
Carter D, Inglis I, Ellis RS, Efstathiou G,
Godwin JG - MNRAS 212:471 (1985)
Chandrasekhar S - "Principles of Stellar Dynamics",
[New York:Dover] (1960)
Christiansen WN, Frater RH, Watkinson A, O'Sullivan JD,
Lockhart IA, Goss WM - MNRAS 181:183 (1977)
Cousins AWJ - Mem RAS 81:25 (1976)
Da Costa GS, Freeman KC, Kalnajs AJ, Rodgers AW,
Stapinski TE - AJ 82:810 (1977)
Davies RL - PhD, Cambridge (1979)
Davies RL - MNRAS 194:879 (1981)
Davies RL, Efstathiou G, Fall SM, Illingworth G,
Schechter PL - ApJ 266:41 (1983)
Davies RL, Illingworth G - ApJ 266:516 (1983)
de Vaucouleurs G - Annales d'Astrophysique 11:247 (1948)
de Vaucouleurs G - MNRAS 113:134 (1953)
de Vaucouleurs G, de Vaucouleurs A, Corwin HG
- "Second Reference Catalogue of Bright Galaxies",
[Austin:University of Texas Press] (1976)
de Vaucouleurs G, Capaccioli M
- ApJ (Suppl) 40:699 (1979)
de Vaucouleurs G, Olson DW - ApJ 256:346 (1982)
Dressler A - ApJ 223:765 (1978a)
Dressler A - ApJ 226:55 (1978b)
Dressler A - ApJ 231:659 (1979)
Dressler A - ApJ 236:351 (1980a)
Dressler A - ApJ (Suppl) 42:565 (1980b)
Dressler A - ApJ 243:26 (1981)
Dressler A - ApJ 286:97 (1984a)

Dressler A - Ann Rev Astr Astrophys 22:185 (1984b)
Dressler A, Thompson IB, Schectman SA
- ApJ 288:481 (1985)
Duncan MJ, Farouki RT, Shapiro SL - ApJ 271:22 (1983)
Ellis RS, Gray PM, Carter D, Godwin JG
- MNRAS 206:285 (1984)
Efstathiou G, Ellis RS, Carter D - MNRAS 193:931 (1980)
Efstathiou G, Ellis RS, Carter D - MNRAS 201:975 (1982)
Faber SM, Jackson RE - ApJ 204:668 (1976)
Faber SM - "The Evolution of Galaxies & Stellar
Populations", ed Tinsley BM & Larson RB,
[New Haven:Yale University Observatory] (1977)
Faber SM, Burstein D, Dressler A - AJ 82:941 (1977)
Farouki RT, Shapiro SL, Duncan MJ - ApJ 265:597 (1983)
Fish RA - ApJ 139:284 (1964)
Ftaclas C, Struble MF - ApJ 274:521 (1983)
Gallagher JS, Ostriker JP - AJ 77:288 (1972)
Geller MJ, Peebles PJE - ApJ 206:939 (1976)
Godwin JG - DPhil, Oxford (1976)
Godwin JG - Nature 277:364 (1979)
Goodman J, Binney JJ - MNRAS 207:511 (1984)
Green MR - DPhil, Oxford (1977)
Green MR, Godwin JG, Ellis RS, Carter D - in prep (1984)
Griffen RF - ApJ 148:465 (1967)
Gunn JE, Gott JR - ApJ 176:1 (1972)
Gunn JE, Oke JB - ApJ 195:255 (1975)
Gunn JE, Tinsley BM - ApJ 210:1 (1976)
Hausman MA, Ostriker JP - ApJ 224:320 (1978)
Hickson P, Richstone DO, Turner EL - ApJ 213:323 (1977)
Hoessel JG, Gunn JE, Thuan TX - ApJ 241:486 (1980)
Hoessel JG - ApJ 241:493 (1980)
Hoessel JG, Borne KD, Schneider DP - ApJ 293:94 (1985)
Humason ML, Mayall NU, Sandage A - AJ 61:97 (1956)
Illingworth G, Freeman KC - ApJ 188:L83 (1974)
Illingworth G - ApJ 204:73 (1976)

Illingworth G - ApJ 218:L43 (1977)
Jenner DC - ApJ 191:55 (1974)
Jones C, Mandel E, Schwartz J, Forman W, Murray SS,
Harnden FR - ApJ 234:L21 (1979)
Jones C, Forman W - ApJ 276:38 (1984)
Kellog E, Murray SS - ApJ 193:L57 (1974)
King IR - AJ 67:471 (1962)
King IR - AJ 71:64 (1966)
King IR - ApJ 174:L123 (1972)
Kormendy J - ApJ 218:333 (1977)
Kormendy J, Illingworth G - ApJ 256:460 (1982)
Kristian J, Sandage A, Westphal JA - ApJ 221:383 (1978)
Kron RB, Albert CE - PASP 94:887 (1982)
Lampton M, Margon B, Bowyer S - ApJ 208:177 (1976)
Leir AA, van den Bergh S - ApJ (Suppl) 34:381 (1977)
Lugger PM - AJ 84:1677 (1979)
Lugger PM - ApJ 286:106 (1984)
Lynden-Bell D - MNRAS 136:101 (1967)
Malumuth EM, Kirshner RP - ApJ 251:508 (1981)
Malumuth EM, Richstone DO - ApJ 276:413 (1984)
Malumuth EM, Kirshner RP - ApJ 291:8 (1985)
Materne J, Chincarini G, Tarenghi M, Hopp U
- Astr Astrophys 109:238 (1982)
Matthews TA, Morgan WW, Schmidt M - ApJ 140:35 (1964)
Melnick J, White SDM, Hoessel JG - MNRAS 180:207 (1977)
Melnick J, Quintana H
- Astr Astrophys (Suppl) 44:87 (1981a)
Melnick J, Quintana H - AJ 86:1567 (1981b)
Merritt D - ApJ 264:24 (1983)
Merritt D - ApJ 276:26 (1984a)
Merritt D - ApJ 280:L5 (1984b)
Michie RW - MNRAS 125:127 (1963)
Miller GE - ApJ 268:495 (1983)

AAT

Minkowski R - IAU Symposium 15, "Problems of Extragalactic Research", ed McVittie G, [New York:MacMillan], p112 (1962)
Morbey C, Morris S - ApJ 274:502 (1983)
Morgan WW - PASP 70:364 (1958)
Morgan WW, Lesh JR - ApJ 142:1364 (1965)
Morgan WW, Kayser S, White RA - ApJ 199:545 (1975)
Morton DC, Chevalier RA - ApJ 174:489 (1972)
Morton DC, Chevalier RA - ApJ 179:55 (1973)
Morton DC, Thuan TX - ApJ 180:705 (1973)
Morton DC, Elmergreen BG - ApJ 205:63 (1976)
Morton DC, Andereck CD, Bernard DA - ApJ 212:13 (1977)
Oemler A - ApJ 180:11 (1973)
Oemler A - ApJ 194:1 (1974)
Oemler A - ApJ 209:693 (1976)
Ostriker JP, Tremaine S - ApJ 202:L113 (1975)
Ostriker JP, Hausman MA - ApJ 217:L125 (1977)
Ostriker JP - IAU Symposium 79, "The Large Scale Structure of the Universe", ed Longair MS & Einasto J, [Dordrecht:Reidel], p357 (1978)
Pritchet C - ApJ 221:507 (1978)
Qunitana H, Lawrie DG - AJ 87:1 (1982)
Quintana H, Melnick J - AJ 87:972 (1982)
Richstone DO, Sargent WLW - ApJ 176:91 (1972)
Richstone DO - ApJ 200:535 (1975)
Richstone DO - ApJ 204:642 (1976)
Richstone DO, Malumuth EM - ApJ 268:30 (1983)
Rood HJ, Sastry G - PASP 83:313 (1971)
Rood HJ, Page TL, Kintner EC, King IR - ApJ 175:627 (1972)
Rood HJ, Leir AA - ApJ 231:L3 (1979)
Roos N, Norman CA - Astr Astrophys 76:75 (1979)
Rubin VC, Ford WK, Thonnard N - ApJ 225:L107 (1978)
Sandage A - ApJ 173:485 (1972a)
Sandage A - ApJ 176:21 (1972b)

Sandage A - ApJ 178:1 (1972c)
Sandage A - ApJ 183:711 (1973a)
Sandage A - ApJ 183:731 (1973b)
Sandage A, Hardy E - ApJ 183:743 (1973)
Sandage A - ApJ 202:563 (1975)
Sandage A - ApJ 205:6 (1976)
Sandage A, Visvanathan N - ApJ 223:707 (1978)
Sargent WLW, Schechter PL, Boksenberg A,
Shortridge K - ApJ 212:326 (1977)
Sargent WLW, Young PJ, Boksenberg A, Shortridge K,
Lynds CR, Hartwick FDA - ApJ 221:731 (1978)
Schechter PL - ApJ 203:297 (1976)
Schechter PL, Peebles PJE - ApJ 209:670 (1976)
Schechter PL, Gunn JE - ApJ 229:472 (1979)
Schild R, Davis M - AJ 84:311 (1979)
Schneider DP, Gunn JE, Hoessel JG - ApJ 264:337 (1983a)
Schneider DP, Gunn JE, Hoessel JG - ApJ 268:476 (1983b)
Semeniuk I - Acta Astronomica 32:337 (1982)
Sersic JL - Zeitschrift für Astrophysik 53:256 (1961)
Sersic JL - Astrophysics & Space Science 28:365 (1974)
Shanks T, Stevenson PRF, Fong R, MacGillivray HT
- MNRAS 206:767 (1984)
Simkin SM - Astr Astrophys 31:129 (1974)
Smith RM, Efstathiou G, Ellis RS, Frenck CS,
Valentijn EA - MNRAS in press (1985)
Stewart GC, Fabian AC, Jones C, Forman W
- ApJ 285:1 (1984)
Stock J, Schueking E - AJ 62:98 (1957)
Strom SE, Strom KM - ApJ 225:L93 (1978)
Struble MF, Rood HJ - AJ 87:7 (1982)
Terlevich R, Davies RL, Faber SM, Burstein D
- MNRAS 196:381 (1981)
Thuan TX, Romanishin W - ApJ 248:439 (1981)
Tonry JL, Davis M - AJ 84:1511 (1979)
Tonry JL - ApJ 251:L1 (1981)

Tonry JL, Davis M - ApJ 246:666 (1981)
Tonry JL - ApJ 266:58 (1983)
Tonry JL - ApJ 279:13 (1984)
Tonry JL - ApJ 291:45 (1985)
Tremaine S - ApJ 203:72 (1976)
Tremaine S, Richstone DO - ApJ 212:311 (1977)
Tremaine S - "The Structure & Evolution of Normal
Galaxies", ed Fall SM & Lynden-Bell D,
[Cambridge:Cambridge University Press], p67 (1981)
van den Bergh S - PASP 89:746 (1977)
Vidal N - PASP 87:625 (1975)
Weinberg S - "Gravitation & Cosmology",
[New York:Wiley] (1972)
West RM, Fransden S
- Astr Astrophys (Suppl) 44:329 (1981)
Westerlund BE, Smith LF - Aust J Phys 19:181 (1966)
Westerlund BE, Wall JV - AJ 74:335 (1969)
White RA - ApJ 226:591 (1978)
White SDM - MNRAS 177:717 (1976)
Whitmore BC, Kirshner RP, Schechter PL
- ApJ 234:68 (1979)
Whitmore BC, Kirshner RP - ApJ 250:43 (1981)
Whiteoak JB - Aust J Phys 25:233 (1972)
Williams TB - ApJ 214:685 (1977)
Williams TB - ApJ 244:458 (1981)
Young PJ - AJ 81:807 (1976)
Zwicky F - "Morphological Astronomy",
[Berlin:Springer] (1957)

ACKNOWLEDGEMENTS

Principal thanks are due to my supervisor Professor Richard Ellis, for providing great academic and bureaucratic assistance over the years during which this work has been done.

This work is the result of a collaborative effort. Outside Durham, thanks go to my long-suffering collaborators: Drs George Efstathiou, Dave Carter and Jon Godwin.

Thanks go to all my colleagues at Durham, but particularly to Dr Ray Sharples, who set me off on finding a consistent method for calculating velocity dispersions.

Financial assistance from the SERC enabled the research work for this thesis to be carried out, both in Durham and at observatories overseas. I am also very grateful to staff at the two Royal Observatories for use of their computing and library facilities.